Setup and application of modulation excitation infrared spectroscopy for mechanistic elucidation of heterogeneously catalyzed reactions

Aufbau und Anwendung der Modulations-Anregungs-Infrarot-Spektroskopie zur Mechanismusaufklärung heterogen katalysierter Reaktionen

Zur Erlangung des Grades eines Doktors der Naturwissenschaften (Dr. rer. nat.)
genehmigte Dissertation von Jakob Weyel aus Gelnhausen
Tag der Einreichung: 30. Mai 2023, Tag der Prüfung: 27. Juli 2023

1. Gutachten: Prof. Dr. Christian Hess
2. Gutachten: Prof. Dr. Rolf Schäfer
3. Gutachten: Prof. Dr. Rolf Jürgen Behm

Darmstadt, Technische Universität Darmstadt

TECHNISCHE UNIVERSITÄT DARMSTADT

Chemistry Department
Eduard Zintl Institute for Inorganic and Physical Chemistry
Hess research group

Setup and application of modulation excitation infrared spectroscopy for mechanistic elucidation of heterogeneously catalyzed reactions
Aufbau und Anwendung der Modulations-Anregungs-Infrarot-Spektroskopie zur Mechanismusaufklärung heterogen katalysierter Reaktionen

Doctoral thesis by Jakob Weyel

1. Review: Prof. Dr. Christian Hess
2. Review: Prof. Dr. Rolf Schäfer
3. Review: Prof. Dr. Rolf Jürgen Behm

Date of submission: 30. Mai 2023
Date of thesis defense: 27. Juli 2023

Darmstadt, Technische Universität Darmstadt

Erklärungen laut Promotionsordnung

§8 Abs. 1 lit. c PromO

Ich versichere hiermit, dass die elektronische Version meiner Dissertation mit der schriftlichen Version übereinstimmt.

§8 Abs. 1 lit. d PromO

Ich versichere hiermit, dass zu einem vorherigen Zeitpunkt noch keine Promotion versucht wurde. In diesem Fall sind nähere Angaben über Zeitpunkt, Hochschule, Dissertationsthema und Ergebnis dieses Versuchs mitzuteilen.

§9 Abs. 1 PromO

Ich versichere hiermit, dass die vorliegende Dissertation selbstständig und nur unter Verwendung der angegebenen Quellen verfasst wurde.

§9 Abs. 2 PromO

Die Arbeit hat bisher noch nicht zu Prüfungszwecken gedient.

Darmstadt, 30. Mai 2023

J. Weyel

Publications

Parts of this thesis have been published so far in peer reviewed journals and at national and international conferences.

Journal articles

- M. Ziemba, J. Weyel, C. Hess, Elucidating the mechanism of the reverse water–gas shift reaction over Au/CeO_2 catalysts using *operando* and transient spectroscopies, Appl. Catal. B Environ. **2022**, 301, 120825.

- J. Weyel, M. Ziemba, C. Hess, Elucidating Active CO–Au Species on $Au/CeO_2(111)$: A Combined Modulation Excitation DRIFTS and Density Functional Theory Study, Top. Catal. **2022**, 65, 779–787.

- M. Ziemba, J. Weyel, C. Hess, Approaching C1 Reaction Mechanisms Using Combined *Operando* and Transient Analysis: A Case Study on Cu/CeO_2 Catalysts during the LT-Water–Gas Shift Reaction, ACS Catal. **2022**, 12, 9503–9514.

- L. Schumacher, J. Weyel, C. Hess, Unraveling the Active Vanadium Sites and Adsorbate Dynamics in VO_x/CeO_2 Oxidation Catalysts Using Transient IR Spectroscopy, J. Am. Chem. Soc. **2022**, 144, 14874–14887.

Oral presentations

- J. Weyel, C. Hess, DRIFT-MES of CO oxidation over Au/CeO_2: temporal classification of CO adsorbates within the mechanism, Modern Concepts in Catalysis: From Science to Engineering – The South-West-German Catalysis Course, 30 September-2 October 2020, Annweiler am Trifels, Germany.

- J. Weyel, M. Ziemba, C. Hess, Elucidating active species over Au/CeO_2 catalysts during CO oxidation with modulation excitation IR spectroscopy, ExpReS 2021, 3rd IMPRS RECHARGE, 19-21 May 2021, online.

- J. Weyel, M. Ziemba, C. Hess, Unraveling active species in gold-ceria catalysts using IR-modulation excitation spectroscopy, Vibrational Spectroscopy Gordon Research Seminar, 30-31 July 2022, Smithfield, RI, USA.

- J. Weyel, M. Ziemba, C. Hess, Combining transient IR spectra with DFT to elucidate the active Au sites during CO oxidation on $Au/CeO_2(111)$, Bunsentagung 2022, 7-9 September, 2022, Gießen, Germany.

Poster presentations

- J. Weyel, C. Hess, *In situ* IR modulation excitation spectroscopy of Au/CeO_2 catalysts for CO oxidation: new insight into the mechanism and the state of gold, GeCatS Infoday "*Operando* Spectroscopy in Catalysis", 29 January 2020, Frankfurt a. M, Germany.
- J. Weyel, M. Ziemba, C. Hess, Infrared modulation excitation spectroscopy over Au/CeO_2 catalysts: temporal assignment of active CO adsorbates, 54th Annual Meeting of German Catalysts, 16-19 March 2021, online.
- J. Weyel, M. Ziemba, C. Hess, Elucidating active species over Au/CeO_2 catalysts during CO oxidation with modulation excitation IR spectroscopy, ExpReS 2021, 3rd IMPRS RECHARGE, 19-21 May 2021, online.
- J. Weyel, M. Ziemba, C. Hess, Detailed understanding of reaction mechanisms by unravelling hidden active species on Au/CeO_2 catalysts using modulation excitation spectroscopy, 55th German Catalysis Meeting, 27-29 June 2022, Weimar, Germany.
- J. Weyel, M. Ziemba, C. Hess, Unraveling active species in gold-ceria catalysts using IR-modulation excitation spectroscopy, Vibrational Spectroscopy Gordon Research Conference, 31 July-5 Aug 2022, RI, USA.
- J. Weyel, M. Ziemba, C. Hess, Unraveling active species on gold- and copper-ceria catalysts using IR-modulation excitation spectroscopy, 56th German Catalysis Meeting, 15-17 March 2023, Weimar, Germany.

Danksagung

Bedanken möchte ich mich von ganzem Herzen bei allen aktuellen und ehemaligen Wegbegleitern und Wegbereitern, Freundinnen und Freunden, Kolleginnen und Kollegen, Vorgesetzten und Bekannten, ohne die mir das Anfertigen der vorliegenden Arbeit nicht oder kaum möglich gewesen wäre.
Zuallererst gilt mein größter Dank Prof. Dr. Christian Hess für das Ermöglichen der Arbeit an einem so fesselnden Thema, dass ich es nur schwer aus der Hand geben mag und die begleitende, großartige Betreuung dieser Arbeit. Danke für alle Frei- und Spielräume in der doch nicht ganz so geradlinig verlaufenden Forschung und auch der Lehre, für Verständnis, hilfreiche Ideen, Anregungen und Ratschläge die so manchen gordischen Knoten durchtrennt haben. Das ist keine Selbstverständlichkeit, dafür bin ich sehr dankbar.
Dem wenig an Wichtigkeit für die gelungene Promotionszeit in kaum etwas nachstehend zu erwähnen sind Claudia Jochem und Karl Kopp für Ihre unfassbar gute Arbeit im Sekretariat und als Techniker. Ohne Claudia hätte kaum eine Bestellung, Rechnung oder Vertrag so schnell und gründlich abgewickelt werden können, ohne dich hätte es nie genug Bureaumaterialien gegeben und mit dir gab es immer eine interessante neue Teesorte im Schrank. Eine bessere Rückendeckung aus dem Sekretariat kann ich mir eigentlich nicht vorstellen. Danke dir, Karl, neben all dem offensichtlichen, wenn du mal wieder ein offenes Ohr für die technischen Herausforderungen des Laboralltags hast, für den riesigen Erfahrungsschatz, den du gerne Tag für Tag an der Arbeit oder auch im Biergarten mit uns teilst, für die Übernahme eines riesigen Teils der Lehre im Grundpraktikum, das Herumärgern mit Gasflaschenlieferungen und ganz besonders für all die Aufgaben und kleinen Ämter, die du ohne groß Worte zu verlieren und meist ohne unser Wissen ausführst und innehast, damit gibst du uns Doktoranden die Möglichkeit, noch mehr und noch besser zu forschen. Jede Publikation ist auch dein Verdienst.
Weiterhin kann ich mich nur glücklich schätzen, mit einer so großartigen Gruppe an Kolleginnen und Kollegen zusammengearbeitet zu haben. Mein Dank für spannende Diskussionen, aufbauende Gespräche und Hilfestellungen in allen Lebens- und Arbeitsfragen geht an Xu Cheng, Dr. Matthias Enders, Dr. Anastasia Filtschew, Dr. Marcel Heber, Joanna Müller, Maximilian Pfeiffer, Dr. Mariusz Radtke, Dr. Simone Rogg, Dr. Philip Ruff, Leon Schumacher, Jun Shen, Jan Welzenbach und Dr. Marc Ziemba.
Besonders hervorzuheben als ganz große Inspirationsquelle ist die Zusammenarbeit und Freundschaft mit Leon Schumacher und Dr. Marc Ziemba, mit denen ich seit unseren etwa zeitgleich begonnenen Masterarbeiten und während der gesamten Promotion eine unvergleichliche Zeit erlebt habe. Sie war geprägt von viel großartiger Forschung, kreativen Abenden im Café Hess und stets spannenden Diskussionen auf fachlicher Ebene und manchmal auch abseits davon. Es waren tolle >3 Jahre mit euch als gegenseitige Ansporner im positiven Sinne, wir sehen uns gewiss noch öfters.
Auf keinen Fall zu vernachlässigen sind auch die Beiträge der von mir betreuten Bachelor- und Masterstudierenden Pascal Schwager, Lisa Steuernagel, Maximilian Pfeiffer, Linus Hofmann und Henrik Hoyer. Jeder von euch hatte eine nichttriviale Fragestellung aus dem Umfeld meines Forschungsthemas zu bearbeiten und ihr habt mit euren Beiträgen sehr zu dessen Vorankommen beigetragen, sei es durch den Aufbau von Messapparaturen, die Durchführung langwieriger Messreihen, das sondieren neuer Reaktionen und Katalysatoren oder die Diskussionen auf wirklich hohem Niveau, die wir im Labor oder am Tischkicker führen konnten. Ihr wart tolle Mitstreiter auf Zeit!
Stellvertretend für die Mechanik- und Elektronikwerkstatt der TU Darmstadt sowie all ihrer Mitarbeiter

möchte ich Matthias Guse, Martin Schwarz und Jürgen Ühlken danken. Ohne eure zündenden Ideen, das viele Wissen und die stets schnelle Hilfe bei Reparaturen, Entwürfen und Verbesserungen von Apparaturen, Messzellen, Steuerelementen und Kabeln, hätte ich kaum Zeit für die eigentliche Forschung gehabt. Nichts hätte auch nur annähernd so gut funktioniert und die Bauteile hätten lange nicht so gut ausgesehen, vielen Dank!
Dem Fonds der Chemischen Industrie im Verband der Chemischen Industrie e.V. danke ich für das mir verliehene Promotionsstipendium, das einige teurere Anschaffungen und internationale Konferenzbesuche überhaupt erst ermöglicht hat und damit erheblich zu einem gelungenen Abschluss meiner Promotionsphase beigetragen hat.
Aus meinem Nichtfachlichen Umfeld bedanke ich mich sehr bei meiner Familie, meinen lieben Freundinnen und Freunden, den Mitgliedern meiner 2-3 Bands, den zwei besten Mitbewohnern der Welt und ganz besonders meiner Freundin. Ihr habt (in nach hinten exponentiell ansteigender Intensität) viel von meiner Arbeit mit- oder gar abbekommen, wart nachsichtig, wenn die Gesprächsthemen darum kreisten oder es im Labor mal wieder etwas länger dauerte, wenn ich verhindert war und gemeinsame Pläne wegen der schwer planbaren Forschung (oder gar einem gänzlich fehlenden Plan) *in situ* geändert werden mussten. Ihr gabt mir Ratschläge, die erfrischenderweise auch mal nichtfachlicher Natur waren und viel Kraft, weiter mit Freude Tag für Tag am Werk zu bleiben.

Zusammenfassung

Die grundlegende Eigenschaft eines Katalysators ist die Beschleunigung chemischer Reaktionen, ohne dass er dabei verbraucht wird. Dies macht katalytisch aktive Verbindungen zu einem der wichtigsten Werkzeuge in der industriell angewandten Chemie. Katalysatoren an sich stellen jedoch keine große Neuheit dar, vielmehr sind sie seit Jahrzehnten Standard in einer Vielzahl von Anwendungen. So werden beispielsweise bei mehr als 85 % aller großtechnischen Prozesse in der chemischen Industrie heterogene Katalysatoren eingesetzt [1].
Die Bedeutung der heterogenen Katalyse ist jedoch nicht auf die mit fossilen Brennstoffen betriebene Industrie beschränkt, sondern bildet auch eine hervorragende Grundlage für zukunftsweisende Anwendungen einer emissionsfreien Industrie, die sich auf Techniken wie Carbon Capture and Utilization (CCU) verlassen könnte. Hierbei sind insbesondere die Aktivierung und Umwandlung von CO_2 in reaktivere Moleküle wie Methanol oder CO über Reaktionen wie die Reverse Wasser-Gas-Shift-Reaktion (RWGSR) hervorzuheben [2, 3]. Auch die Deckung des Bedarfs an hochreinem Wasserstoff, z. B. für Brennstoffzellenanwendungen, ist auf katalytische Reaktionen angewiesen, weshalb z. B. die Niedertemperatur (*Low Temperature*)-Wasser-Gas-Shift-Reaktion (LT WGSR), die den CO-Anteil reduziert und gleichzeitig die H_2-Produktion nach der Dampfreformierung deutlich steigert, derzeit auf großes Interesse stößt [4, 5]. Katalysatoren sind aber auch in heutzutage alltäglichen Situationen anzutreffen, wie z. B. bei der Abgasnachbehandlung in Verbrennungsmotoren, wo mittels CO-Oxidation giftiges CO in weniger schädliches CO_2 umgewandelt wird [6].
Dennoch sind viele Details solcher katalytischer Prozesse noch weitgehend ungeklärt, obwohl deren tieferes Verständnis wesentlich zur anwendungsorientierten Optimierung beitragen könnte [1]. So kann insbesondere ein detaillierteres mechanistisches Verständnis der ablaufenden katalytischen Reaktionswege dazu beitragen, den Umsatz oder die Selektivität zu erhöhen. Der Nutzen der mechanistischen Aufklärung geht jedoch über den Aspekt der Optimierung dieser Parameter hinaus, denn ein bekannter Reaktionsmechanismus ist auch ein erster Schritt zur wissensbasierten Erklärung von Aktivierungs- und Deaktivierungsprozessen [7].
Ein solch tiefes Verständnis katalytischer Prozesse wird in der Regel durch Techniken zur Charakterisierung ermöglicht, die in den meisten Fällen aus dem Bereich der Spektroskopie stammen. Im besten Fall werden Messungen *in situ* durchgeführt, was bedeutet, dass die Charakterisierung während der Reaktion stattfindet oder sogar *operando*, wobei die *in situ*-Routine um laufende Aktivitätsmessungen ergänzt wird.
Die DRIFT-Spektroskopie (Diffuse Reflexions-Infrarot-Fourier-Transformations-Spektroskopie, *diffuse reflectance infrared fourier transform spectroscopy*) beispielsweise ist ein wichtiges und weit verbreitetes Werkzeug, das breite Anwendung gefunden hat, etwa für die schwingungsspektroskopische Untersuchung von pulverförmigen Proben in der Katalysatorforschung. Aufgrund der großen Informationsdichte dieser Messmethode ist jedoch auch die Komplexität der Spektren sehr hoch. So ist es selbst bei Modellreaktionen, wie z. B. der Au/CeO_2-katalysierten CO-Oxidation, kaum möglich, sauber zu unterscheiden, welche Spezies bei der Reaktion entstehen und ob sie am Reaktionsmechanismus beteiligt sind oder nur als Beobachter auftreten.
Eine allgemeine Herausforderung ist hier die Aufklärung von Spektren, die Überlagerungen einer großen Anzahl von Signalen auf der Oberfläche adsorbierter Neben- und Zwischenprodukte zeigen. Deren Einordnung in die Kategorien der Beobachter- und der aktiv beteiligten Spezies ist nicht nur für die konventionelle DRIFT-Spektroskopie, sondern auch für die meisten anderen Charakterisierungstechniken eine schwierige Aufgabe, bei der selbst *in situ*- oder *operando*-Methoden an die Grenzen ihrer Aussagekraft stoßen.
Die Einführung eines transienten Ansatzes in die *in situ*- oder *operando*-Methoden kann diese Lücke schließen

und eine Unterscheidung zwischen verschiedenen Signalen ermöglichen, z. B. auf der Grundlage des Kriteriums, ob sie an der Reaktion beteiligt sind oder nicht, oder zwischen Signalen, die zwar an sehr ähnlichen spektralen Positionen auftreten, aber während der Reaktion eine sehr unterschiedliche Dynamik aufweisen und daher zu unterschiedlichen Zeiten auftreten können.
Eine Methode, die diese beiden Vorteile vereint, ist die sogenannte Modulations-Anregungs-Spektroskopie (*Modulation Excitation Spectroscopy*, MES). Bei dieser wird zeitaufgelöste Spektroskopie mit einer periodischen Stimulation des untersuchten Systems durch Variation eines externen Parameters, z. B. der Konzentration, sowie einer gezielten Datennachbearbeitung, der sogenannten phasensensitiven Detektion (PSD), kombiniert. Diese Methode wurde in der Vergangenheit bereits erfolgreich zur Trennung der Signale aktiver Spezies von Hintergrund und Beobachtern eingesetzt, nachdem sie 2001 erstmals von Baurecht und Fringeli als eigenständige spektroskopische Methode am Beispiel der ATR-IR-Spektroskopie (abgeschwächte Totalreflexion, *attenuated total reflexion*) von Säure-Base-Reaktionen vorgestellt wurde [8]. Trotz ihrer Leistungsfähigkeit beim selektiven Nachweis aktiv beteiligter Spezies, bei relativ geringem apparativem Aufwand, konnte sich diese Technik bisher nicht als Standardmethode für die mechanistische Untersuchung katalytischer Prozesse etablieren [8, 9].
In dieser Arbeit wird das Design und die Optimierung eines Systems zur Anwendung von ME-DRIFTS auf eine Vielzahl von katalytischen Reaktionen wie der CO-Oxidation, Wasser-Gas-Shift-Reaktion (WGSR), reversen Wasser-Gas-Shift-Reaktion (RWGSR) sowie der CO_2-Aktivierung zur MeOH-Herstellung bei erhöhten Drücken über gold- und kupferbeladenen Ceroxid-Katalysatoren beschrieben. Für diese Reaktionen konnte das mechanistische Verständnis der eingesetzten Katalysatoren bei der Arbeit grundlegend erweitert werden, indem der Reaktionsweg der Moleküle auf der Katalysatoroberfläche direkt nachverfolgt werden konnte.
Im Falle der WGSR über Cu/CeO_2 beispielsweise konnte anhand der MES-PSD-Spektren beurteilt werden, ob der Mechanismus über Adsorbate (assoziativ) verläuft oder einem Redox-Mechanismus folgt, wobei sich der zuletzt genannte als der vorherrschende Mechanismus herausstellte.
Bei der CO-Oxidation über Au/CeO_2 wurde festgestellt, dass Carbonat- und Hydroxylspezies nicht an der Produktbildung beteiligt sind. Alle potentiell aktiven Spezies wurden in der Carbonylregion gefunden, wo (dynamisch gebildete) einzelne Goldatome als aktive Spezies identifiziert wurden.
Die RWGSR über Au/CeO_2 zeigte einen assoziativen, durch Adsorbate vermittelten Reaktionsmechanismus als vorherrschend. Als aktive Spezies wurden bidentate Carbonate und einzelne Hydroxylgruppen identifiziert, Formiat, das in der Literatur ebenfalls als Intermediat diskutiert wurde, konnte jedoch ausgeschlossen werden, da es erst nach der Reaktion entsteht.
Die Untersuchung der Hochdruck-CO_2-Aktivierung mit *operando*-MES hat in ersten Experimenten gezeigt, dass die Bildung von CO, Methan und MeOH parallel abläuft, was die eindeutige Interpretation der mittels PSD gewonnenen mechanistischen Informationen erschwerte. Trotzdem konnten erste Anhaltspunkte für einen möglichen Weg zu MeOH über adsorbierte Methoxy-Spezies gesammelt werden. Die Anwendung einer neu entwickelten *in situ*-Zelle mit geringem Hohlraumvolumen führte zu einer erheblichen Verbesserung der Spektrenqualität, sodass ein Mechanismus der MeOH-Bildung über Au/CeO_2 bei hohen Drücken formuliert werden konnte.
Die speziell angefertigte Reaktionszelle hat auch das Verständnis der bereits ausgiebig studierten CO-Oxidation über Au/CeO_2 und Cu/CeO_2 signifikant verbessert. Da sie einen schnellen Austausch der Gasphase innerhalb von Sekunden ermöglichten, wurden die Periodenlängen der Experimente verkürzt, was bei der Suche nach schnell reagierenden Intermediaten der Reaktion von Vorteil ist. Bei der CO-Oxidation über Au/CeO_2 ermöglichte der schnelle Austausch in der neuen Zelle eine drastische Verringerung der Intensität stabiler, nichtreaktiver Spezies. Im Falle der CO-Oxidation über Cu/CeO_2 lag das Hauptaugenmerk auf den potentiell aktiven Oxidationszuständen von Kupfer während der Reaktion, wobei sich Intermediate wie das an Cu^{2+} adsorbierte CO identifizieren ließen.

In dieser Arbeit konnte somit anhand verschiedener heterogen katalysierter Beispielreaktionen gezeigt werden, dass die MES-PSD in Kombination mit der DRIFT-Spektroskopie eine geeignete Methode darstellt, um einen schnellen Zugang zu mechanistischen Informationen heterogen katalysierter Reaktionen zu erhalten. Die verschiedenen in dieser Arbeit vorgestellten Einsatzmöglichkeiten der Methode erlauben es, einerseits schnell einen allgemeinen Überblick über die untersuchte Reaktion und die beteiligten aktiven Spezies zu erhalten, andererseits aber auch sehr gezielte Fragestellungen z. B. zu Dynamiken einzelner Reaktionsintermediate zu beantworten. Eine zukünftige Erweiterung des Repertoires um weitere Spektroskopiearten wie Raman- und UV/Vis-Spektroskopie verspricht hierbei noch zusätzliche Synergien.

Abstract

The fundamental characteristic of a catalyst is the acceleration of chemical reactions without its consumption during the latter. This makes catalytically active compounds one of the most important tools in industrially applied chemistry. Yet catalysts *per se* do not represent a great novelty in chemistry. In fact, they have been standard in a vast variety of applications for decades. For example, more than 85 % of all large-scale processes in chemical industry use heterogeneous catalysts [1].
However, the benefits of heterogeneous catalysis are not limited to the fossil fuel driven industry, but will also be a sound foundation for pioneering applications in a future emission-free industry relying on techniques such as Carbon Capture and Utilization (CCU). Here, the activation and conversion of CO_2 to more reactive molecules such as methanol or CO via reactions such as the reverse water-gas shift reaction (RWGSR) should be emphasized [2, 3]. As Meeting the demand for high-purity hydrogen, e. g. for fuel cell applications, also relies on catalytic reactions, there has been great interest in e. g. the low temperature water-gas shift reaction (WGSR), which reduces the CO amount whilst pushing H_2 production to new heights after steam reforming [4, 5]. But catalysts are also encountered in everyday situations such as exhaust gas aftertreatment in internal combustion engines, where the CO oxidation transforms toxic CO to less harmful CO_2 [6].
Nevertheless, many details of catalytic processes have remained largely unexplained, although their understanding could significantly contribute to application-oriented optimization [1]. In particular, a more detailed mechanistic understanding of the catalytic reaction pathways can facilitate the development of catalysts with increased conversion or selectivity. However, the benefits of mechanistic elucidation go far beyond the single aspect of optimizing these parameters, as a known reaction mechanism is also a first step toward a knowledge-based understanding of both activation and deactivation processes [7].
Such a deep understanding of catalytic processes is in most cases facilitated by the use of characterization techniques, mostly stemming from the field of spectroscopy. In a best case scenario, measurements are rolled out *in situ*, which means, that characterization takes place during the reaction, or even *operando*, which adds an activity measurement to the *in situ* routine.
DRIFT spectroscopy (diffuse reflectance infrared Fourier transform spectroscopy) is an important and widespread tool that has found wide application, for example for the vibrational spectroscopic study of powdered samples in catalyst research. However, due to the information density of this method, the complexity of the spectra is also very high. Thus, even in model reactions, such as the Au/CeO_2-catalyzed CO oxidation, it is hardly possible to distinguish between different species produced in the reaction and to decide, which species are actively involved in the reaction mechanism and which are just present as spectators.
A general challenge in this context is the elucidation of spectra showing a superposition of a large number of signals of adsorbed by- and intermediate products. Their classification as spectators or active participants is a difficult task not only for conventional DRIFT spectroscopy but for most characterization techniques, where even *in situ* or *operando* methods reach their limits.
The introduction of a transient approach to *in situ* or *operando* methods can fill this gap by enabling the discrimination between different signals, e. g., by separating signals from species actively involved in the reaction from inactive ones, or by distinguishing between signals with overlapping spectral positions based on their different dynamic behavior, depending on the time of their occurrence.
A method that combines both of these advantages is so-called modulation excitation spectroscopy (MES),

where conventional spectroscopy methods are combined with a periodic stimulation of the investigated system by variation of an external parameter, e. g. the concentration, as well as deliberate data post-processing, so-called phase-sensitive detection (PSD). This approach has been successfully applied to separate the signals of active species from the background and spectator species, after it was first introduced as a distinct spectroscopic method in 2001 by Baurecht and Fringeli, using ATR (attenuated total reflectance) infrared spectroscopy of acid base reactions as an example [8]. Despite its performance in the selective detection of actively involved species while requiring little additional equipment, this technique has not yet been widely adopted as a standard method for the mechanistic study of catalytic processes [8, 9].
This work describes the design and optimization of a setup for the application of ME-DRIFTS to a variety of catalytic reactions, such as CO oxidation, water-gas shift reaction, reverse water-gas shift reaction, as well as CO_2 activation for MeOH production at elevated pressures using gold- and copper-loaded ceria catalysts. In particular, it was possible to enrich the mechanistic understanding of these catalysts at work and provide direct evidence for the pathway taken during the catalytic reaction.
For example, for the WGSR over Cu/CeO_2 catalysts, MES-PSD enabled an assessment of the type of mechanism dominating, that is, an adsorbate-driven (associative) or redox mechanism. In this case, a redox mechanism was found to be at work.
In the case of CO oxidation over Au/CeO_2, carbonate and hydroxyl species were found not to be involved in product formation. All potentially active species could be attributed to the carbonyl region, where (dynamically formed) single atomic gold sites were identified as active species.
RWGSR over Au/CeO_2 revealed an associative reaction mechanism mediated by adsorbates as the predominant route. Bidentate carbonates and specific hydroxyl groups were identified as active species, but formate, which was also discussed as an intermediate in the literature, could be excluded due to its formation only after the reaction.
The analysis of the high pressure CO_2 activation with *operando*-ME-DRIFTS has revealed, that the formation of CO, methane and MeOH occur in parallel, which has hindered the unambiguous interpretation of the mechanistic information extracted via PSD. Nevertheless, it was possible to gather evidence for a possible pathway to MeOH via adsorbed methoxy species. The application of a newly developed low void volume *in situ* cell has greatly improved the spectra quality, so that a mechanism of MeOH formation over Au/CeO_2 at high pressures could be postulated.
The newly developed cell has also advanced the mechanistic understanding of the CO oxidation over Au/CeO_2 and Cu/CeO_2. Because of a rapid total gas phase exchange within seconds, the period lengths in the experiments could be reduced, which is advantageous when targeting fast-reacting reaction intermediates. For example for the CO oxidation over Au/CeO_2, the rapid exchange drastically reduced the abundance of stable but non-reactive species. In the case of CO oxidation over Cu/CeO_2, the focus was primarily on the active oxidation states of copper during the reaction. In particular, intermediate species such as CO adsorbed on Cu^{2+} were identified.

In this work it could thus be demonstrated that MES-PSD in combination with DRIFT spectroscopy represents a powerful method to gain rapid access to mechanistic information of heterogeneously catalyzed reactions. The various possible applications of the method presented in this work make it possible, on the one hand, to quickly obtain a general overview of the reaction under investigation and the active species involved, and on the other hand, to answer very specific questions, e. g., about the dynamics of individual reaction intermediates. A future extension of the repertoire to include other spectroscopic techniques such as Raman and UV/Vis spectroscopy promises additional synergies.

Contents

1 Introduction

1.1 Concentration Modulation Excitation Spectroscopy (MES) and Phase Sensitive Detection (PSD)

1.1.1 Spectroscopy for mechanistic investigation

A major challenge in the elucidation of reaction mechanisms is the identification of the species actively involved in the reaction (gas phase molecules, adsorbates, vacancies, electronic states, etc.). Since these are often present only in low concentrations due to their short lifetimes and are thus lost in the background noise or are hardly detectable next to much more intense observer species (s. fig. 1.1), specially developed spectroscopy methods have to be used for this purpose.

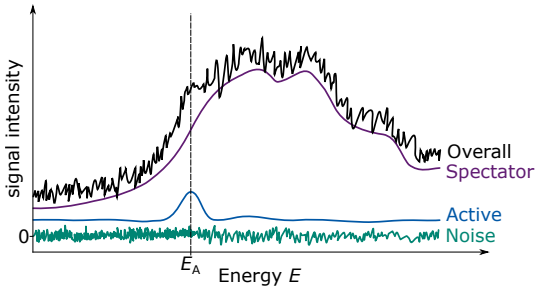

Figure 1.1: Hypothetical total spectrum (black) and its possible components: Observer species (purple), active species (blue), and noise (green).

To obtain a comprehensive picture of these active species of a reaction, it is usually necessary to combine the results of several experiments with the aid of different spectroscopic methods. *In situ* and *operando* experiments have proven to be particularly helpful in this respect. In both cases, the spectroscopic investigation of a sample is performed during the reaction.
The *operando* approach further extends the spectroscopic experiment by the simultaneous measurement of the catalytic activity. Here, certain signals can be clearly correlated with the simultaneously measured activity of the sample (structure-activity relationship). In most cases, however, *in situ* and *operando* experiments do not follow the reactions under consideration in a time-resolved manner, but only represent snapshots of selected states before, during or after the reaction. If additional transient (i. e., time-resolved) measurements are made in conjunction with the *in situ* or *operando* approach, details of the reaction mechanism are accessible.
Modulation Excitation Spectroscopy (MES) is such a transient measurement method, which is used in catalyst research to elucidate complex processes and mechanisms under *in situ* and *operando* conditions. By periodically changing (modulating) a process variable (here: c), the signals of active species in time-resolved spectra also exhibit periodic behavior, in contrast to the time-constant signals of the spectator species and the statistical background noise. Using the mathematical tool of phase sensitive detection (PSD), the active signals can be completely isolated and information about the processes occurring at the catalyst can be obtained. These are often only accessible to a limited extent or not at all with conventional spectroscopic approaches due to band overlaps and low intensities of the active species.

1.1.2 Technical requirements for MES

To set up a MES-capable apparatus, automated communication between different devices is necessary. Connections are required between the respective spectrometer, an actuator for the periodic modulation of the

concentration (here: valve) and a computer, which serves as a control unit but also for post-processing of the data (see fig. 2.1).
In addition, the recording of the spectra must be faster than the relaxation of the investigated processes during the periodic excitation (cf. Nyquist-Shannon sampling theorem).

1.1.3 Phase sensitive detection (PSD)

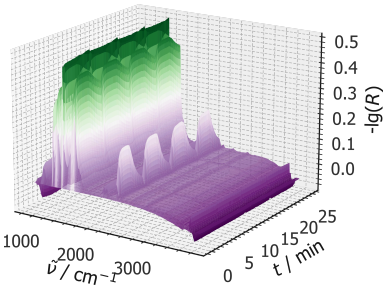

Figure 1.2: Section of the 3D spectra.

The 3D data sets obtained in the course of the modulated measurement (intensity versus wavenumber and time, see fig. 1.2) contain the information relevant for the PSD whether a signal periodically responds to the modulation frequency or not. It is contained in the time-dependent intensity curve (at a given wavenumber value).
The periodic modulation of the gas phase concentration causes active species on the catalyst surface to change their concentration at the same frequency. This causes their infrared signals to also periodically become stronger or weaker. The Discrete Sine Transform (DST) shown in eq. (1.1) (related to the more familiar Fourier Transform) causes only those signals to remain in the spectrum that change with the same frequency by convolving the signal function $I(\tilde{\nu}, t)$ with a periodic function that approximates the concentration modulation (here for simplicity a sine function was chosen but depending on the residence behavior of the spectroscopic cell used, rectangular functions may be considered, which will be addressed later).
Depending on the reaction kinetics of the active species under consideration, the response also occurs with a specific time shift. This can be described mathematically more easily as the phase shift φ of the measured periodic data. If this was not taken into account, some of the active signals would not be observable, depending on the time shift of the species considered. Therefore, it is necessary to vary φ over an entire period (360 °), resulting in a whole set of phase spectra that is always evaluated together. This also has the advantage that the phase angle with the maximum intensity of a signal can be used for mechanistic investigation. The DST shown here

$$I(\tilde{\nu}, \varphi) = \frac{2}{T} \int_{t_0}^{t_{\text{end}}} I(\tilde{\nu}, t) \cdot \sin(2\pi\nu t + \varphi) \mathrm{d}t \tag{1.1}$$

converts the set of spectra from the time to the phase domain, where I is the signal intensity, $\tilde{\nu}$ is the considered wavenumber of the radiation, φ is the phase shift of the response signal with respect to the excitation, t is the time, T is the duration of one period, and ν is the frequency of the periodic excitation.
The result of the transform given in eq. (1.1) is shown in fig. 1.3 and can be summarized as follows: **1**. Only the signals with $I(\tilde{\nu}, t)$ showing the same periodicity as the sinusoidal function convolved with it remain in the spectrum. **2**. Signals of spectator species whose intensity shows a saturation curve as well as the statistical background noise are removed from the spectrum by this mathematical operation.
This is achieved by the transformation into the so-called “phase domain”, which describes a multitude of possible phase shifts φ that the signal function $I(\tilde{\nu}, t)$ as well as the sinusoidal function convoluted with it can take. The phase shift of the sinusoidal function is varied from 0 to 360 ° in an arbitrary step size within the framework of a PSD algorithm, which is described in more detail in section 3.2 and is always compared anew with the signal function by means of eq. (1.1).
If there is a coincidence of the phase shifts of signal and modulation function (sine), the overlap of both functions is maximum and the corresponding phase angle is called $\varphi_{\max}$ (see fig. 1.3). The transformation in eq. (1.1) results in the maximum of the transformed signal function $I(\tilde{\nu}, \varphi)$ in this case. If the phase shifts do not match, the calculated value moves increasingly away from its maximum.

The unwieldy value of the maximum phase angle φ_{max} can be converted back into a time value t_{max} by referencing to the period duration:

$$t_{\mathrm{max}} = \frac{360° - \varphi_{\mathrm{max}}}{360°} \cdot t_{\mathrm{Period}} \tag{1.2}$$

If this information is collected over all the signals in the spectrum, it is thus possible to identify signals that belong together on the basis of the same time values and to obtain mechanistic information about the course of the reaction by arranging the values in time.

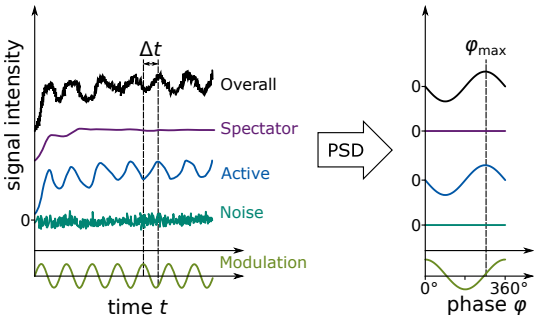

Figure 1.3: Effect of the PSD on the total spectrum (black) as well as its components based on the transformation of an exemplary I-t curve from the time to the phase domain.

2 Experimental

2.1 MES setup

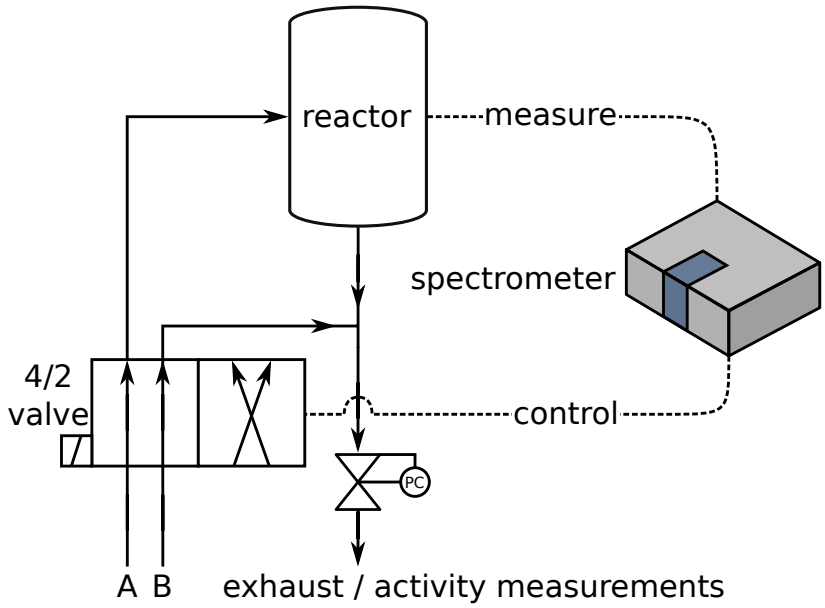

Figure 2.1: Schematic picture of the utilized apparatus for MES and its three core components (4/2 valve, reactor, FTIR spectrometer) as well as an additional back pressure controller (PC) for experiments at higher pressures. For simultaneous activity measurements, an additional FTIR spectrometer can be fed with the exhaust.

The core of the modulation experiment is an apparatus that is set up according to the scheme as depicted in fig. 2.1.

Valve The 4/2 valve used for all the experiments is an electronically switchable type 724ED44UWE by Valco Instruments.

Spectrometer For all experiments either a Vertex 70 or an INVENIO-R by Bruker, equipped with a Globar (SiC) light source and a liquid nitrogen cooled mercury cadmium telluride (MCT) detector have been employed. Both spectrometers are controlled via a PC with the spectrometer's software OPUS 8.7.

Reactor cell The reactor cell used for most of the experiments is a commercially available High Temperature Reaction Chamber with the associated Praying Mantis™ mirror setup by Harrick Scientific Products. Samples are placed in a specially designed overflow tray (Ø: 8 mm; depth: 0.5 mm) containing ≈25-35 mg of catalyst.

High pressure equipment In case of high pressure experiments, a digital back pressure controller (Bronckhorst, type P-702CV-M10A-RGD-33-E) after the T piece joining reactor and direct exhaust, depicted in fig. 2.1 can be used to set pressures of up to 27 bar, as the 4/2 valve used has a limit of 400 psi (27.58 bar). However, it should be noted that higher pressures significantly increase the residence time in the reactor, a problem which will be addressed in later chapters.

Communication between spectrometer and valve The communication between spectrometer (Vertex 70 or INVENIO-R) and valve (depicted in fig. 2.1 as "control" as well as more detailed in fig. 2.2) is the prerequisite for the temporal assignment of the spectra to the respective modulation period and its progress. Communication

between the spectrometer's computer and the spectrometer is possible via a network cable (type RJ-45), where the software (OPUS 8.7), distributed by Bruker, provides access for the user.

With this software and after installing the Rapid Scan extension of the OPUS software, it is possible to both set the measurement parameters of the FTIR spectrometer (aperture, resolution, mirror speed, etc.) and control the valve. The control of the valve position is programmed in OPUS as an executable script, the so-called method. The method also includes instructions to the spectrometer on when to take how many measurements. The commands of the method are processed by the spectrometer and forwarded to the valve via the trigger box (E525/Z) provided by Bruker. From the trigger box's four output channels (DO0-3) two are needed in our current setup to address each of the two valve positions, so two BNC cables are required. These are connected via an adapter to the ten-core digital I/O cable required on the valve side. The adapter was made by the electronics workshop of the TU Darmstadt's chemistry department.

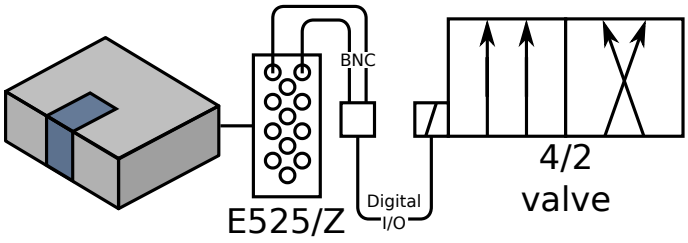

Figure 2.2: Sketch of the device interconnections with designation of the cables used.

2.2 Process gases used in catalytic experiments

All gases were dosed using digital mass flow controllers (MFC) by Bronckhorst. Water that has been used for the WGSR experiments was dosed using a controlled liquid evaporation unit in combination with an MFC.

Table 2.1: List of gases used in the experiments together with their purities and manufacturers.

Gas	Purity / %	Manufacturer
CO	99.997	Westfalen
O_2	99.999	Westfalen
Ar	99.996	Westfalen
H_2	99.999	Westfalen
CO_2	99.995	Westfalen

2.3 Synthesis of ceria supported noble metal catalysts

Thermal decomposition at 600 °C of $Ce(NO_3)_3 \cdot 6\,H_2O$ (Alfa Aesar, 99.5 %) was used to prepare polycrystalline ceria sheets. This has been described in detail in our previous studies [10, 11].
Preparation of ceria cubes and rods was carried out by hydrothermal synthesis of $CeCl_3 \cdot 7\,H_2O$ (Alfa Aesar, 99 %) and $Ce(NO_3)_3 \cdot 6\,H_2O$ (Alfa Aesar, 99.5 %) in NaOH solution (98 %, Grussing GmbH) which has also been described in our previous studies [12, 13].
Ceria polyhedra / octahedra were commercially available from Sigma-Aldrich (<25 nm (BET)).
Loading ceria with copper was achieved via deposition–precipitation (DP) using 10^{-3} M $CuCl_2 \cdot 2\,H_2O$ solution (Sigma-Aldrich, 99.5 %). First, ceria samples were dispersed in deionized water at a ratio of 1:150 while the pH was adjusted to 9 using a solution of 0.1 M NaOH (98 %, Grussing GmbH). Then, the pH of the copper chloride solution was set to 8 and mixed into the suspended ceria to obtain the intended loading. After adding,

the pH was adjusted to 9 again. Thereafter, the reaction mixture was heated at 65 °C for 2 h and after cooling was placed in an ultrasonic bath for 30 min. The resulting residue was centrifuged, washed four times with deionized water, and dried at 85 °C for at least 24 h.
The loading of the ceria nanoparticles with gold is carried out by electrolyte deposition. For this purpose, the ceria samples are dispersed at a ratio of 1:150 in deionized water, the pH of which is adjusted to 9 with a 0.1 M NaOH solution (98 %, Grüssing GmbH). The 10^{-3} M $HAuCl_4 \cdot 3\,H_2O$ solution (Carl Roth, 99.9 %) is prepared, which is also adjusted to pH 9. Then, as much of the $HAuCl_4 \cdot 3\,H_2O$ solution is added to the ceria dispersion until a loading of 0.5 wt % is achieved. The reaction mixture is then heated to 65 °C for two hours and, after cooling, placed in an ultrasonic bath for 30 min. Finally, the residue is centrifuged and washed four times with deionized water before the product is dried for about 24h at 85 °C in a drying oven.

3 Modulation Excitation Spectroscopy and Phase Sensitive Detection

3.1 Progress to date in MES

Modulation Excitation Spectroscopy (MES) in combination with Phase sensitive Detection (PSD) has been used since its emergence in 2001 as a tool to study the dynamics of heterogeneously catalyzed reactions. MES is the spectroscopic experiment, while PSD is a mathematical data post-processing tool. The conditions that the design of the experiment must meet are a combination of technical limitations and irrefutable facts that depend on the nature of the process or reaction under study.
Briefly said, the chosen measurement technique must be temporally sufficiently fine resolved so that occurring dynamics of the process under consideration can be captured and tracked. Achieving the best possible time resolution together with the best possible spectral resolution and minimum data volume is a dominant challenge in MES and will also be discussed later in this thesis based on the given examples.
Nonetheless different work groups have been able to execute MES measurements utilizing various techniques. A large part being IR based studies such as ME-DRIFTS of various reactions such as CO oxidation, PROX or EtOH dehydration over mostly metal loaded or bare oxides, such as Cu, Au or Pd on CeO_2, ZrO_2 or Al_2O_3, to name just a few [14–16].
Another IR technique is ATR-IR-MES, which is mostly used to carry out catalytic studies at the solid-liquid interface. As an example, reactions such as benzyl alcohol oxidation over Au/ZnO can be mentioned [17, 18].
Furthermore, ME-PM-IRRAS as a highly surface sensitive method has been used for tracking dynamics on thin films, where the difference between gas phase and adsorbed species is of great importance [19].
ME-XAS has been a particularly strong technique, when it comes to process-induced changes in oxidation state or coordination of active catalytic sites such as shown by Serrer *et al.* [20] in the case of Ni-Fe on Al_2O_3, where they were able to unravel redox cycles within the active iron particles.
ME-XRD is a method, that is currently gaining momentum. Being capable of investigating quick changes in bulk structure, it has already proven its value for unraveling dynamic changes in crystal structure *in situ* shown by Ferri *et al.* for Pd on ceria/zirconia or Al_2O_3 catalysts [21].
Finally there are some basic studies on Raman and UV/Vis spectroscopy by Nuguid *et al.* from 2019 [22, 23], that investigated the dynamics during selective catalytic reduction (SCR) of NO_x and some earlier works by Urakawa *et al.* [24] but until now the full potential of the modulation approach for this technique seems to be unexplored, which will be discussed in a later chapter of this work.

Apart from these advancements in making new measurement techniques work in combination with modulated excitation, there has been a significant gain of momentum when it comes down to combining different modulated spectroscopic techniques to obtain a more complete picture of the process. Some notable ones are the combination of ME-DRIFT, UV/Vis and Raman spectroscopy in one cell by Nuguid *et al.* [23], ME-XRD and XAS by Ferri *et al.* [21], or ME-XRD with DRIFTS by Marchionni *et al.* [25].
Another field showing only slight progress so far is the modulation of other parameters than concentration, such as temperature [24] and electrochemical potential [26]. One may also think about pressure modulation,

as this method has been explored within the kinetics community following the groundbreaking works of Eigen and coworkers in the 50s [27], applying sound waves to periodically trigger and track ultrafast kinetics.

3.2 The PSD approach and its scope of application in this work

Concerning the code on which all PSD calculations in this work are based As PSD is a pure data post-processing technique, it is in the first place set up completely independent of any experimental setup. The only need is a decently fast computer providing sufficient hard disk space and memory (from a current point of view) for storage of vast amounts of data within the terabyte range, and handling of single measurements that can easily consume several gigabytes.
The post-processing program used has been self-written and consists of today of roughly 600 lines of python code but out of which only about five are the PSD itself, whereas the rest comprises data handling, some useful PSD-specific visualizations and an overarching but simplistic graphical user interface (GUI) enabling the use of this PSD-program to people completely inexperienced in programming. The code and an extended readme file including explanations of each function is available at GitHub for free (**https://github.com/Ja-We/Phase_Sensitive_Detection_for_Spectroscopy**).
The sine transform discussed in chapter 1 and shown in eq. (1.1) is implemented in the program in the following code segment (see listing 3.1).

Listing 3.1: Code snippet of the PSD-function with a sine function.

```
1 for i in range(1,len(phi)+1):
2
3         for j in range(0,len(data[:,0])):
4                 dummy[j,i] = 2/t_inp[int(n_sp),0]*igr.trapz(data[j,1:]
5                 *np.sin(omega*t_inp[0:n_sp,0]+phi[i-1]*2*np.pi/360))
6
7 spectra[:,1:] = spectra[:,1:]+dummy[:,1:]
```

The array $data$ contains all time-resolved spectra to be processed. Its first column (with index 0) contains the wavenumbers at which a measured value is available. Each of the following columns contains a spectrum that can be assigned to a specific time. $omega$ is the given angular frequency of the periodic excitation, t_inp contains all time values for the spectra collected in $data$ and phi is a vector predefined by the user, containing a set of phase angles between 0 and 360 ° to which the transformed spectra will be calculated.
The code snippet comprises two for loops, the inner one iterating over j contains the actual sine (or rectangular function) transform and builds up a spectrum line by line. From one row of the array $data$ (i. e. a bunch of intensities at one particular wavenumber over time) a single decimal number is generated as value for the new phase spectrum in the array $dummy$ by convolution with the periodic sine (or rectangular) function shifted by a fixed value phi and the subsequent trapezoidal integration ($igr.trapz(...)$) over time (cf. line 4). The outermost loop over i creates the phase resolution of the spectra by varying the phase shift contained in the vector phi and appending the spectra calculated by the loop over j column-wise. In line 7, the sum of the current spectrum ($dummy$) and the sum of all previous spectra ($spectrum$) is formed.
If wanted and especially if the residence times of the experimental data are short enough to allow for its application, a rectangular function ($signal.square(...)$) can be used instead of a simple sine, which is shown in the following code snippet.

Listing 3.2: Code snippet of the PSD-function with a rectangular function.

```
for i in range(1,len(phi)+1):

        for j in range(0,len(data[:,0])):
                dummy[j,i] = 2/t_inp[int(n_sp),0]*igr.trapz(data[j,1:]
                *signal.square(omega*t_inp[0:n_sp,0]+phi[i-1]*2*np.pi/360))

spectra[:,1:] = spectra[:,1:]+dummy[:,1:]
```

What parameters have to be optimized for ME-DRIFTS Measuring good modulation spectra that can be processed with the PSD program is a balancing act between good spectral resolution, good temporal resolution, signal intensity and file size. In the best case high signal intensities are desired for a good signal-to-noise (S/N) ratio, the finest possible sampling of time (Δt) for well-resolved dynamics, a maximum resolution of the signals ($\Delta\nu$) and all of this while not creating excessively large files.
With the available DRIFT spectrometers (INVENIO-R and Vertex 70, both from Bruker) important parameters to optimize are aperture, mirror speed, resolution and interferogram accumulations per spectrum. An optimization has to take place every time drastic changes in the setup are executed or a new reaction is addressed, which is why in almost none of the following chapters you will find the exact same experimental parameters.
To obtain high signal intensities, a high aperture is desirable because it allows more light to pass through. But as in photography, this makes the "image" i. e. the spectrum blurry, thus limiting spectral resolution.
The measurement time of one spectrum depends on the speed and the distance to be covered by the moving mirror (distance is not alterable for the available spectrometers) and is generally independent of the spectral bandwidth as long as the mirror speed does not limit the sampling rate of the ADC (analogue digital converter) as this would also limit the number of data points per interferogram too much. According to the Nyquist-Shannon sampling theorem, decreasing the number of data points per interferogram will decrease the accessible spectral range, therefore the mirror speed cannot be increased without keeping the desired spectral range in mind.

Table 3.1: Parameters to optimize in MES-PSD and their positive (+), negative (-) and neutral (o) effects on various characteristics of the modulation spectra.

Parameter	S/N	Δt	$\Delta\nu$	Spectral range	File size
aperture	+	o	-	o	o
mirror speed	o	+	o	(-)	-
resolution	-	o	+	o	-
accumulations	+	-	o	o	o

For the Vertex 70 the best possible spectral resolution is $0.5\,\mathrm{cm}^{-1}$, for the INVENIO-R it is $0.2\,\mathrm{cm}^{-1}$. As stated above, this will limit the apparatus's aperture so that signal intensities worsen. To counter that, it can be considered to increase the number of accumulated interferograms per spectrum which will increase the overall quality of the spectrum obtained but at the cost of temporal resolution. Hence, all this must be considered in context, as the optimization of one parameter will inevitably have a limiting influence on the other parameters as presented in more detail in table 3.1.
Finally large three dimensional data sets are created, that consume up to several gigabytes of memory. So with

the aim of not being limited in the amount of experiments to execute, all of the above mentioned parameters only need to be optimized to a point, where the requirements of the process under consideration are met. Therefore, when selecting the parameters, it should always be critically questioned whether a resolution that shows the rotational fine structure of gas phase species is needed and whether the sampling rate of the spectra might already be too good for the time scales of the observed reactions. This may drastically decrease the amount of memory used as well as the time for data procession with the PSD program.

Altering the modulation period length influences the species observed Depending on the complexity of the reaction under consideration, many different species are expected, each of which having a unique rate of formation. A slower reacting species will thus be detectable at a later point in time than a fast reacting one if only parallel reactions are considered. When taking successive reactions into account, the intermediate species will be detectable earlier as well. For MES-PSD experiments this leads to the conclusion, that by changing the period length of the external modulation, one may change the spectral selectivity towards species with different temporal behaviors. By choosing short period lengths, faster reacting species and intermediates are favored, while choosing long periods shifts the focus towards the final product and other stable species.
This can roughly be illustrated by the concentration curve of the simplest possible consecutive reaction in a batch reactor ($A \rightarrow B \rightarrow C$) shown in fig. 3.1, where when looking after a short time, the intermediate concentration is significantly higher than the final product and would therefore be dominant in a hypothetical spectrum. A measurement at a later time would then show a clear increase in product intensity.

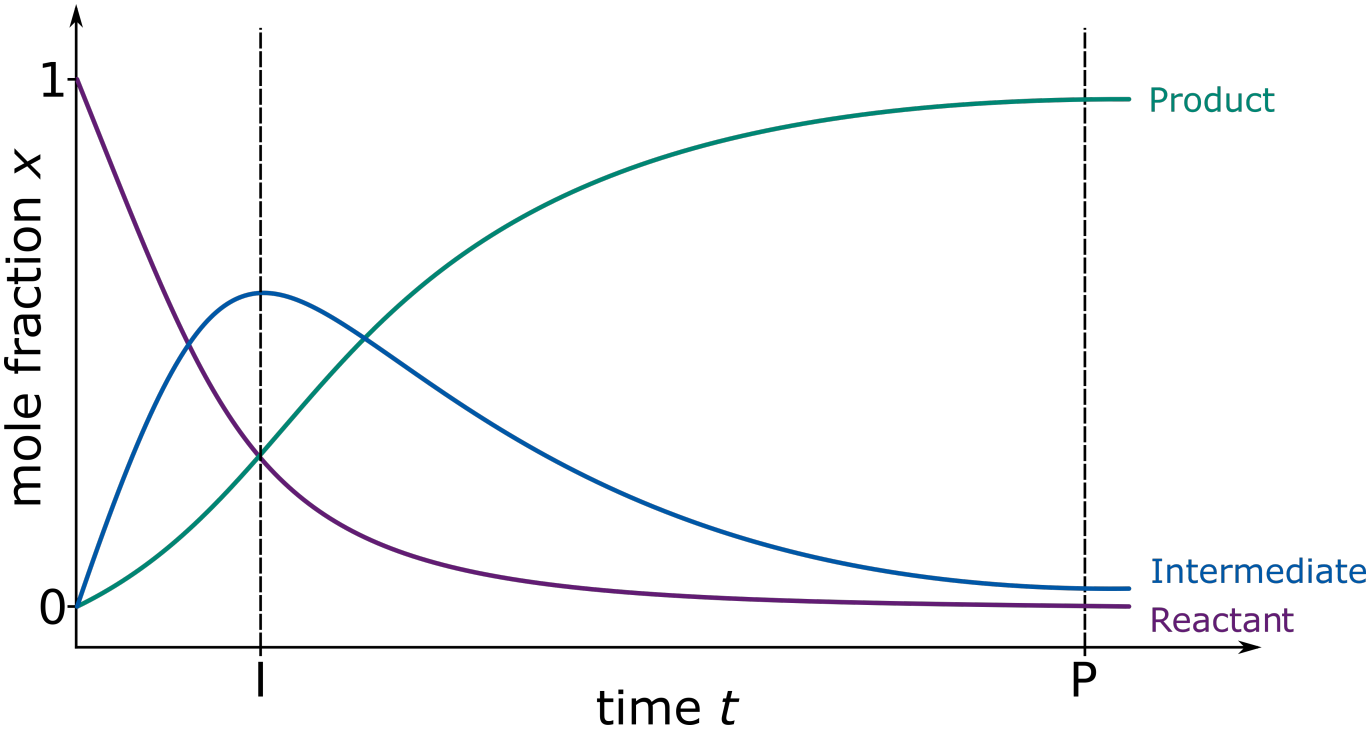

Figure 3.1: Schematic course of the mole fractions of the most simple consecutive reaction of the type $A \rightarrow B \rightarrow C$. The dashed lines show positions, where the signals of an intermediate species (I) or the Product (P) would dominate a hypothetical spectrum.

Influence of the initial state and the modulated gas Another influence on the modulation spectra of the same reaction with e. g. two reactants A and B is the possibility to modulate either the concentration of A or B. This can lead to drastically different results. To stick with the example of heterogeneous catalysis, this would be equivalent to a different pretreatment of the catalyst. This can lead to different species being preferentially deposited on the catalyst surfaces and can also lead to different states of the catalyst material during modulation, i. e. in terms of the abundance of electrons or vacancies of different types. Combining such experiments, that probe the system from two sides may provide a holistic view of the reaction, but depending on the importance of the pretreatment to the system, may also probe completely different initial and final states of the material, thus yielding data sets that are difficult to reconcile. This challenge is illustrated schematically in fig. 3.2, where the modulation from different initial states is shown. In the best-case scenario, the final state would be expected to be shared even when coming from different initial states, e. g. the purple and blue curves in fig. 3.2 should touch with their respective maxima/minima. The intensity of this response, shown in fig. 3.2, depends on the system itself and its specifics, as well as on the period length, which is compared in the left and right panels of fig. 3.2.
So in a reaction with two reactants, all different combinations shown in fig. 3.2 are imaginable, including applying constant A or B and periodically pulsing the other species. Or the modulation might start from the reaction gas atmosphere with both reactants present and periodically switch off one or both of them. All these approaches are designed to study the response of the system/reaction to different external stimuli to obtain different views of the same system, as it is not expected to behave the same when either species A or B is pre-adsorbed or when starting from reaction conditions. Another possibility, not shown in fig. 3.2 for simplicity, is the approach of applying constant A or B and completely exchanging it with the other species. The latter approach is thought to probe only the reaction of the already adsorbed reactant with a specific pulse of the other reactant and then replace it to undergo the same procedure.
The combination of this initial state approach with the application of different period lengths helps to find out if there is such a transition, as will be discussed in section 6.2.

Isotope-labeled MES can further deepen understanding There is preliminary work by Pavelko *et al.* from 2014 [28] combining steady-state isotope transient kinetic analysis (SSITKA) and MES-PSD, but there have never been follow-up studies using this approach, although it seems quite promising. This technique was also implemented in the apparatus presented in this work and applied to propane ODH as part of one project [29]. This approach narrows down the field of species that appear to be active, as the reaction is not switched on and off, but continues, while only a differently labelled reactant (A / A') is exchanged. This makes it easier to separate and study the active species. Thus, it is not the concentration of A or B that is modulated, but rather A is replaced by A' while the reactant B remains constant. Although the implementation of this technique was part of this doctoral project, it will not be discussed here in detail, as its application was done in my colleague's project and can better be followed there [29].

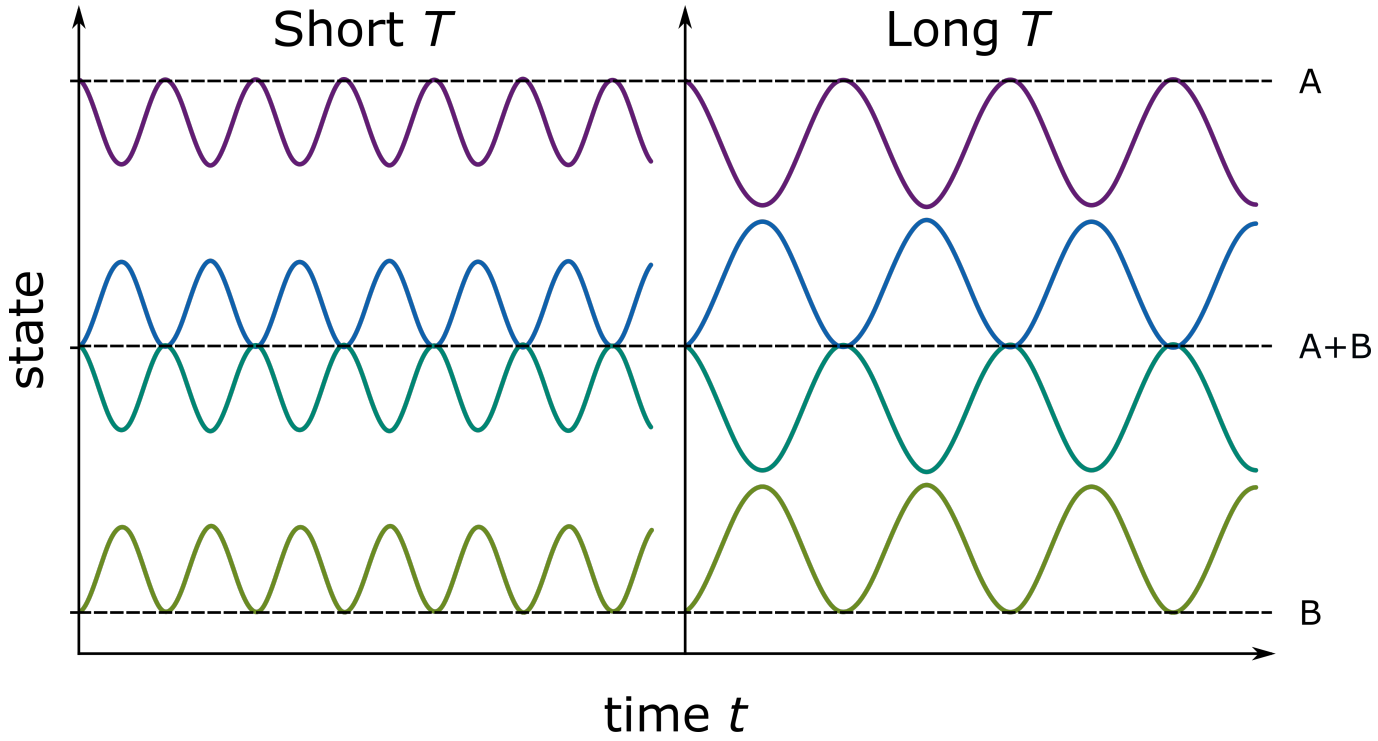

Figure 3.2: Schematic depiction of how the state of the catalyst system may change, when starting from different pretreatments, which in this case are gas A, B or both (A+B). During a modulation experiment starting from these pretreatments, either the lacking reaction gas can be pulsed, while keeping the flow of the other gas constant (e. g. violet and green) or it is possible to start with both gases in the atmosphere and turn the supply of one of the gases off (e. g. blue and turquoise).The other possibility of starting with one gas and periodically exchanging it with the other reactant is also possible but not shown in the figure for simplicity. The amplitudes of the sine curves depicted here are chosen arbitrarily and will differ from system to system and with different period lengths as shown in the left and right panels.

4 Unraveling active adsorbates over Au/CeO_2 during CO oxidation

4.1 Elucidating which gold carbonyl of many is the active species

Large parts of the following chapter have been adapted with permission from already published work [30], which is open access.

As a starting point to apply the modulation excitation apparatus to a real world system, CO oxidation was chosen, an important prototype reaction in heterogeneous catalysis. The system was selected based on prior works of our group by Ziemba and Schilling [31], where the CO oxidation mechanism over Au/CeO_2 was adressed with means of steady state DRIFT spectroscopy and DFT calculations but important mechanistic details remained speculative.
They were able to get a first idea of active and site blocking species during the reaction, with the gold state being of particular interest, as $O_{lattice}$-Au^+-CO appeared to be correlated to product formation and different carbonates were postulated to inhibit the reaction. The aforementioned gold carbonyl species was observed on single isolated gold atoms (single sites) and/or on single gold atoms abstracted from larger clusters (pseudo single sites), while larger gold clusters as a total or nanoparticles were considered to only play a minor role during the reaction.
Using the novel method of MES-PSD, the aim was to deepen the understanding of the reaction mechanism as it frees the spectra obtained from all signals related to species that are not actively participating in the reaction. Via PSD, characteristic time values of each species of interest for the reaction are calculated, i. e. whose signals appear later than those of the pulsed reactant CO and earlier than the product CO_2.
The first studies presented here relied on a commercial DRIFTS cell by Harrick Scientific, which will further be referenced to as “H2021” [30]. This cell and its large volume only allowed to apply long period lengths, as a total gas phase exchange was only achieved after about 47 s (see fig. 4.7 and table 4.5).
Nevertheless information on the reaction mechanism was extracted allowing to sort groups of surface species such as carbonates, hydroxyls, carbonyls as well as the gas phase species temporally and postulate a sequence. These results were then compared to proposals from earlier papers, such as Schilling *et al.* [31], to prove the principle of the measurement method. After validating the setup, the knowledge about carbonyl species that participate in the reaction was enlarged by focusing on that particular spectral region, where there was clear evidence that dynamically formed single gold atoms are the active site.

Experimental details For the modulation experiments, 20 periods with a length of 374 s were cycled. During these, CO concentration was switched between 0 and 2 mol%, while O_2 concentration was kept constant at 10 mol%, using Ar as inert and at an overall flow of 100 $mL_n min^{-1}$. After baking out the samples at 250 °C in 10 % O_2/Ar to remove any residuals, they were treated for 15 min in the same atmosphere at reaction temperature, which was chosen to be 37 °C. Background spectra were collected after one modulation period (turning reaction on and going back to O_2/Ar) at reaction temperature as pretreatment. Spectra were measured

Table 4.1: Observed carbonyl signals and their time values for gold-loaded ceria polyhedra. The same experiment has been executed three times yielding the maximum deviation $\Delta t_{\max}$ for each signal in s.

$\tilde{\nu}$ / cm^{-1}	t(Au/CeO2 I) / s	t(Au/CeO2 II) / s	t(Au/CeO2 III) / s	$\Delta t_{\max}$ / s
2092	18	21	21	3
2122	8	9	9	1
2133	9	11	11	2
2156	26	27	27	1
2171	42	43	42	1
2359	21	23	23	2

from 850 to 3800 cm^{-1} with a resolution of 0.5 cm^{-1}, an aperture of 8 mm and a mirror speed of 40 kHz on a Bruker Vertex 70.
During modulation experiments a maximum conversion of 3.4 % was observed for the Au/CeO_2 sheets and 1.2 % for the polyhedra samples. The gold-free samples taken as reference show no activity.
Each interferogram measured was converted into a spectrum so that one spectrum is acquired approximately every 1.5 s. In order to estimate potential uncertainties of the time values derived from the PSD, the MES experiment on Au/CeO_2 polyhedra was exemplary performed three times (see table 4.1). This resulted in a maximum deviation of time values of 3 s as determined from the weak signal at 2092 cm^{-1}. The other signals discussed show a maximum deviation of 1 or 2 s. So for some signals the time resolution between two consecutive measurements of 1.5 s is decisive, for others it is the maximum deviation (see table 4.1). Intensities and peak positions were checked several times and found to be constant for all measured data sets.

Mechanistic findings with Au/CeO_2 sheets as an example As an example for the mechanistic findings on gold-ceria catalysts, the gold-ceria sheets sample is taken for the sake of simplicity, as results for the polyhedra do not differ a lot, while the latter are still given in table 4.3.
So it can be seen from table 4.2, that all important signals in figs. 4.1 and 4.2 but those of some CO adsorbates in the carbonyl region around 2000 to 2200 cm^{-1} appear later than the product CO_2 and are thus considered not to be actively involved in the mechanism. Discussion of the results will thus be focused primarily on the carbonyl region with the possibly actively participating species.
But coming back to the overall picture, it can be stated, that the mechanism follows a path in which adsorption of CO from the gas phase (starting at 7 s) onto gold single sites and pseudo single sites (after 9 and 8 s respectively) is followed by its reaction to CO_2 (20 s) using surface oxygen in a Mars-van Krevelen-type of mechanism. The therefore necessary oxygen dynamics have been elucidated in earlier studies of our group [31, 32]. Formation of diverse carbonates (CO_3), the response of the OH species and formation of CO adsorbed to bare CeO_2-sites seem to take place after the product CO_2 appears.
These mechanistic findings are all in line with earlier studies [31, 32] and thus served as a validation and starting point for more in-depth analyses of the system's dynamics in the carbonyl region.

In depth analysis of the carbonyl region Starting with spectra from the carbonyl region of the bare ceria samples, it is obvious, that the sheets exhibit three signals at 2122, 2156 and 2171 cm^{-1}, while the polyhedra only show one at 2156 cm^{-1}. In an ascending manner, these signals are attributed to an electronic transition related to Ce^{3+} (2122 cm^{-1}) [33, 34], CO adsorbed onto an ideal ceria (111)-surface (2156 cm^{-1}) [35–37] and CO adsorbed onto a reduced and more defect-rich surface (2171 cm^{-1}) [35, 38].

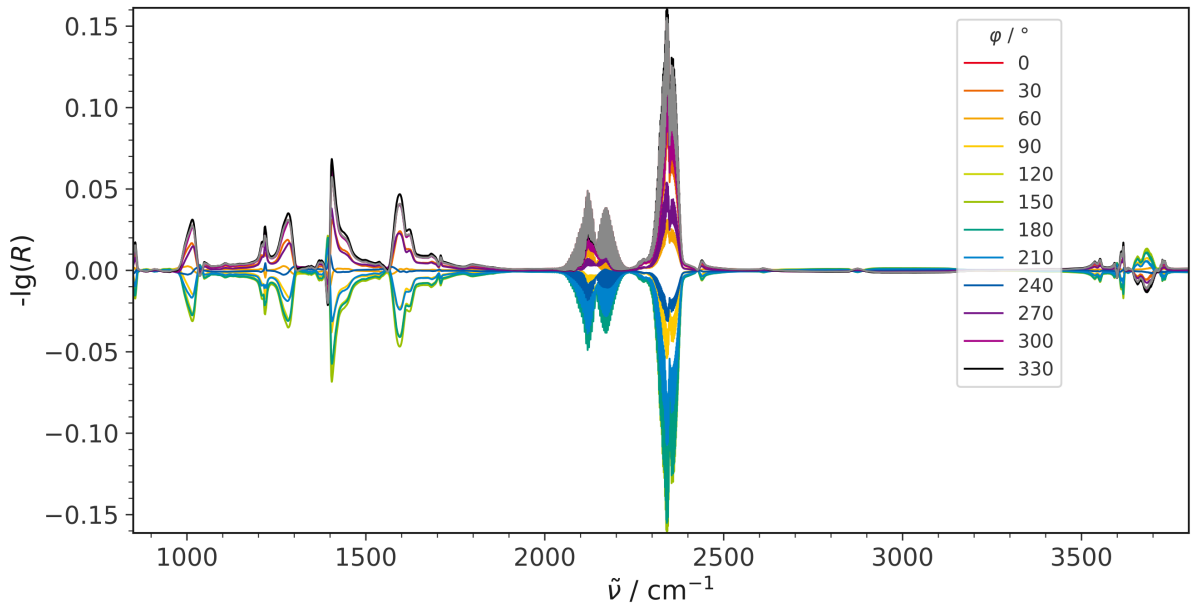

Figure 4.1: Complete set of PSD spectra of the CO oxidation over Au/CeO_2 sheets with a legend showing the phase angle of each spectrum. Since in the discussion the phase angles are always immediately transformed into time values by eq. (1.2), phase angles are only given in this chapter.

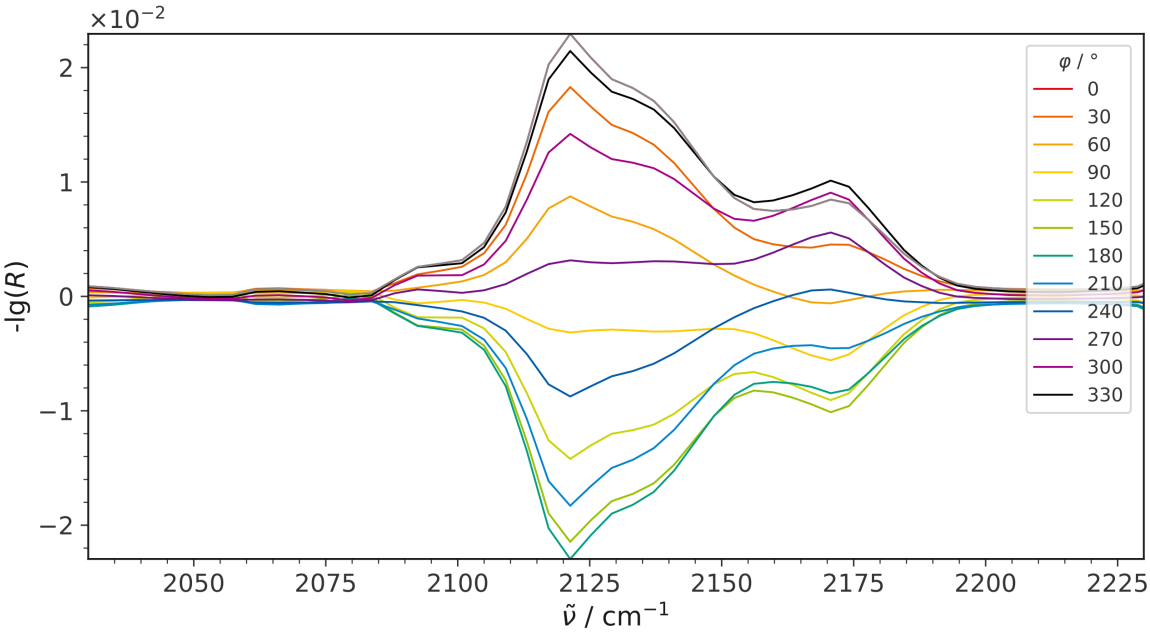

Figure 4.2: Carbonyl region of the PSD spectra of the CO oxidation over Au/CeO_2 sheets after gas phase removal with a legend showing the phase angle of each spectrum. Since in the discussion the phase angles are always immediately transformed into time values by eq. (1.2), phase angles are only given in this chapter.

Table 4.2: The most prominent signals, their time values derived from PSD and assignments from the full spectrum of the CO oxidation over Au/CeO_2 sheets in fig. 4.1. Period length was 374 s. Signals with a negative sign tend to decrease in the reaction phase, while all other signals increase.

$\tilde{\nu}$ / cm^{-1}	t / s	Assignment
2073	7	CO (g)
2122	14	CO-Au_1 (pseudo single site)
2092	9	CO-Au_n
2133	9	CO-Au_1
2359	**20**	**CO_2 (g)**
3729	21	OH
3537	25	OH
1270	26	Carbonates
3552	26	OH
1207	27	Carbonates
856	28	Carbonates
1281	28	Carbonates
1015	29	Carbonates
3611	29	OH
1595	30	Carbonates
1621	30	Carbonates
1709	30	Carbonates
3617	33	OH
1221	34	Carbonates
2171	34	CO-CeO_2
3656	(-) 35	OH
3681	(-) 36	OH
1217	36	Carbonates
1219	41	Carbonates
1400	50	Carbonates
1560	125	Carbonates

The lack of the signal ascribed to reduced ceria as well as the electronic transition for the polyhedra samples indicates, that the sheets are initially more defect-rich, which may come from the additional existence of steps for the sheets, that reportedly have a positive impact on the reduction behavior [11].
Regarding the time values there are differences between the samples as well. For the sheets all signals appear in between 11 to 15 s and at low wavenumbers, where the already weak electronic transition signal fades out. A steep increase in time can be seen, which may be attributed to the increasing and undefined contribution of the background, thus holding no viable information.
The polyhedra exhibit time values in between 13 to 20 s for the signal around 2156 cm^{-1}, while for the background surrounding it, another steep increase is observed but can be ignored, as the background is not known to hold any crucial information.
The appearance of the signal at 2156 cm^{-1} at different time values of 11 s for the sheets and 15 s for the polyhedra is a significant deviation, as the error for the time values of these signals is 1.5 s, equal to the rate of spectra measurement in this case. A reason for that may be the effect, exerted by a signal's surrounding like other signals or, in the case of very weak ones, the background. It is clearly visible, that in case of the sheets, signals are way more intense and surrounded by other signals that may exhibit the same time values, while the signal in case of the polyhedra is only about one third as intense as its homologue from the sheets and may thus be much more affected by a possible overlap with the surrounding background "noise".

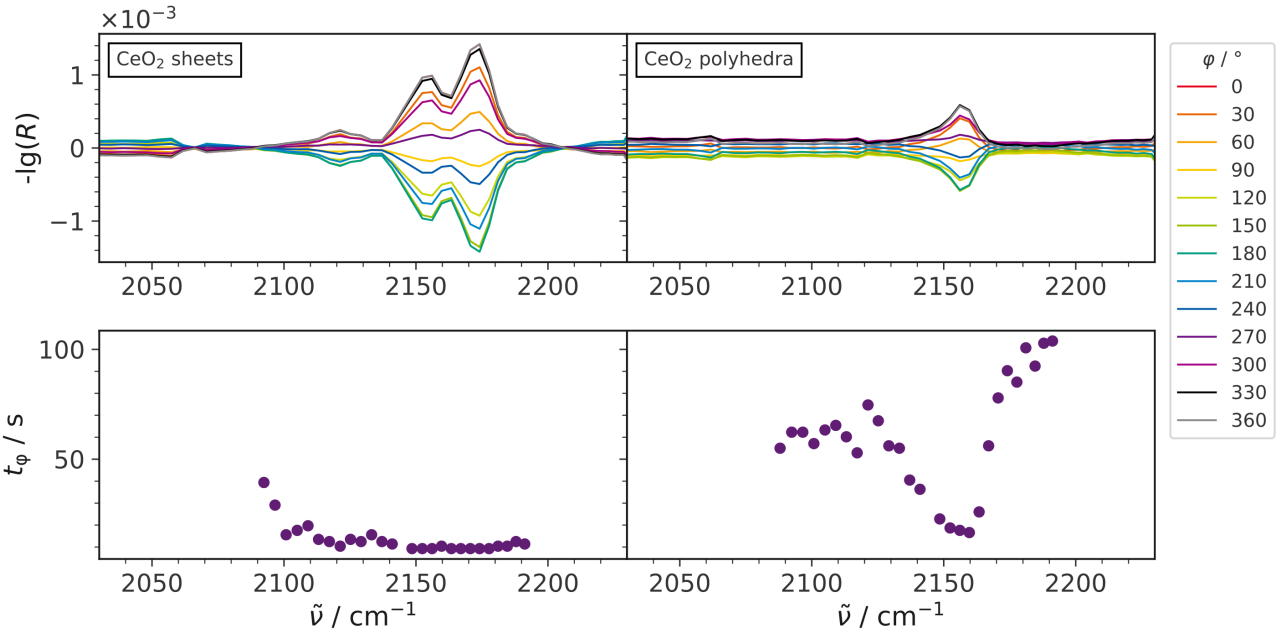

Figure 4.3: Comparison of the carbonyl regions of the PSD spectra of CeO_2 sheets (left) and polyhedra (right) after gas phase removal in the top row as well as the adjacent time values of each spectral position in the bottom row. Modified image taken from [30].

In fig. 4.4 PSD spectra of Au/CeO_2 sheets (left) and polyhedra (right) in the top row are shown together with the corresponding time values in the bottom row.
For both data sets a huge similarity is visible with dominating signals at 2122 cm^{-1}, assigned to CO on pseudo-single atomic gold sites [31] and 2171 cm^{-1} to CO on reduced ceria [35, 38]. In both cases a broad signal centered around 2133 cm^{-1}, which has previously been ascribed to CO on top of single gold atomic sites [31] as well as a small contribution at 2092 cm^{-1} of CO on larger clusters are visible [31]. One obvious

Table 4.3: Time values of signals in the carbonyl region for Au/CeO_2 and CeO_2 sheets and polyhedra (in brackets).

$\tilde{\nu}$ / cm-1	$t(Au/CeO_2)$ / s	$t(CeO_2)$ / s	assignment
2073	7 (8)	10 (11)	CO (g)
2122	8 (9)	– (–)	CO-Au pseudo-single site
2133	9 (10)	– (–)	CO-Au pseudo-single site
2092	14 (18)	– (–)	CO-Au_n cluster
2359	**20 (21)**	**– (–)**	**CO_2** (g)
2156	24 (26)	11 (15)	CO-$CeO_{2,ideal}$
2171	34 (39)	10 (–)	CO-$CeO_{2,reduced}$
2122	– (–)	12 (–)	Ce^{3+} electr. transition

difference is a pronounced asymmetry of the signal around 2171 cm^{-1} towards lower wavenumbers for the sheets.
In accordance to previous studies the increased signal intensity of CO on reduced ceria relative to the contribution of CO on an ideal surface on gold-loaded samples is attributed to the higher surface oxygen defect density in that case [32, 39]. The electronic transition, that can be observed for bare ceria sheets at around 2125 cm^{-1} can be excluded for gold-loaded samples, as previous isotope experiments have shown [31].
The time values, that are shown in the bottom row of fig. 4.4 but are as well listed in an ascending manner in table 4.3 show, that for gold-ceria sheets the first signals that appear after 8 and 9 s are associated to CO adsorbed to (pseudo-) single gold atomic sites at 2122 and 2133 cm^{-1}, respectively. These are followed by CO adsorbed to larger clusters at 14 s and 2092 cm^{-1}. The next signal to appear is already the product CO_2 after 20 s at 2359 cm^{-1}. The signals of CO adsorbed to bare ceria, that are situated at 2156 and 2171 cm^{-1} do appear after product formation at 24 and 34 s, respectively, and therefore way later than in case of bare ceria (about 10 s), which indicates a different mechanism leading to the formation of these species.
Interestingly, the CO-CeO_2 signals are about ten times more intense than they were for bare ceria (see fig. 4.3) which as well is indicative for a different mechanism at work for their formation. But as they only appear after CO_2 is already formed, they seem not to be involved in the mechanism leading to the product. A facilitated formation of these species can be speculated by a spillover / displacement mechanism of CO adsorbed to the gold single site, which is thought to be the active site, to the ceria surface. At first such a spillover seems not to be expected when looking at adsorption energies ($E_{ads,CO}(Au_1)$ = –2.58 eV; $E_{ads,CO}(CeO_2)$ = –0.19 eV) [31, 40]. But recent DFT calculations have shown, that on an already oxygen depleted ceria surface, CO from an e. g. single gold atom can be displaced by a second CO atom from the gas phase, not leading to product formation [30].
This mechanism may explain, why the time values as well as intensities for CO adsorbed to CeO_2 in case of the gold-loaded catalysts are so much different to those of bare and inactive ceria, where the signals are thought to be caused by sorption dynamics only. CO adsorbates due to this sorption behavior are expected to be present in case of gold-loaded catalysts as well, but of way smaller intensity than those due to the spillover/displacement mechanism, as a comparison of intensities in figs. 4.3 and 4.4 indicates.
Discussing now the signals of Au/CeO_2, the ones at 2092, 2122 and 2133 cm^{-1} appear to be active, as they show time values lower than that of the product CO_2. Although the one at 2092 cm^{-1} is way less intense than the others and thus seems to be much less important or may even be only due to CO sorption dynamics when switching gas phases. DFT calculations of adsorbed CO on different cluster sizes (Au_2, Au_3, Au_4) indicate, that all of these may contribute to this signal, due to large similarities in the obtained vibrational frequencies [30]. Further contributions from CO on other cluster sizes are also thinkable but the calculations available are

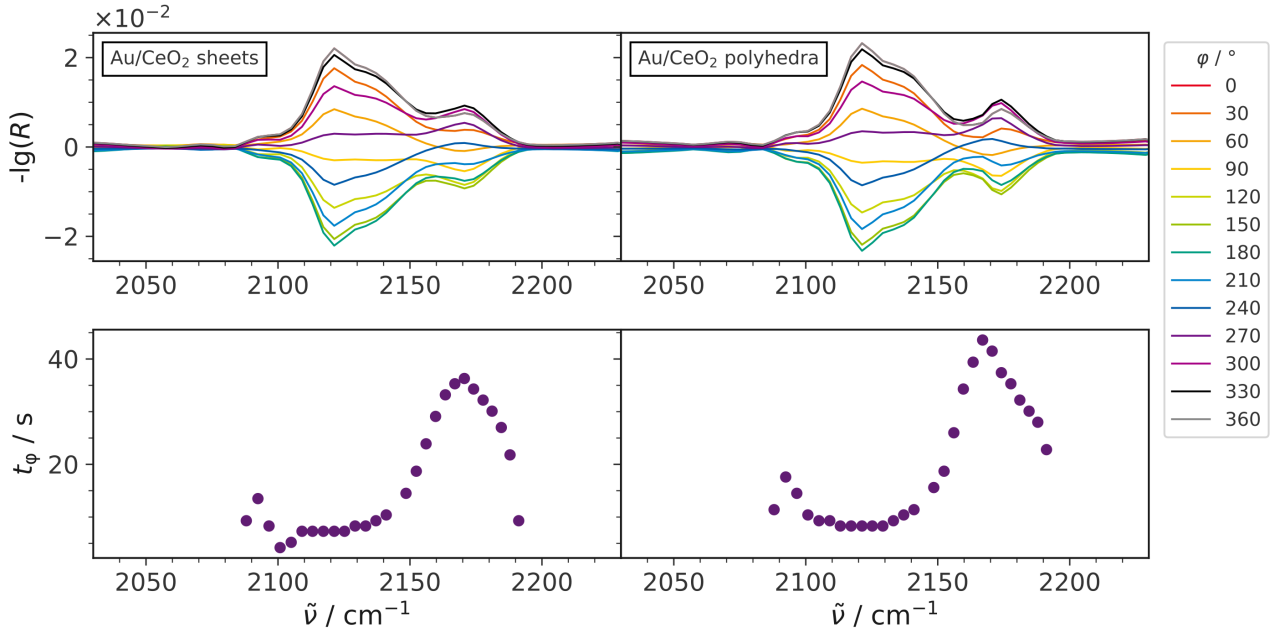

Figure 4.4: Comparison of the carbonyl regions of the PSD spectra of Au/CeO_2 sheets (left) and polyhedra (right) after gas phase removal in the top row as well as the adjacent time values of each spectral position in the bottom row. Modified image taken from [30].

limited to the aforementioned species.
The signals at 2122 and 2133 cm^{-1} are obviously the most prominent and thus promising signals to be attributed to the active species. According to literature they are assigned to single gold atoms that are abundant on the surface (2133 cm^{-1}) or similar single atoms but dynamically formed out of larger clusters (2122 cm^{-1}) [31, 41]. In this context it has to be stated, that there is evidence in literature, that completely isolated single gold atoms tend to block sites after catalyzing the reaction once, due to formation of a strongly bound and nonreactive negatively charged Au species [40, 41]. Therefore, it seems unlikely that there are completely detached Au atoms and, consequently, that the signal at 2133 cm^{-1} also belongs to a dynamically formed species.

Mechanistic conclusions In summary, mechanistic conclusions can be drawn about the active species, which appears to be CO adsorbed on (dynamically formed) Au_1 single atomic sites, as its signals are quite strong and they appear in between the reactant (CO) and the product (CO_2) signals. The following discussion is once again focused on Au/CeO_2 sheets, as results for the polyhedra do not differ much. A graphic representation of the obtained mechanistic picture can be seen in fig. 4.5.
First, CO from the gas phase (7 s) adsorbs on a gold cluster on the surface (8 s), leading to abstraction of the active CO-Au_1 single atomic site. Following earlier studies, according to a Mars-van Krevelen-type reaction mechanism this adsorbed CO tilts towards the ceria surface, where it binds to an available surface oxygen [31, 40]. This creates the product CO_2, that can quickly desorb to the gas phase (20 s), leaving a negatively charged oxygen vacancy behind. The contribution of larger clusters is considered insignificant, even though falling into that time window between CO and CO_2 observation, as it is marginalized by its very weak intensity. A minor activity of these sites is at this point not completely unthinkable, but further experiments presented in

section 4.3 point toward no activity. Another possibility for the appearance of those signals might be sorption dynamics at work. This can make signals appear as active in MES-PSD, as in case of adsorption and desorption in response to the gas phase exchange, concentrations at the surface change in line with the external trigger too. And as it is not be the reaction, that is the source of this "activity", it is expected to be way lower than the signals of a species actively participating in product formation.
CO adsorbed to bare ceria seems to only appear in the aftermath of the reaction at 24/34 s, i. e. at a time, when the surface is already depleted of oxygen, due to its consumption in the Mars-van Krevelen-type of reaction. As discussed above, CO adsorbed to an active (pseudo) single gold atomic site may spill over or be displaced by another CO to the already oxygen depleted surface, where it may further disperse as shown in fig. 4.5, which will be discussed in more detail based on further experimental evidence in section 4.3. In the same chapter, CO adsorbates on larger clusters are also further discussed based on new evidence for their inactivity.

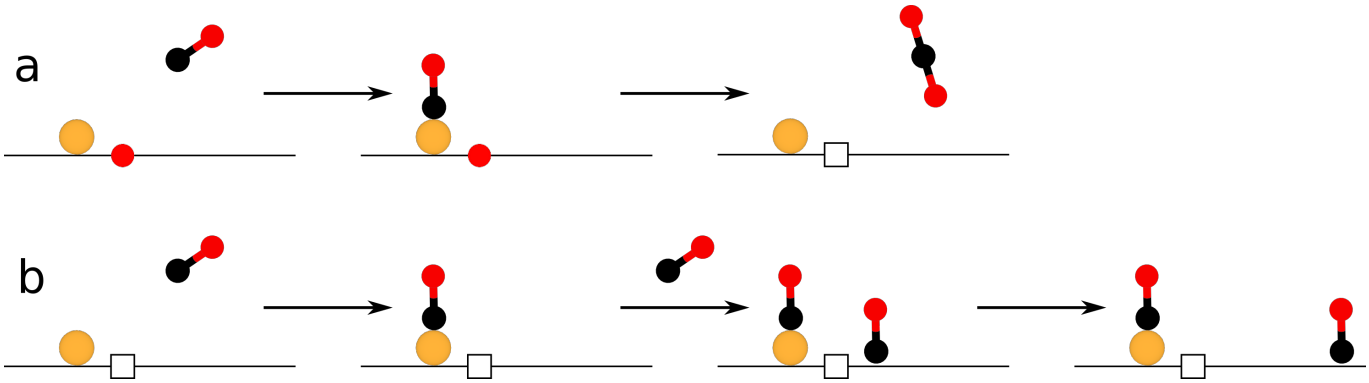

Figure 4.5: Proposed mechanisms for **a:** CO_2 formation and **b:** CO spillover/displacement. For simplicity, a depiction of the dynamic formation of the gold single atomic sites has been omitted. Modified image taken from [30].

4.2 Design of a low void volume reaction cell to overcome long residence times

To overcome the limitations of the aforementioned commercial cells by Harrick Scientific Products, especially the long residence times, a low void volume cell has been built as part of this work. It was designed using the free and open source 3D CAD software FreeCAD (Version 0.19, **`https://www.freecad.org/`**) and produced by the mechanical workshop of the chemistry department of the Technical University of Darmstadt. The resulting low void volume cell (LVVC) has a total volume of 1.33 mL including the reactor chamber and its direct supply lines, in comparison to the 14 mL volume of the commercial cells by Harrick Scientific Products [42].

Temperature calibration Temperature calibration of the cell was executed using a VOLTCRAFT M-4660A multimeter equipped with a Type K thermocouple. For this purpose, the spectroscopy window was replaced by a Teflon plate with a small perforation for inserting the thermocouple. After insertion, the thermocouple was firmly contacted with the bottom of an empty sample tray. The calibration was executed at atmospheric pressure and at a flow rate of 100 $mL_n min^{-1}$ Ar. The cooling circuit was not connected. The results can be

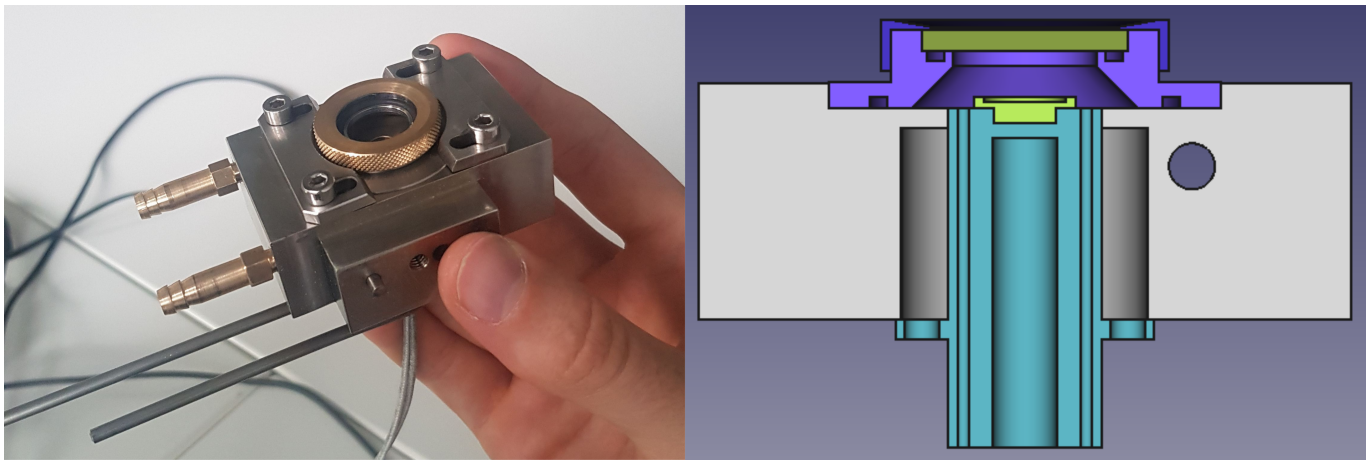

Figure 4.6: Final version of the LVVC both as it looks in reality (left) as well as in a cross sectional view (right), depicts the most important parts, that is the cell body (gray), the container for heating cartridge, gas feed and exhaust (cyan), the sample tray (bright green), the spectroscopy window (green) and the window holder (violet))

seen in table 4.4 which yielded the following equation of calibration:

$$T_{\text{sample tray}} = 0.74 \cdot T_{\text{controller}} + 5.73\,^{\circ}\text{C} \tag{4.1}$$

Table 4.4: Results of the newly designed LVVC's temperature calibration.

$T_{\text{controller}}$ / °C	$T_{\text{sample tray}}$ / °C
30	28
50	43
100	82
150	116
200	154
250	191
300	228
350	266

Determination of fluid dynamic parameters For determination of fluid dynamic parameters such as residence time ($\bar{\tau}$) and dispersion during experiments, the reaction setup has been tested by using a Harrick cell (H2021) and the newly designed low void volume cell (LVVC).
A step input experiment was carried out to measure the cumulative distribution curve $F(t)$ of the reactor and its supply lines. In this experiment different gas flows (100, 50, 20, 10 $\text{mL}_\text{n}\text{min}^{-1}$) of 100 $\text{mL}_\text{n}\text{min}^{-1}$ pure Ar were introduced, that were switched to 2 mol% CO in Ar. Spectra are measured in DRIFTS-mode, utilizing the investigated reaction cell with inert KBr in its sample tray, which is why the contributions of reactor and supply lines to the residence time behavior could unfortunately not be entangled. 200 spectra are collected prior to switching and 800 afterwards to allow for a complete gas phase exchange to happen. $F(t)$ is obtained via

$$F(t) = \frac{A(t)}{A_{\text{end}}} \tag{4.2}$$

where A describes the integrated area of the IR signal of CO. The original raw data were smoothed by fitting the convolution of a heavyside and a gaussian function to the time-resolved data, the results of which are shown in fig. 4.7 for both reactors. The first ($< t >$) and second moment ($< t^2 >$) of $F(t)$ are calculated via

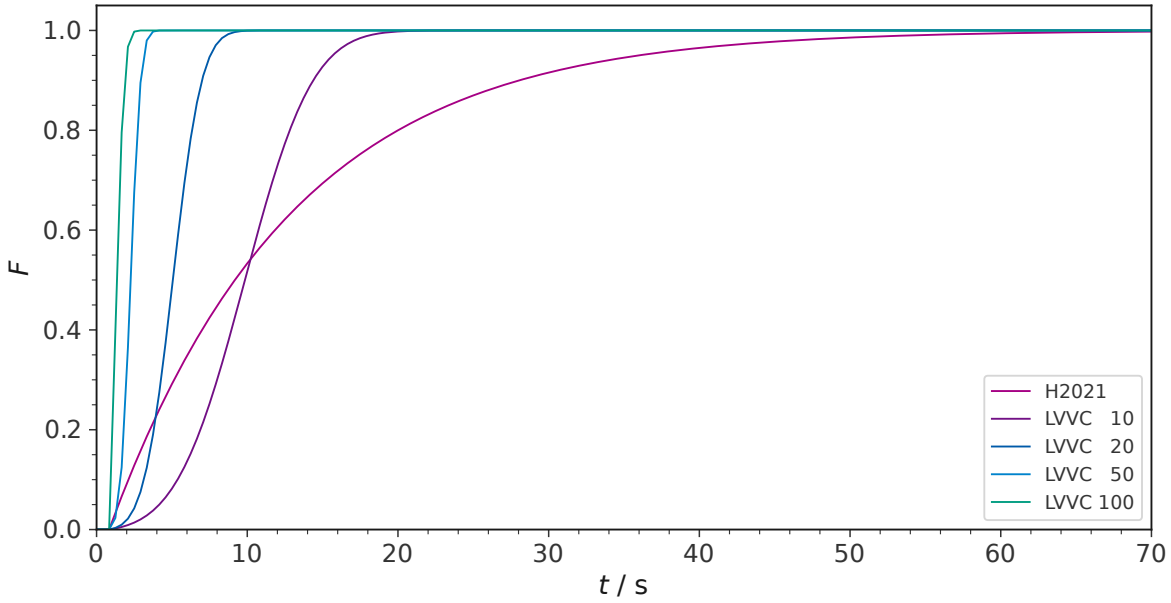

Figure 4.7: Cumulative distribution curves of the step input experiment for the commercial H2021 cell at 100 $mL_n min^{-1}$ and the self built LVVC cell at multiple flow rates given as numbers in $mL_n min^{-1}$ in the legend. At a time of 0 s the valve was switched from pure Ar to 2 mol% CO in Ar. The sample (KBr) temperature was 110 °C

$$\bar{\tau} = < t > = \int_0^1 t \mathrm{d}F(t) \tag{4.3}$$

$$< t^2 > = \int_0^1 t^2 \mathrm{d}F(t) \tag{4.4}$$

yielding the mean residence time $\bar{\tau}$ of the setup. The dispersion $\sigma^2 = < t^2 > - < t >^2$ and the standard deviation $\sigma = \sqrt{\sigma^2}$ are calculated from those two moments and results for both cells are shown in table 4.5. According to the interpretation of σ about 68 % of the change in concentration happens within a time interval of $\pm\sigma$ around the mean residence time, 95 % within $\pm 2\sigma$, 99.7 within $\pm 3\sigma$ etc. The value of $\bar{\tau} + 3\sigma$ is therefore also given in table 4.5 and will be discussed as the time of nearly complete gas phase exchange.
The experiments shown in fig. 4.7 prove, that the concentration step which results from switching the valve and should therefore resemble a rectangular signal shape is almost conserved in case of the specially developed LVVC at high flow rates of e. g. 100 $mL_n min^{-1}$ but broadened and dispersed largely when decreasing the flow rate in that cell. The retention time distribution of the commercial H2021 reactor and its supply lines further prolong the residence time even at high flow rates of 100 $mL_n min^{-1}$. In case of the commercial H2021 cell it is obvious that every experiment with a single pulse time below 47 s (see table 4.5) will not come close to enter the state of complete gas phase exchange and thus a steady CO content at its respective maximum. This diminishes the amplitude of possible signal intensity changes within the time domain which will be

transmitted by PSD to the phase spectra as smaller peaks. This makes interpretation of the data in this area less revealing and the slow exchange may increase the error of the obtained time values although interpretation is by no means impossible. But in case of the LVVC it is possible to apply almost complete gas phase changes within a few seconds (depending on the selected flow rate, see fig. 4.7 and table 4.5). Therefore this cell maximizes the effects on the signal intensity, so that it is perfectly suited for the type of rapid exchange experiments needed in MES.

Table 4.5: Fluid dynamic parameters that have been calculated for the commercial (H2021) and the newly developed cell (LVVC).

Cell	$\dot{V}$ / $mL_n min^{-1}$	$\bar{\tau}$ / s	$<t^2>$ / s^2	σ^2 / s^2	σ / s	$\bar{\tau} + 3\sigma$ / s
H2021	200	5.1	47.5	21.1	4.6	18.9
H2021	100	12.3	285.7	134.8	11.6	47.1
LVVC	100	1.0	1.1	0.2	0.4	2.2
LVVC	50	1.9	3.7	0.3	0.6	3.5
LVVC	20	4.7	23.9	2.3	1.5	9.2
LVVC	10	9.5	101.6	12.1	3.5	19.9

4.3 Varying the period length to point out spectators that appear active

Utilizing the newly built cell (LVVC), it is now finally possible to go to lower period lengths and still observe an almost total gas phase exchange. According to the literature, this will enhance the visibility of short-lived species in comparison to more stable ones [43]. Furthermore, this should allow to decrease the intensity of species that are only due to slow processes, such as the sorption dynamics of CO on bare ceria discussed in section 4.1.
Period lengths of 4, 2 and 1 min (which equals 160, 80 and 40 spectra per period, respectively) were applied using the LVVC, while keeping all other parameters the same as in section 4.1. Results for the carbonyl region are shown in fig. 4.8, all spectra are plotted in absolute intensities and without normalization. For both CO-Au signals at 2122 and 2133 cm^{-1} almost no further intensity changes can be observed for period lengths above 1 min, indicating that these species have almost reached their maximum abundance after only 1 min, which indicates, that the reaction is quite fast and most of the interesting effects should be observable at short period lengths.
But an opposing observation can be made for those signals that have been proposed not to be linked to active sites. This is the case for the small signal of CO adsorbed to larger gold clusters at 2092 cm^{-1}, which almost disappears when the LVVC is used. The other stark difference is visible for the CO-CeO_2 signal, which is shifted from 2171 to 2164 cm^{-1}. And when comparing the PSD spectra recorded with the LVVC at decreasing period lengths it can be seen, that the intensity in

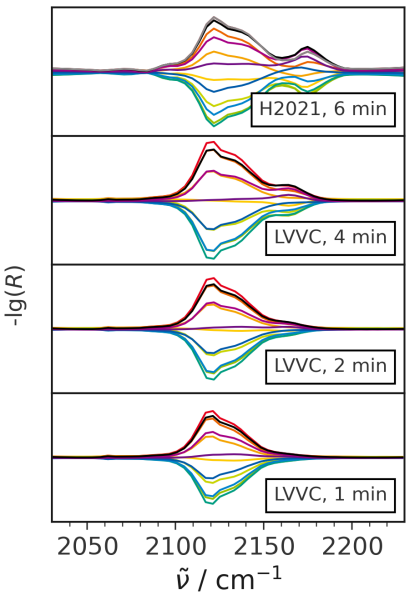

Figure 4.8: From top to bottom: Comparison of the PSD spectra recorded utilizing the old Harrick cell (H2021) to those recorded utilizing the LVVC at different period lengths (4, 2, 1 min).

the range of CO-CeO_2 signals decreases when shortening the period length.
This period length-related behavior supports the assumptions made utilizing the old cell, that CO adsorbed to bare ceria as well as to larger clusters is not linked to activity toward product formation but different processes such as simple sorption dynamics. The fact that these species are more abundant in case of the experiments with the H2021-cell may result from the longer exposure of the system to CO because of the very slow gas phase exchange (see fig. 4.7 and table 4.5). So there is always more of these species detectable than in case of the LVVC with its fast exchange rates, where they seem to never accumulate in large enough quantities to even become measurable and all CO available to the surface seems to be consumed by the active gold sites.

5 MES of CO_2 activation and the influence of pressure

5.1 Discovering previously hidden reactive gold hydrides during the reverse water-gas shift reaction (RWGSR) over Au/CeO_2

Preliminary results published in an earlier work concerning the reverse water-gas shift reaction's mechanism already indicated, that the activity is not mainly driven by surface defects but that the abundance of adsorbed species such as diverse carbonates, formates and gold hydrides (see fig. 5.1) correlates with increased activity [11]. These findings were made with the aid of non-modulated transient DRIFT experiments, where one of the reactants (H_2 or CO_2) was turned on or off after well-defined pretreatments in reaction atmosphere or in the presence of one of the reactants. This procedure yielded viable information about possible active species and allowed for a correlation of abundance and activity but not all of those signals could be sorted according to their time of emergence. So it remained unclear, which of these species appeared prior to product formation or in the aftermath, which may indicate sorption processes as already discussed for CO oxidation in section 4.1.
Thus the application of ME-DRIFTS to this important catalytic reaction appears promising in narrowing the field of the already identified signals that may play a role as active species and to provide a mechanistic succession that will further enhance the understanding of the reaction.

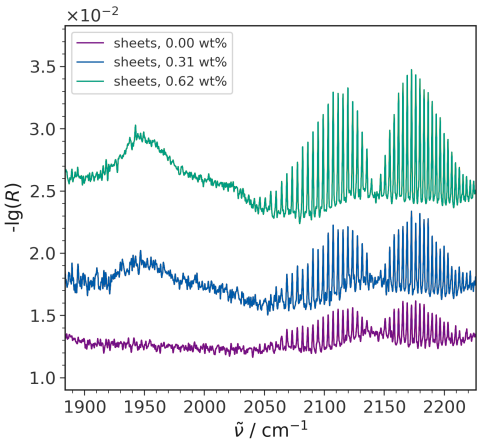

Figure 5.1: Conventional DRIFT spectra of the region with the potential gold hydrides, already published in [11]. Spectra were measured after CO_2 supply was switched on, while H_2 remained constant. For clarity only the last spectra of a measurement series with a duration of 6 min are shown. To increase the intensity of gold-related signals, spectra of Au/CeO_2 sheets with higher gold loading (0.62 wt%) are shown.

Experimental details For the modulation experiments, 20 periods with a length of 123 s each were cycled. Shorter period lengths were not applied, as the cell used in this case was the commercial H2021 in which a total gas phase exchange was only achieved after about 47 s (see table 4.5) and during one period two exchanges have to take place. In one period either CO_2 concentration was switched between 0 and 2 mol%, while H_2 concentration was kept constant at 4 mol%, or vice versa that is switching the H_2 concentration between 0 and 4 % and keeping a steady flow of 2 % CO_2. As inert carrier gas Ar was used, while the overall flow rate was 100 $mL_n min^{-1}$. Samples were treated for 15 min in a reductive 4 mol% H_2/Ar (for CO_2 modulation) or the more oxidative 2 % CO_2/Ar (for H_2 modulation) at a reaction temperature of 250 °C. Background spectra were measured after one modulation period as pretreatment at reaction temperature. Spectra were measured from 850 to 3800 cm^{-1} with a resolution of 0.5 cm^{-1}, an aperture of 8 mm and a mirror speed of 40 kHz on a Bruker Vertex 70.
Unfortunately, catalytic activities were never measured during modulation experiments. But activity data of

these catalysts during conventional steady-state experiments exist, where after 1 h of operation under the same conditions Au/CeO_2 sheets exhibited constant conversions of 5.4 %, while unloaded ceria sheets showed 1.6 %. All samples used in these experiments were the same as those discussed in section 4.1.
Each interferogram resulted in one spectrum, so that approximately every 1.5 s one spectrum is acquired, which was as well taken as experimental uncertainty for the derived time values.

5.1.1 First mechanistic insights from CO_2 modulation

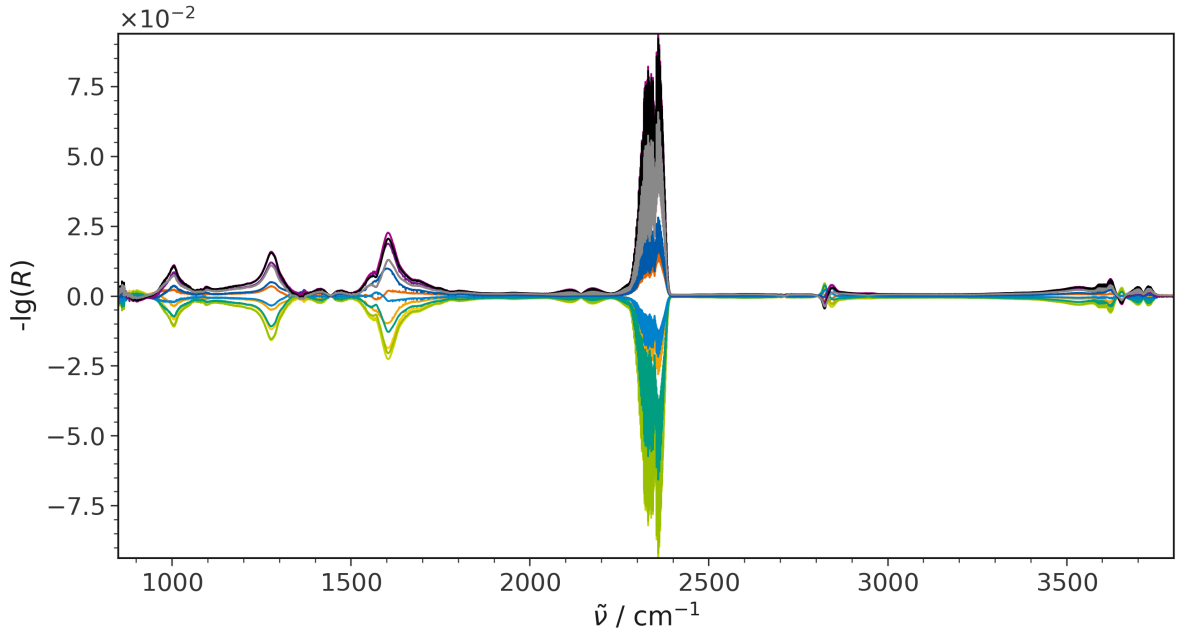

Figure 5.2: Full PSD spectra of the RWGSR over Au/CeO_2 sheets during CO_2 modulation (switching CO_2 concentration between 0 and 2 mol%, while H_2 concentration was kept constant at 4 mol%).

PSD signals show potential active signals The set of overview PSD spectra in fig. 5.2 shows, that besides the two gaseous species CO_2 (reactant) and CO (product) there are no CO adsorbates visible in the carbonyl region from 2000 to 2400 cm^{-1}, as can be seen in an enlarged view in fig. 5.3. Other signals, that are visible in the PSD spectra can be found in the carbonate region below 1800 cm^{-1}, in the CH stretch region around 2800 cm^{-1} and in the hydroxyl region above 3500 cm^{-1}. When increasing the zoom, a weak signal at 1953 cm^{-1} becomes visible as well. All signals together with their relative time values are listed in table 5.1. Unfortunately, the other product, H_2O did not appear in large enough quantities to be tracked in CO_2 modulation spectra, thus its place in the following mechanism (see fig. 5.5) is based on findings from complementary H_2 modulation experiments, which are discussed later on.

Time values deepen mechanistic understanding The time values in table 5.1 show, that there is a multitude of signals appearing prior to product (CO) formation. The reactant CO_2 appears at 16 s together with a signal assigned to (partially) dissociatively adsorbed H_2 on a single gold atom [11], followed by two carbonate vibrations at 17 s, two signals of doubly (II-B) and triply (III) bridging OH groups at 17 and 18 s [44] as well as another carbonate vibration at 19 s before the product CO appears at 20 s. The OH vibration appearing at 20 s, which can be assigned to OH on a more reduced surface (II*-B) [44] may as well be involved in

Table 5.1: The most prominent signals, their time values derived from PSD and assignments from the full spectrum of the RWGSR during CO_2 modulation shown over Au/CeO_2 in fig. 5.2. Negative signs indicate signals that decrease when turning CO_2 on. The period length is 123 s.

$\tilde{\nu}$ / cm^{-1}	t / s	Assignment
2824	(-) 12	Formate
2363	16	CO_2 (g)
1953	16	Au-H_2
1007	17	Bidentate carbonate
1278	17	Bidentate carbonate
3537	17	OH (II-B)
3613	18	OH (III)
1604	19	Bidentate carbonate
2173	**19**	**CO (g)**
3654	(-) 20	OH (II*-B)
1570	23	Formate
2847	24	Formate
1332	26	Formate
2946	27	Formate
1369	41	Formate

the mechanism as its error range of 1.5 s overlaps with the one of CO. This would be in alignment with its assumed role from literature, where this species of OH on reduced surfaces (II*-B) is reported to transform into the corresponding OH species at a more oxidized surface (II-B) which can be seen at 3537 cm^{-1} (17 s) [44]. According to literature, the carbonate signals at 1278 (17 s), 1007 (17 s) and 1604 cm^{-1} (19 s) can be assigned to bidentate carbonate on ceria [3, 11, 45, 46]. The deviation of their time values is within the overlap of each signal's error range of 1.5 s and can thus be assumed to coincide, which makes sense for different vibrations of the same molecule.
In [11] another signal at about 2134 cm^{-1} was observed, which was assigned to a hydrogen atom adsorbed to a single gold atom. Unfortunately, this signal is not very pronounced in case of the RWGSR over Au/CeO_2 sheets in comparison to polyhedra samples (see [11]). E. g. in fig. 5.1 there is almost no difference to be seen in the area around 2134 cm^{-1} when comparing the higher loaded Au/CeO_2 samples to bare CeO_2, although the intensity of the other signal assigned to gold hydrides at about 1953 cm^{-1} correlates perfectly with gold loading. So for the spectra of Au/CeO_2 sheets discussed here, there is no indication for a carbonyl-related signal (see fig. 5.3).
Interestingly, the signal at 2824 cm^{-1} appears prior to the modulated reactant CO_2. It was assigned to the CH stretching vibration of a formate [11, 45–48]. An interesting behavior of this signal was already reported in [11], where a similar signal shifted to higher wavenumbers, when exposed to the more oxidizing conditions of the reaction phase including CO_2, and shifted back to lower wavenumbers, when CO_2 supply was turned off and only H_2 remained, which strongly reduced the catalyst. This signal behavior can lead to the twisted appearance of the signal pair in the PSD spectra in fig. 5.4, which in the end would just be due to an oxidation-state dependent cycling between the low and high wavenumber position of the same signal as shown in [11]. This leads to the conclusion, that this CH stretching vibration of formates may for this system act as a sensitive probe towards changes in surface oxidation state. This signal's very early appearance at (-) 12 s (4 s before the reactant CO_2) seems odd in the first place but may be due to an overlap of the two opposing signals, which is shown in detail in fig. 5.4. As already discussed in section 4.1, a broad overlap of

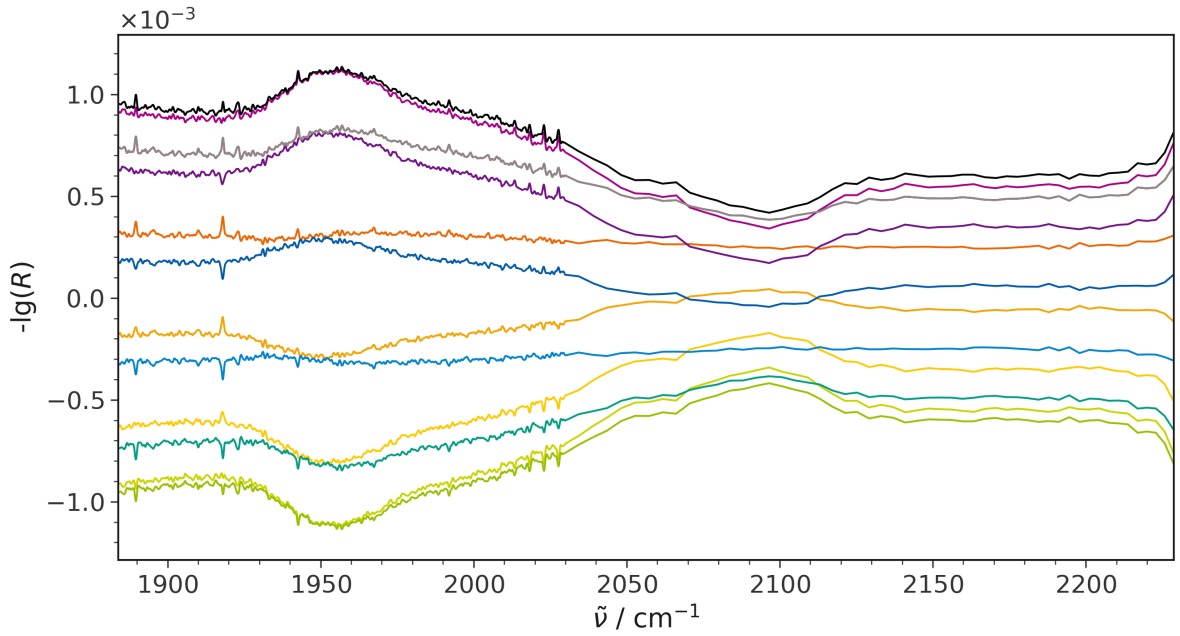

Figure 5.3: Carbonyl region of the PSD spectrum of the RWGSR over Au/CeO_2 sheets during CO_2 modulation after gas phase removal.

neighboring signals means, that both have a strong influence on each other's time value that is extracted via PSD. This drastically increases the error of the calculated time values, so that the interpretation of the latter has to be done carefully or even left out.
After the product (CO) formation there are still many signals, mostly of formates whose time values range from 23 s to 41 s. The most undisturbed formate signal, free of neighbors, is the one at 2946 cm^{-1} (27 s), which should provide the best reference point according to what was already discussed above, where it was stated, that the overlap of two signals has an effect on their time values derived from PSD, increasing the uncertainty. Therefore the solitary signal at 2946 cm^{-1} was chosen, as it is the least error-prone formate signal. Furthermore, the signals at 1570 (23 s), 2847 (24 s), 1332 (26 s) and even 1369 cm^{-1} (41 s), that all have as well been discussed in previous studies [11], may still be linked to the same species, even without overlapping error regions. The reasons for this can be the same as discussed for the weak CO adsorbate signals during CO oxidation in section 4.1, where neighboring strong bands or even the remaining background affect the calculated time values.

Construction of a mechanistic picture Combining all findings from MES-PSD with the existing knowledge published in [11], it is possible to exclude the participation of formates during CO formation but emphasize the importance of bidentate carbonates during that process, confirm the involvement of gold hydrides as well as a certain number of hydroxyls in the mechanism and exclude CO adsorbates to take part in the reaction. Thus a potential reaction mechanism may look like the one shown in fig. 5.5, where first H_2 (partially) dissociatively adsorbs to single gold atoms on the surface. CO_2 from the gas phase can then adsorb into an oxygen vacancy on the surface in proximity of the Au-H_2 species and, by including a neighboring surface oxygen atom, form a stable bidentate carbonate. One of the H atoms may then spill over to the bidentate carbonate and facilitate its disintegration into gaseous CO and a surface hydroxyl with gaseous CO immediately leaving the reaction

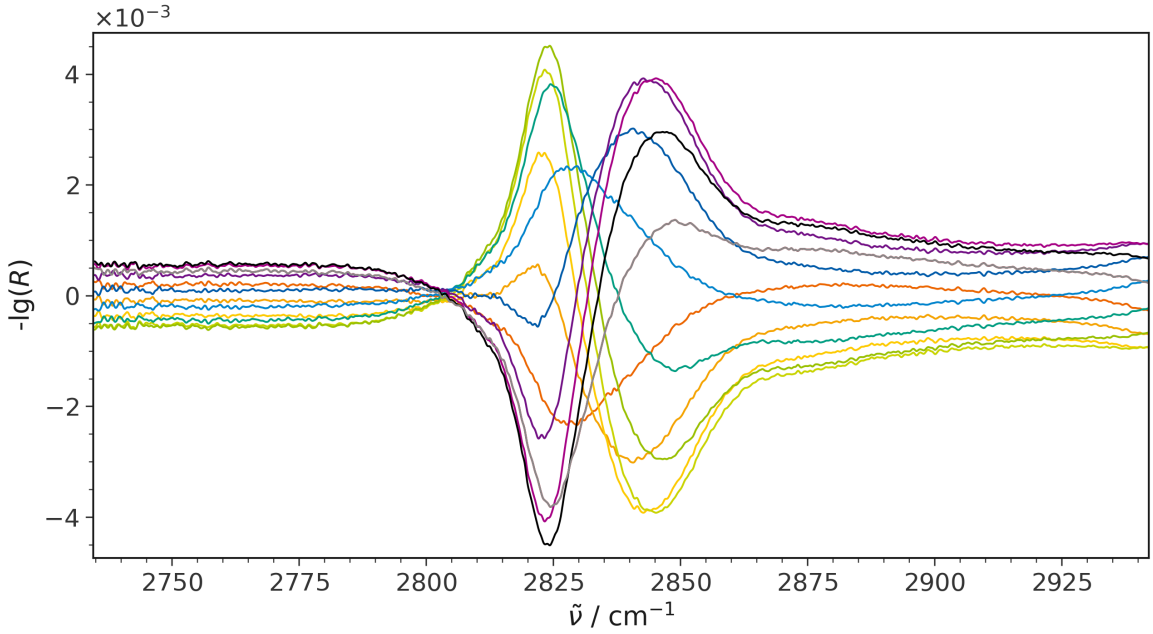

Figure 5.4: The formate signal's "twisted" behavior in the PSD spectrum of the RWGSR over Au/CeO_2 sheets during CO_2 modulation.

site. To close the catalytic cycle, the formation of the second product, H_2O is still needed. This may happen via spillover of the remaining H atom still attached to the gold atom to the newly formed OH in its vicinity. Water may then leave the system via the gas phase, leaving the surface in its initial state.
As another possibility, Ziemba *et al.* [11] proposed a reaction of the adsorbed carbonate that has been formed from CO_2 with hydrogen from the gas phase without its prior adsorption to the gold site. From the available data it is not possible to prove or refute this potential pathway, so it might as well be a potential side-reaction. Anticipating the results of the high-pressure CO_2 activation in section 5.2.1, it can be noted that the RWGSR observed there does not appear to proceed via gold hydrides, making a reaction of adsorbed CO_2 with H_2 from the gas phase more likely as a possible reaction pathway. However, further experiments will be needed to confirm this proposal.

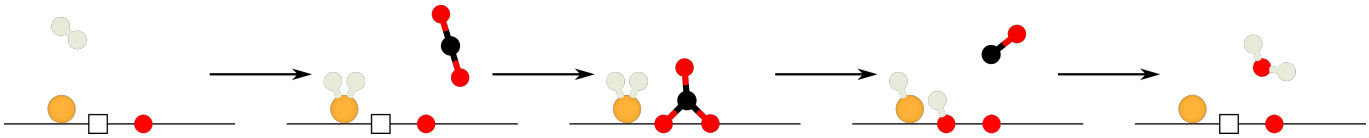

Figure 5.5: Proposed mechanism for the RWGSR over Au/CeO_2 based on MES-PSD results.

5.1.2 Deepening the mechanistic understanding by complementary H_2 modulation

The signals observed are complementary, the findings as well To gain a more complete picture of the reaction mechanism, the modulation procedure was inverted by now periodically pulsing H_2 while keeping the CO_2 flow constant. Spectra collected under these conditions are shown in fig. 5.6. Basically all the important signals that have been visible when applying CO_2 modulation in the previous chapter can be observed too.

These signals together with their respective time values are summarized in table 5.2.

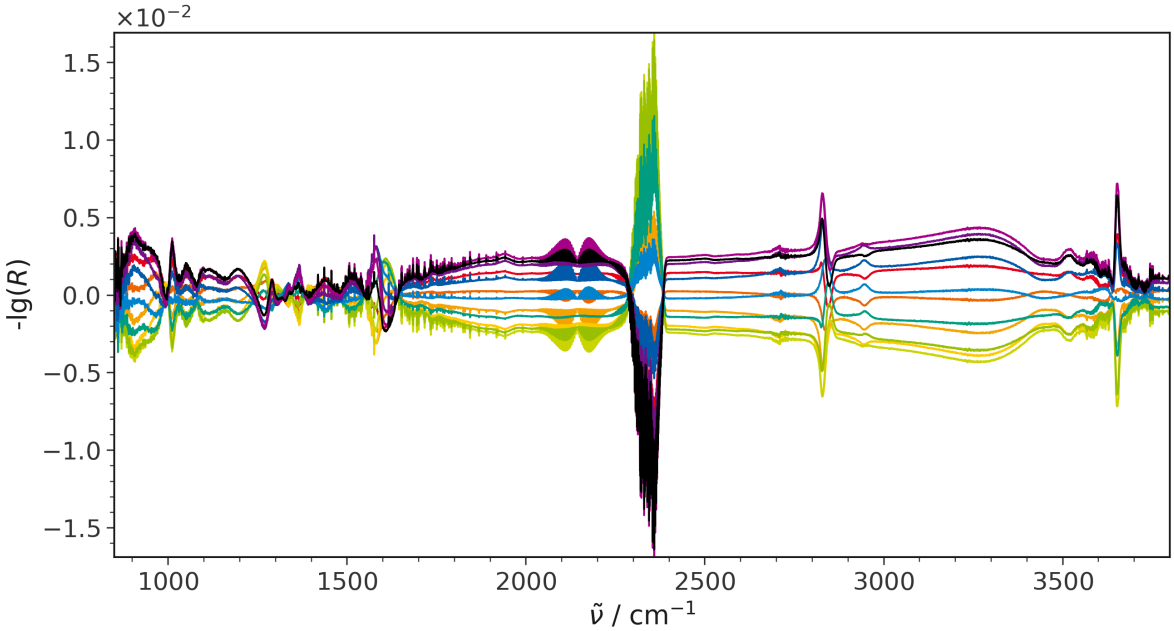

Figure 5.6: Full PSD spectra of the RWGSR over Au/CeO_2 sheets during H_2 modulation (switching H_2 concentration between 0 and 4 mol%, while CO_2 concentration was kept constant at 2 mol%).

What immediately catches the eye is a broad absorption that can be attributed to weakly adsorbed water [31], ranging from about 1700 cm^{-1}, where the carbonyl region ends, to 3500 cm^{-1}, where the hydroxyl region begins. Such broad absorption features are detrimental to the sensitivity of MES-PSD because any signal in the region covered by this broad responsive feature will appear in the PSD spectra due to the non-selective nature of PSD, which amplifies any spectral position if any response to the modulation frequency is detectable there. Even in the case where another signal appearing on top of the broad absorption feature behaves as a spectator species. The underlying dynamics of the broad active contribution cannot be separated from the signal appearing on top by the means of conventional PSD, so the latter gets "transported" into the PSD spectra via the broad active feature. The problem is therefore basically the same as that discussed for neighboring and overlapping signals in previous chapters such as section 4.1. But unlike the problems posed by inseparable neighboring bands, those arising due to broad periodic background effects can be overcome. This has already been described by in [49], where a supposed electronic background effect was modeled and subtracted from the spectra, generating an adjusted data set, to which it was possible to again apply PSD and retrieve information on the sharp signals in the same region as that background.
In the present case such a procedure will not further clarify the mechanistic insights from the data set shown in fig. 5.6. All signals in the range covered by that broad water absorption have either already been excluded from being active species in CO_2 modulation experiments, which applies for formates that only appeared after product formation, or have been confirmed in preceding non-modulated transient experiments (see [11]), where Au-H_2 adsorbates appeared under reductive as well as oxidative conditions. For these species CO_2 modulation experiments have only provided even clearer evidence for Au-H_2 to be active by proving that this species definitely appears prior to product formation (see table 5.1). Nonetheless, time values for the species that overlap with the broad water signal between roughly 1700 and 3500 cm^{-1} in fig. 5.6 still have been calculated and seem to be in line with the findings from the previous chapter (appearance before or after

Table 5.2: The most prominent signals, their time values derived from PSD and assignments from the full spectra of the RWGSR over Au/CeO_2 during H_2 modulation shown in fig. 5.6. Negative signs indicate signals that decrease when turning H_2 on. The period length is 123 s.

$\tilde{\nu}$ / cm^{-1}	t / s	Assignment
1291	3	Carbonates
1609	(-) 9	Bidentate carbonate
2363	(-) 17	CO_2 (g)
1940	19	Au-H_2
3655	20	OH (II*-B)
3519	21	OH (III)
3745	**22**	**H_2O (g)**
3275	**22**	**H_2O (ads)**
2173	**23**	**CO (g)**
2946	25	Formate
2829	26	Formate
1270	(-) 29	Bidentate carbonate
1583	36	Formate
2850	36	Formate
1368	37	Formate
1337	39	Formate

product formation) but their absolute numbers must be considered carefully, as due to the overlapping broad absorption feature they may be subjected to a large error, whose calculation has not been part of this work.
The other signals, mainly in the carbonate and hydroxyl region, show some interesting behavior. First, it has to be noted, that under these modulation conditions it is finally possible to see the second product, water. But it is not only visible in its adsorbed form, centering around 3275 cm^{-1} with a time shift of 22 s, which has been broadly discussed above, but also as a gas phase species. An example is the sharp signal at 3745 cm^{-1}, appearing at the same time of 22 s. The CO signal at 2173 cm^{-1} appears at 23 s, so formation of both products seems to take place at about the same time.
In the carbonate region signals are observable, that can be assigned to formates at 1337, 1368 and 1583 cm^{-1}, which appear at 39, 36 and 36 s, respectively. This is a further indication, that formates are only formed in the aftermath of the reaction at a surface that has enough hydrogen containing species present due to sufficient H_2 exposure. The formate-related signals in the CH region at 2829, 2850 and 2946 cm^{-1} all overlap completely with the broad water absorption and their time values are therefore not fully reliable. They all still show quite similar time values of 26, 36 and 25 s respectively, which are all later than product formation and in the broader range of the other formate-related signals in the carbonate region. But obviously all are higher than the time values of the two products, underlining that formate formation occurs after product formation.
Further signals are visible at 1270 and 1609 cm^{-1}, which are decreasing in the H_2 pulse and can be ascribed to bidentate carbonate. The signal at 1270 cm^{-1} appears at 29 s, while the one at 1609 cm^{-1} is already visible after 9 s. This huge difference may be due to neighboring signals (at 1290 and 1583 cm^{-1}) that are about the same height or even higher and which partly overlap with them. This, as already discussed before, makes the time values overlap too and may increase the error drastically. So even though the signal at 1270 cm^{-1} lies outside the conservative error range of 1.5 s of the product formation, the error can be assumed to be much larger in the case of these overlapping signals, so that its involvement in the mechanism can still be assumed, as indicated by the (also error-prone) signal at 1609 cm^{-1} (9 s), definitely responding before product

formation but even before the reactant CO_2 becomes visible (17 s).
At first it seems surprising, that CO_2 only appears after 17 s, while some other signals at 1291 and 1609 cm^{-1} occur after 3 and 9 s, respectively. However, due to overlaps, the calculated time values must be treated with caution in all three cases. E. g. the CO_2 signal lies in the middle of the broad background absorption, which may blur the calculated time value. The two other signals overlap with intensive features at 1270 and 1583 cm^{-1}, which show the opposite intensity behavior as they do, and therefore a mixing of their time values is likely.
Two hydroxyl signals can be observed at 3655 cm^{-1} (20 s), assigned to doubly bridged hydroxyls on a reduced surface (II*-B), which is decreasing, and at 3519 cm^{-1} (21 s), assigned to triply bonded OH (III), which is increasing during the H_2-pulse (see table 5.2). Both have already been observed for CO_2 modulation and are discussed there (see section 5.1 and table 5.1), and both signals respond at almost the same time as the products. The OH (II*-B) signal has been observed to be decreasing in the case of the reaction phase during CO_2 modulation with a supposed transformation of that species into the corresponding OH species at a more oxidized surface, OH (II-B), red-shifted by about 20 cm^{-1} and transforming back in the second phase of the modulation period, where only H_2 is present. The same signal is decreasing during the reaction phase of H_2 modulation but without the oxidized species being observed in the second (CO_2 only) phase of the modulation experiment, maybe due to an overlap with the CO_2 features visible in that region combined with a low signal intensity of the hydroxyls relative to CO_2.
So a potential explanation might be, that only the transformation of these supposedly redox state dependent doubly bridged hydroxyl species into each other is observed, induced by pulsing a more oxidative (CO_2) or reductive gas (H_2) over the catalyst. This would automatically lead to the conclusion, that the triply bridged OH (III) seems to be the active hydroxyl species according to fig. 5.5, which would make sense, as in the previous steps, the reaction of CO_2 via a carbonate species to CO has refilled an oxygen vacancy in the direct vicinity of the emerging hydroxyl species, thus oxidizing its surrounding. This would also be in line with the signals assigned to OH-groups on reduced surfaces decreasing in intensity, as the surface oxygen vacancies are refilled.

Refining the mechanism From the temporal information gained in the H_2 modulation experiments it is now possible to obtain information on the time at which water emerges, which is the other product besides CO. As shown in table 5.2, gaseous and weakly adsorbed water both appear at about the same time (22 s) as CO (23 s), which is within each signal's error range of 1.5 s. Therefore it can be stated, that the two last steps of product formation in fig. 5.5 are fast and may even appear almost synchronously. This fast formation of water is logical for thermodynamic reasons, since it is a highly stable molecule.
The involvement of formates can again be excluded due to the late emergence of its signals, while the role of bidentate carbonate during the reaction cannot be further clarified by this experiment, as the time values of its features are probably subjected to a large error due to overlaps with neighboring signals. But from the results of CO_2 modulation in the previous section and what was visible in previous works, bidentate carbonate can still be assumed to be the most promising candidate for playing an active role during the associative pathway of the RWGSR.
The H_2 pulse experiments allowed to obtain further information about the active hydroxyl species in the mechanism, which seems to be a triple-bridged OH (III) species. The role of the doubly bridged OH (II*-B) or a reduced surface and its pendant OH (II-B) on its oxidized counterpart were observable in the modulation experiments (CO_2 and H_2) only due to the oxidizing or reducing influence of these gases on the catalyst surface and therefore a possible transformation of these two signals into each other.
More information on the gold-hydrogen species could not be obtained from these experiments, as its characteristic signal overlapped with the intense background absorption, but from CO_2 modulation experiments and

the preliminary studies using non-modulated transient DRIFTS [11], Its crucial role in the associative RWGSR pathway can already be well established.

5.2 Addressing the increasingly complex system of methanol production over Au/CeO_2 at elevated pressure.

As a next step after atmospheric pressure CO_2 activation, higher pressures were targeted to shift the equilibrium towards methanol formation, as the RWGSR towards CO formation is not the only reaction to involve CO_2 hydrogenation, which can be seen in the following equations.

$$\begin{aligned} \mathrm{CO_2 + H_2} &\longrightarrow \mathrm{CO + H_2O} \\ \mathrm{CO_2 + 3\,H_2} &\longrightarrow \mathrm{CH_3OH + H_2O} \\ \mathrm{CO_2 + 4\,H_2} &\longrightarrow \mathrm{CH_4 + 2\,H_2O} \end{aligned}$$

Earlier studies have already shown, that catalytic systems similar to ours can yield promising results, as shown by Rezvani *et al.* [50], where gold-loaded reducible oxide catalysts such as Au/ZnO or Au/CeO_2 appear as suitable systems for this type of reaction, exhibiting higher activities and selectivities than current commercial catalytic systems like Cu/ZnO [51, 52]. The latter are known to be good at forming MeOH from CO but when switching the reactant to CO_2, their selectivity towards MeOH suffers as they are highly active in the RWGSR as well, thus preferably forming CO [53–55]. According to earlier studies [56, 57], activity towards MeOH on Au/ZnO correlated with O vacancy formation, thus a highly reducible oxide such as CeO_2 is claimed to be an excellent system for CO_2 activation and MeOH formation [58, 59].

5.2.1 Using a commercial cell to obtain first insights into the mechanism

Experimental details During the first set of high pressure experiments the commercially available H2021 cell was used (see section 4.1). The modulation parameters were the following: 10 periods with a length of 1581 s during which 160 spectra were taken with 20 interferograms averaged into one. Thus the time for one spectrum was 9.9 s.
These long times were necessary due to weak and noisy adsorbate signals and very long residence times in the reactor at the chosen pressure of 10 bar. Experiments have shown, that a full gas phase exchange under these conditions was only achieved after roughly 11 min as can be seen in fig. 5.7. Since this value is by far too large for a fast gas phase exchange acceptable in MES, the determination of residence times, comparable to tables 4.5 and 5.5 was omitted for this cell under these conditions (see section 5.2.2).
Nevertheless, experiments were conducted to initially prove the catalyst's ability to produce MeOH. Conditions similar to those applied in the literature were applied. The temperature was chosen to be 250 °C and the gas composition was 25 vol% CO_2 and 75 vol% H_2 at a total flow rate of 60 $mL_n min^{-1}$. Thus a H_2/CO_2 ratio of 3/1 was applied to facilitate MeOH production over the possible side reactions towards CO or CH_4. During modulation experiments, CO_2 was exchanged periodically with the equivalent flow of argon, background spectra were measured after one modulation period at reaction temperature as pretreatment.
These experiments were conducted in an *operando* mode, including an additional IR spectrometer (Vertex 70) equipped with a gas cell (Hellma Axiom Corporation), measuring the exhaust composition in transmission mode as shown in the setup in fig. 2.1.

Observations when applying 10 bar and pulsing CO_2 The PSD spectra of the high pressure CO_2 activation in fig. 5.8 show at first glance, that carbonates are involved (indicated by signals in the region up to 1800 cm^{-1}).

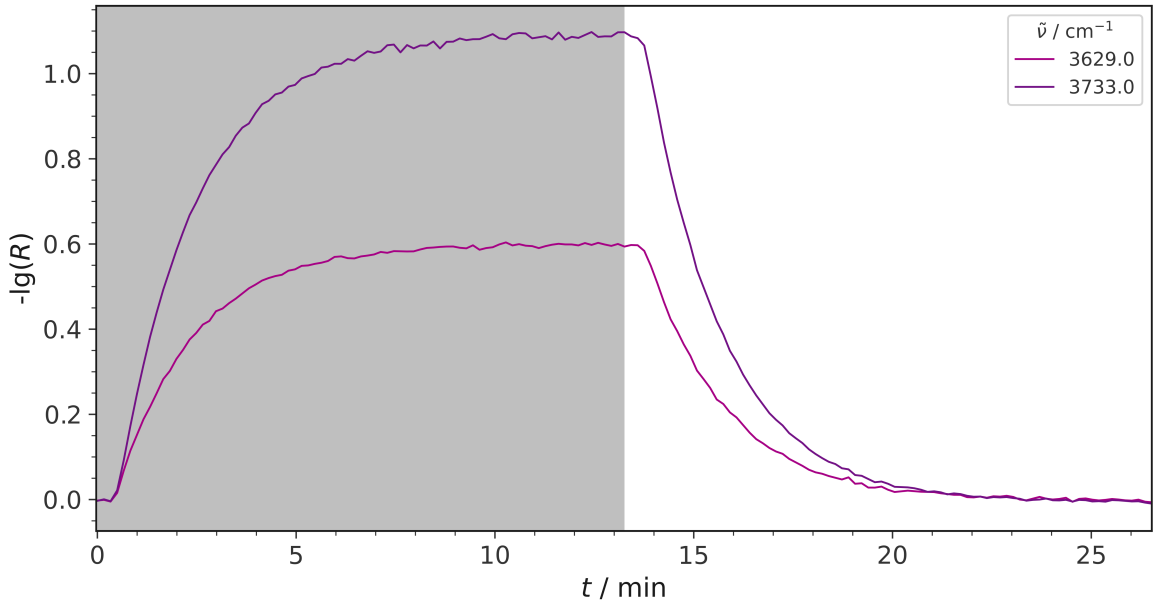

Figure 5.7: Time evolution of two CO_2 signals during one period of CO_2 modulation. CO_2 was switched on in the gray area and switched off in the white area.

Gaseous CO is visible quite well between 2000 and 2300 cm^{-1} indicating the occurrence of the RWGSR as a side reaction. Within the CH region between 2700 and 3100 cm^{-1}, a multitude of signals is visible as well. Besides all of that, highly intense CO_2 signals block the regions between 2200 and 2400 as well as 3500 and 3800 cm^{-1}. Above 3800 cm^{-1} an intense set of signals belonging to gaseous H_2O is visible, which coincides with the adjacent set of signals scattered around 1600 cm^{-1} across the carbonate region.
From the PSD spectra in fig. 5.8, only CO and water are easily apparent as products. Due to the *operando* nature of the experiments, it was possible to prove the abundance of at least three products of the CO_2 activation in the modulation experiments by simultaneously monitoring the exhaust gases with a second IR spectrometer. First, the resulting time-resolved spectra reveal the formation of the desired gaseous MeOH, recognizable by its signals, featuring the P, Q, and R branch at around 1033 and 2845 cm^{-1}, as well as a broad signal group between 2700 and 3150 cm^{-1} [60], which is visible in figs. 5.9 and 5.10. Besides MeOH, CO formed via the RWGSR is detected as well, which is visible in fig. 5.11 and furthermore methane, which can be seen in fig. 5.10, blue-shifted to the signals of MeOH but clearly distinguishable by a rotationally resolved signal with a Q branch at about 3017 cm^{-1} [61].
Unfortunately, these exhaust spectra were only measured qualitatively without calibration of the signals and a quantification of each reaction's share is therefore not possible. Nonetheless, the abundance of three parallel reaction paths proves to be problematic for the extraction of mechanistic information from MES-PSD, as the extracted time values of the species observed cannot be specifically assigned to one reaction or another. Furthermore, the temporal resolution is only 9.9 s and a complete gas phase exchange is only reached after about 11 min (see fig. 5.7), which means that the gas phase stays in contact with the catalyst for a very long time, thus blurring the temporal information. Literature on a comparable but higher-loaded (1 wt% Au) Au/CeO_2 system by Rezvani *et al.* has also only shown MeOH-selectivities of up to 40 %, while already working at 21 bar [50]. Therefore, an easy assignment of reaction intermediates to one particular reaction and thus a separation of mechanisms seems impossible at that point.

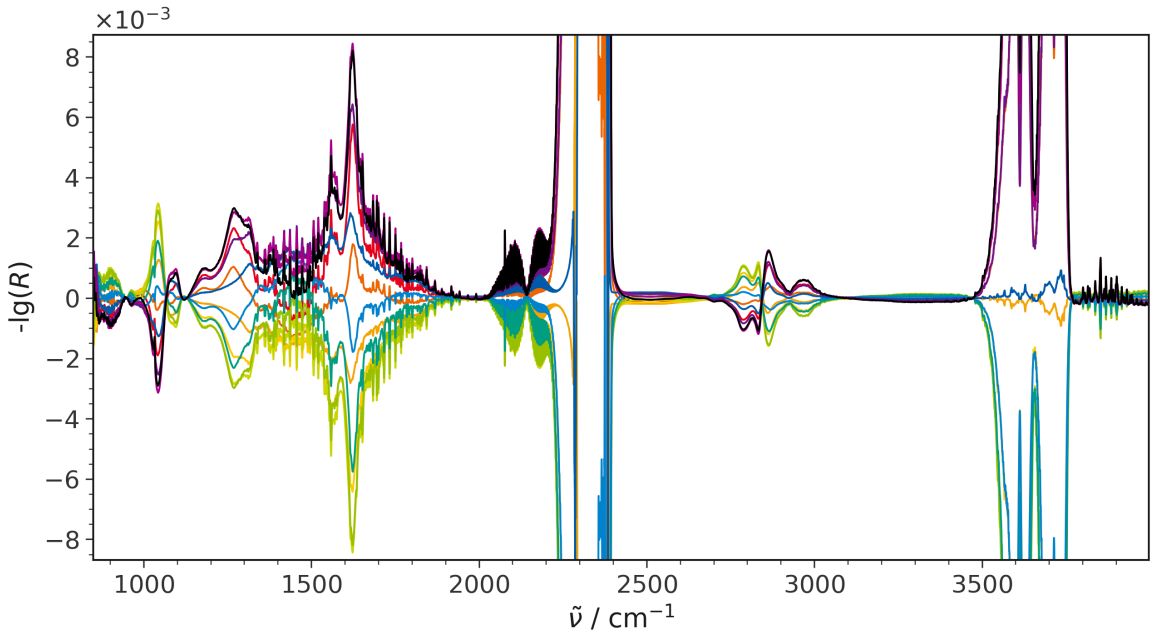

Figure 5.8: PSD spectra of CO_2 activation using the commercial H2021 cell over $AuCeO_2$ at 10 bar for CO_2 modulation.

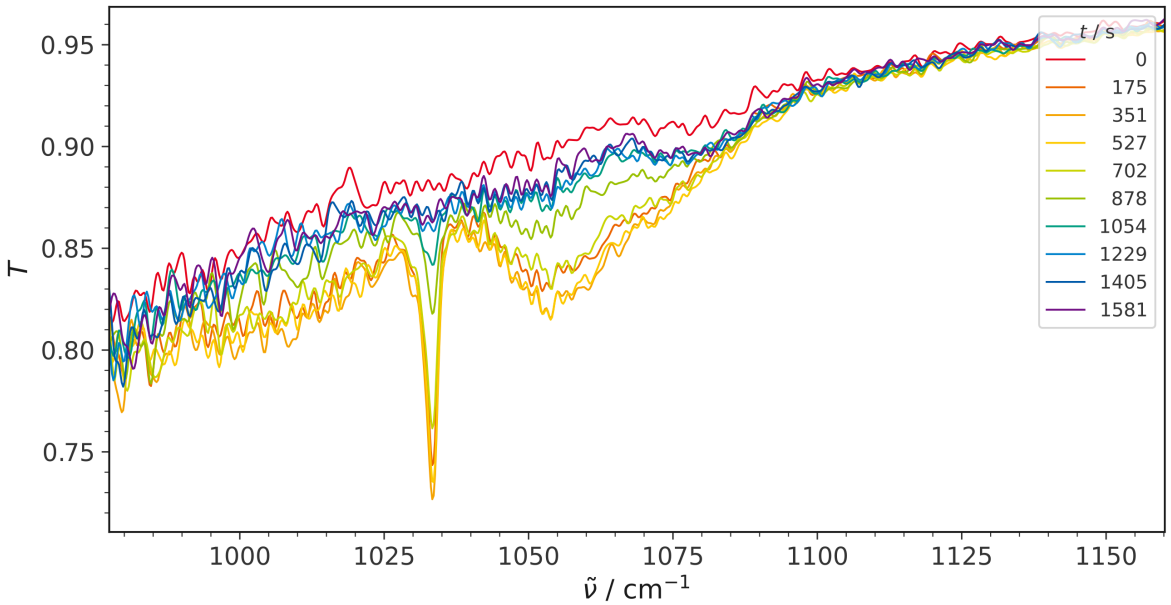

Figure 5.9: Time evolution of the distinct MeOH signal in the exhaust transmission IR spectra of CO_2 activation using the commercial H2021 cell over $AuCeO_2$ at 10 bar during one modulation period for CO_2 modulation.

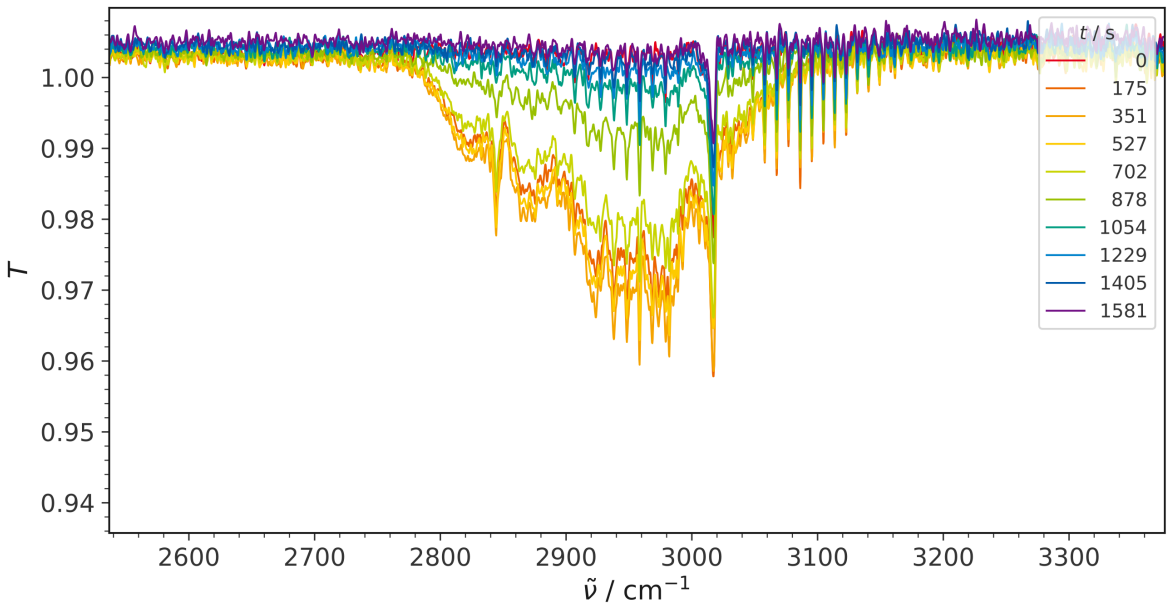

Figure 5.10: Time evolution of the CH region depicting signals associated with MeOH and CH_4 in the exhaust transmission IR spectra of CO_2 activation using the commercial H2021 cell over $AuCeO_2$ at 10 bar during one modulation period for CO_2 modulation.

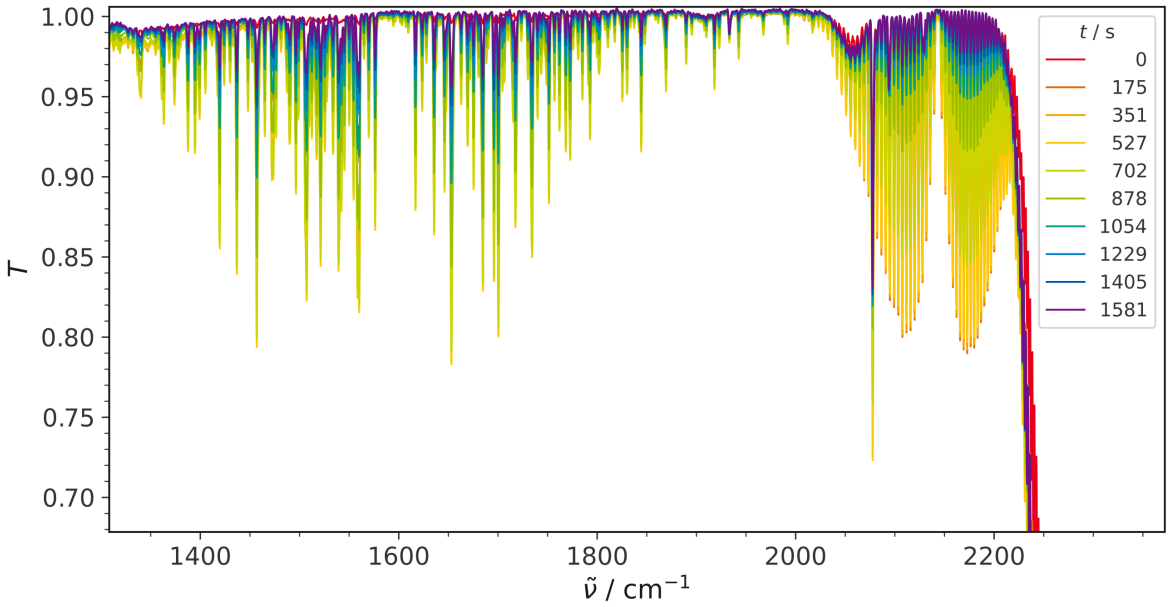

Figure 5.11: Time evolution of the water and CO signals in the exhaust transmission IR spectra of CO_2 activation using the commercial H2021 cell over $AuCeO_2$ at 10 bar during one modulation period for CO_2 modulation.

Data interpretation The only way to gain at least limited mechanistic information from this data set is to discuss some reaction specific intermediates such as methoxy, whose participation in the RWGSR can be excluded but which may lead to MeOH or CH_4 formation [50, 62]. As indicator for the RWGSR, bidentate carbonate can be assumed, which has, according to the chapter on RWGSR (see section 5.1) and earlier literature [11] been identified as an active species during RWGSR. Rezvani *et al.* have, on a comparable catalyst and at a pressure of 5 bar, not proposed bidentate carbonate as an active species in CO_2 activation toward MeOH [50], so it can be assumed, that it is primarily linked to the RWGSR pathway. On the other hand, Rezvani *et al.* reported in the same paper, that formate seems to play an important role in MeOH formation over Au/CeO_2. In the study of the RWGSR within this work it was possible to exclude formate from playing an active role in RWGSR (see section 5.1), so this species may serve as an indicator for the activity of the system towards MeOH production.
Regarding the RWGSR taking place, identifiable by gaseous CO being created, it can be stated, that no hints of adsorbed CO species in the carbonyl region are present besides the signal of gaseous CO (see fig. 5.15). Interestingly, no contributions of gold hydrides are detectable within the PSD spectra either, even though the RWGSR-experiments at atmospheric pressure and with other gas phase compositions (see section 5.1) have pointed out their relevance to the mechanism. This may lead to the conclusion that under these conditions either the ability to detect Au-H species is limited, or that the mechanism takes another route bypassing this type of intermediate species, as discussed in [11], where another active hydrogen species besides the gold hydrides is proposed to be gaseous H_2.
Concerning the mechanistic sequence, previous studies have already pointed out, that there is a non-negligible contribution of a redox mechanism besides the dominating adsorbate-driven associate mechanism for this material during RWGSR [11]. If such a shift towards a redox mechanism would be the case, one would consequently have to doubt, whether bidentate carbonate holds as an indicator for the RWGSR activity. When looking at the time values in table 5.3, signals that may be assigned to bidentate carbonate at 1270 (176 s) and 1623 cm^{-1} (211 s) appear earlier or at least at the same time as that of the RWGSR's product CO (211 s), so an associative mechanism via bidentate carbonates towards CO formation remains at least plausible. But due to the huge experimental uncertainty, all results from these data sets have to be considered carefully and unambiguous statements cannot be given.
Potential methoxy signals can be seen at 2789 and 1044 cm^{-1}, plus a signal at 2833 cm^{-1}. The signal at 1044 cm^{-1} is assigned to methoxy's ν(OC) vibration, while the signals at 2789 and 2833 cm^{-1} can be traced back to its characteristic CH vibrations [44]. But the latter CH vibration at 2833 cm^{-1} may as well be due to the redox-state dependent shifting of the formate CH signal, which was already discussed in the previous chapter concerning the RWGSR (see fig. 5.4).
Formates that, according to Rezvani *et al.*, were identified as indicative of the reaction towards MeOH but that may as well appear in the aftermath of the RWGSR (see section 5.1), can be seen at 2969, 2868, 2833 and 1565 cm^{-1} but the signal at 2833 cm^{-1} coincides with a possible methoxy feature [44]. Interestingly, only the potential formate CH vibrations are visible, while features at lower wavenumbers, that is in the carbonate region between 1300 and 1400 cm^{-1}, are not detected. Except for the signal at 1565 cm^{-1}, which appears as latest of all signals observed (264 s), the time values of these signals are all smaller than for the methoxy species, as can be seen in table 5.3. Usually, this would lead to the conclusion, that these signals may be connected and that methoxy species may be a product of formate transformation. Surprisingly, however, all methoxy species show a decreasing behavior when CO_2 is pulsed, indicated by the negative sign (-) in table 5.3. This is in stark contrast to the increase observed for the putative formate signals, which can be seen in table 5.3. This inverse behavior is puzzling, since the signals identified as belonging to methoxy species are the only ones that show this negative correlation with pulsed CO_2 and thus with the introduction of the reaction gas atmosphere, as can be seen in table 5.3 and for a comparable experiment in fig. 5.19. A negative value in table 5.3 does not only mean a decreasing trend during the first half of one modulation period, where

Table 5.3: Most prominent signals, their time values derived from PSD and assignments from the full spectrum of the high pressure CO_2 activation over Au/CeO_2 in fig. 5.8 (CO_2 modulation) using the commercial H2021-cell. Negative signs indicate signals that decrease when turning CO_2 on, the period length is 1581 s.

$\tilde{\nu}$ / cm^{-1}	t / s	Assignment
3629	136	CO_2 (g)
3733	136	CO_2 (g)
1181	176	Carbonates
1270	176	Bidentate carbonate
3854	180	H_2O (g)
2969	189	Formate
2864	206	Formate
1623	211	Bidentate carbonate
2073	211	CO (g)
2789	(-)215	Methoxy
1044	(-)233	Methoxy
1315	242	Carbonates
2833	(-)242	Formate / Methoxy
1098	259	Carbonates
1565	264	Formate / carbonates

in this case the reaction gas phase with CO_2 and H_2 is present, but also an increasing behavior in the second half, in which only H_2/Ar flows through the reaction cell. This may indicate, that methoxy is not a species that directly succeeds from carbonates or formates that emerge from CO_2 adsorption in the first half of the period, as can be seen from their time values in table 5.3. A possible explanation could be that it still originates from the aforementioned adsorbates, but only during the reductive phase in the second half of the modulation period, when only H_2/Ar flows through the reaction chamber. This would explain, why all other signals in the carbonate region appear during the reaction gas phase and disappear during the reductive phase, while for methoxy it is vice versa.
In addition, further information can be extracted from fig. 5.17 that gaseous MeOH, indicated by a sharp signal originating from its Q-branch at 1033 cm^{-1}, seems to appear in the same half of the modulation period (reaction phase) as all the other signals in the carbonate region, also opposite to methoxy. Unfortunately, this signal's time value cannot be extracted, as it is entirely dominated by the surrounding ν(OC) vibration signal of adsorbed methoxy, only being a small dip in the latter signal. But despite all the caveats, this may still lead to the conclusion that MeOH can only be formed from methoxy and is ultimately released from the surface during the reaction phase in which CO_2 is added to the system, perhaps via displacement of the adsorbed methoxy by the newly formed carbonates. Since all time values in this experiment are not fully reliable, further experiments are definitely needed to make the spectra more interpretable, which will be addressed in the following sections on the design and subsequent application of a new cell adapted to high-pressure conditions.
Further challenges with the data set are illustrated by the water signal and its associated co-products such as gaseous CO or adsorbed methoxy. Looking at table 5.3, there is a large gap of 31 s between the time of CO formation (211 s) and the time of water appearance (180 s), as well as a gap of 35-62 s between the time at which potential methoxy signals respond (215-242 s) and water (180 s). However, since water may also respond when MeOH is released rather than at the time of methoxy formation, these data are further

complicated and the information is blurred. Thus, in this case, no correlation of the signals seems obvious due to the simultaneous presence of multiple reactions. For example, in the experiments on the RWGSR, where there was only one possible reaction pathway, it was observed that CO and water appeared at essentially the same time.

In conclusion, all these findings from the present data should be taken with extreme caution due to the experimental limitations discussed, but can still serve as an interesting preliminary study. In order to overcome the aforementioned design hurdles of the commercial H2021 cell, it will be necessary to completely replace it with a new construction similar to the LVVC already described in section 4.2, which has to have a low cell volume but also be adapted for use at high pressures up to 27 bar, which is not the case for the LVVC presented in section 4.2.

5.2.2 Construction of a low void volume reaction cell for high pressure experiments

The original LVVC discussed in section 4.2 was not applicable to high pressures, as it has not been designed to withstand such conditions. The weak point of the old LVVC when it comes to applying elevated pressures in the reaction chamber is the large inner volume, which was intended to thermally isolate the heating cartridge and the adjacent sample from the surrounding block with the O rings and the dome by limiting the number of thermal bridges (see fig. 4.6). Therefore, a new high pressure low void volume cell (HP LVVC) was designed to resemble the original design of the LVVC's interior but without the weak point created by its hollow body. In particular, the structure of the reaction cell's part through which the gas flows is exactly the same and thus also its fluid dynamic properties are identical to the ones discussed in section 4.2.

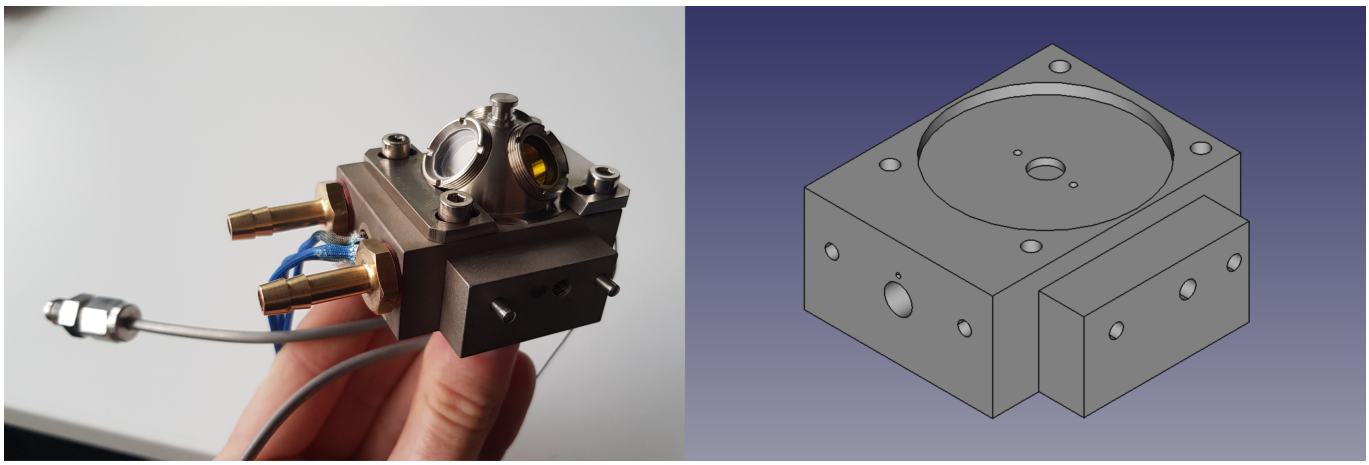

Figure 5.12: Final version of the HP LVVC both as it looked in reality (left) as well as the 3D design of the cell body without the commercially available dome (right).

Temperature calibration Temperature calibration of the cell was executed using a VOLTCRAFT M-4660A multimeter equipped with a Type K thermocouple. For this purpose, the spectroscopy window was replaced by a Teflon plate with a small perforation for inserting the thermocouple. After insertion, the thermocouple was firmly contacted with the bottom of an empty sample tray. The calibration was executed at atmospheric pressure and at a flow rate of 60 $mL_n min^{-1}$ Ar. The optional cooling circuit was not connected. The results can

be seen in table 5.4 which yielded the following equation of calibration:

$$T_{\text{sample tray}} = 0.99 \cdot T_{\text{controller}} \tag{5.1}$$

Table 5.4: Results of the newly designed HP LVVC's temperature calibration.

$T_{\text{controller}}$ / °C	$T_{\text{sample tray}}$ / °C
25	25
50	50
100	100
150	150
200	198
250	248
260	258

Switching experiments to determine the fluid dynamic parameters Switching experiments are designed similar to the ones discussed in section 4.1 but with flows similar to the catalytic experiments that were carried out during CO_2 activation at elevated pressures, that is switching from H_2/Ar to H_2/CO_2 with in both cases a ratio of 3/1 at 60 $mL_n min^{-1}$. Unfortunately, flows higher than that were not accessible due to limitations of the high pressure capable mass flow controllers. The fluid dynamic parameters were measured at pressures of 1, 5, 10 20 and 27 bar. The cumulative distribution curves are shown in fig. 5.13 and the fluid dynamic parameters derived from this are listed in table 5.5.

Table 5.5: Fluid dynamic parameters that have been calculated for the the HP LVVC at a flow rate of 60 $ml_n min^{-1}$.

p / bar	$\bar{\tau}$ / s	$<t^2>$ / s^2	σ^2 / s^2	σ / s	$\bar{\tau} + 3\sigma$
1	2.5	6.9	0.5	0.7	4.6
5	21.3	513.3	61.2	7.8	44.7
10	39.6	1793.0	229.0	15.1	85.0
20	75.3	6500.6	830.4	28.8	161.7
27	95.9	10346.9	1149.1	33.9	197.6

From table 5.5 it can beseen, that at a pressure of 10 bar and by using the HP LVVC, a residence time of 39.6 s is obtained and a full gas phase exchange is observed after 85 s, by far lower than the estimated 11 min that were observed for a complete gas phase exchange in the commercial H2021-cell under these conditions (see fig. 5.7).

5.2.3 Applying the new cell for detailed mechanistic understanding

Experimental details Due to the different behavior of the HP LVVC compared to the commercial H2021 cell discussed previously, the modulation parameters were set as follows: 20 periods with a length of 729 s during which 160 spectra were taken with 5 interferograms averaged into one. Thus the time needed for the accumulation of one spectrum was 4.6 s.

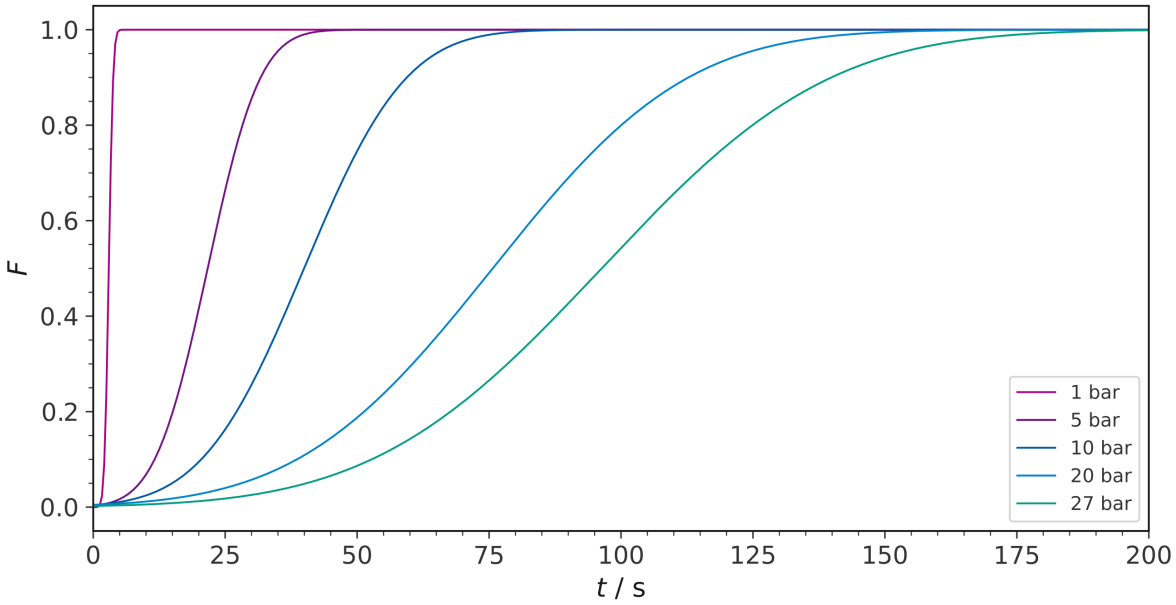

Figure 5.13: Cumulative distribution curves of the step input experiment at 60 $ml_n min^{-1}$ using the custom HP LVVC cell at multiple pressures, which are given in the legend. At a time of 0 s the valve was switched from 75 % H_2/25 % Ar to 75 % H_2/25 % CO_2. The sample (KBr) temperature was 110 °C.

To be able to compare the new results to the ones obtained using the H2021 cell, the same catalyst under the same conditions was used, thus the temperature was chosen to be 250 °C, the gas composition was 25 vol% CO_2/75 vol% H_2, and the flow rate was 60 $mL_n min^{-1}$. During modulation experiments, CO_2 was periodically exchanged with the equivalent flow of argon. Background spectra were measured after one modulation period at reaction temperature as pretreatment.
Unfortunately, these experiments were not conducted in an *operando* mode due to a lack of available spectrometers to monitor the exhaust.

Spectra of HP CO_2 activation with the HP LVVC At first glance, the PSD spectra generated when using the HP LVVC in fig. 5.14 resembles the one acquired during CO_2 modulation using the H2021 cell in fig. 5.8. But when taking a closer look, some major differences can be seen, especially for the products MeOH, CO and CH_4, that have been easily identified in case of the H2021-experiments via a qualitative gas phase analysis but that were also visible in the PSD spectra (see figs. 5.15 to 5.17). In case of the HP LVVC-experiments, there was no analysis of the exhaust gases available and, unfortunately, there is way less gas phase signal visible in the DRIFT spectra (see figs. 5.15 to 5.17).
Most strikingly, there is almost no CO visible in the carbonyl region, as depicted in more detail in fig. 5.15, but rather signals, that can be related to high concentrations of CO_2 as reported by Fehr *et al.* [63]. At first glance this is a good sign, as a low abundance of gaseous CO implicates only a low activity of the catalyst in the RWGSR. Also when looking at the CH-region around 3000 cm^{-1}, no signal is visible related to gaseous CH_4, the other side-product. Such a signal would be present at least in form of a bump at 3017 cm^{-1}, where its Q-branch has been observed in the PSD spectra when taking the H2021-cell in fig. 5.16. Unfortunately, this pattern seems to apply for the desired product, MeOH, as well. When looking at the region around 1000 cm^{-1} a clearly identifiable signal of gaseous MeOH is expected with its intense Q-branch at 1033 cm^{-1} (see fig. 5.9),

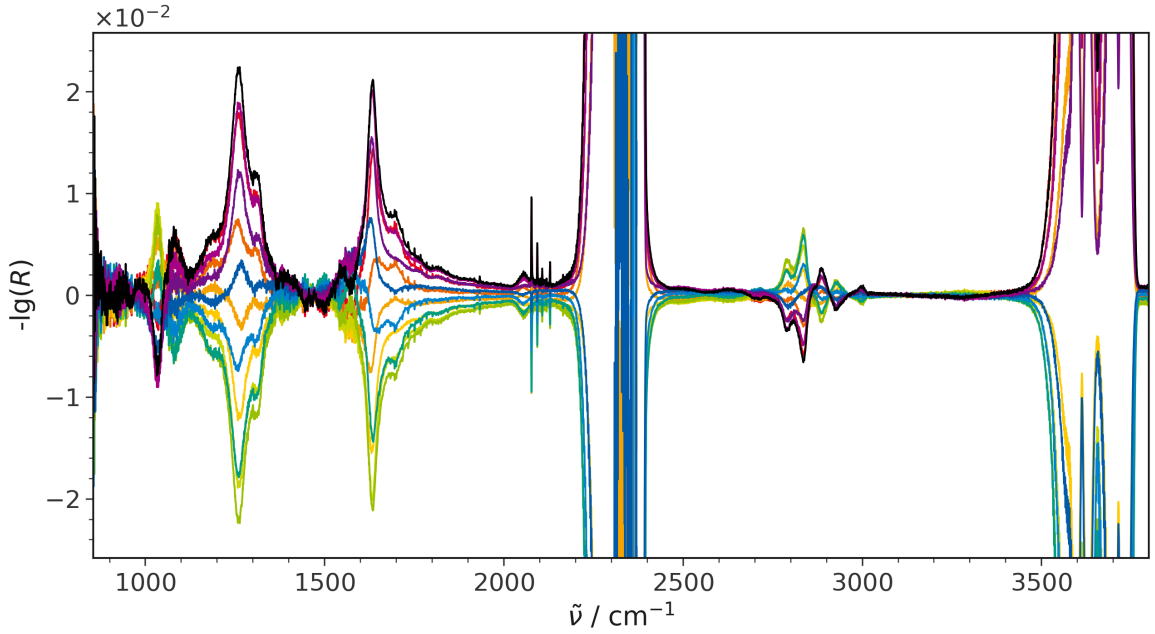

Figure 5.14: PSD spectra of CO_2 activation over $AuCeO_2$ at 10 bar for CO_2 modulation using the HP LVVC.

that can also be observed in the PSD-spectra of the H2021-experiments but not when using the HP LVVC (see fig. 5.17).
When looking at the carbonate region (see fig. 5.18), the abundance of gaseous water for the H2021-experiments can easily be identified via the large amount of sharp signals in the region from 1300 to 1900 cm^{-1} but for the HP LVVC-experiments, these signals are way less pronounced, which may be an indicator for significantly less reaction taking place or due to the faster exchange of the gas phase in the detectable reactor volume.
According to the literature by Badri *et al.* [64], some characteristic signals are detected, that can be assigned to methoxy on a reduced surface. The main signals of CH-vibrations can be found at 2790, 2836 and 2928 cm^{-1}, and the ν(OC) vibration at 1036 cm^{-1}. The signal at 2790 cm^{-1} is assigned to the $\nu_s(CH_3)$ vibration, while the other two are assigned to a Fermi resonance of $\nu_a(CH_3)$ and the $\delta(CH_3)$ vibration's first overtone. All four of these show a somehow similar behavior and decrease when CO_2 is switched on, although the time values do not match for all of these signals (see table 5.6).
Signals of potential carbonate species can be seen at 1082, 1310, 1698, 1260 and 1633 cm^{-1}. The signals at 1310 and 1698 cm^{-1} appear at 41 and 45 s respectively, which is within each signal's experimental uncertainty of 4.6 s and may therefore belong together. The other signals at 1082, 1260 and 1633 cm^{-1} exhibit totally different time values of 26, 59 and 77 s, which is far out of the aforementioned experimental uncertainty. But for all these signals it has to be noted, that there are spectral overlaps between features at 1036 and 1082 cm^{-1}, 1633 and 1698 cm^{-1} as well as 1260 and 1310 cm^{-1}, so that further blurring of the time values cannot be excluded.
Traces of CO that can be seen in fig. 5.15 exhibit time shifts of 77 s, which is earlier than most of the methoxy signals and later or at least simultaneous with all the carbonate signals observed. This is in line with the observations from section 5.1, that the RWGSR towards CO is dominated by an associative mechanism, although the simultaneous presence of at least one other reaction mechanism (toward MeOH) if not two

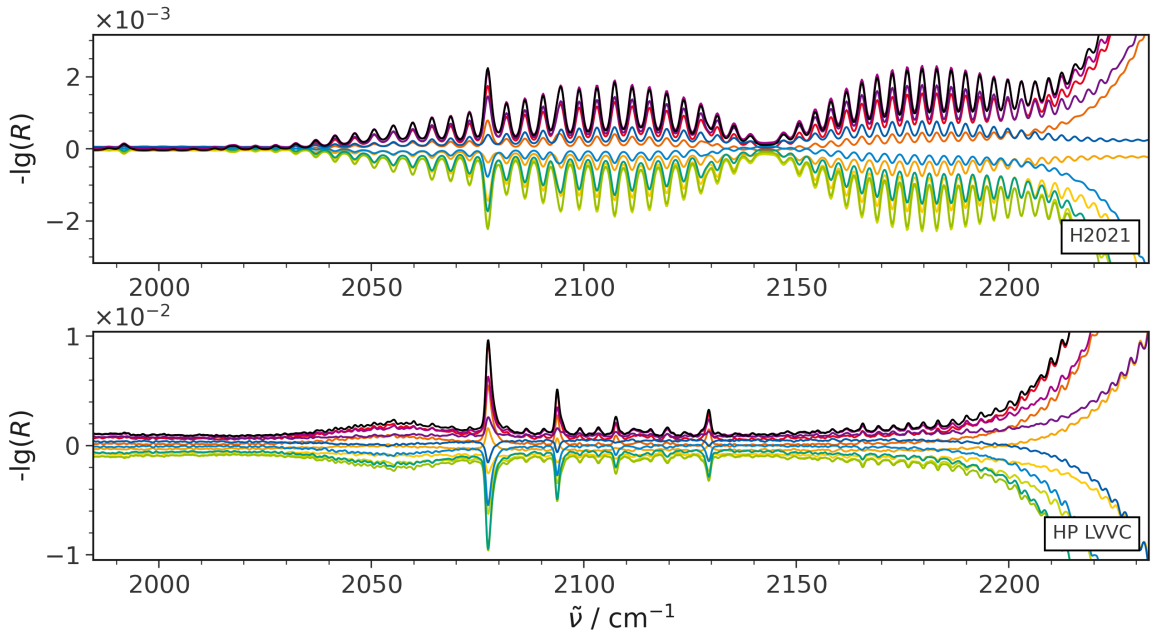

Figure 5.15: Comparison of CO regions of the PSD spectra during CO_2 activation over $AuCeO_2$ at 10 bar for CO_2 modulation using the H2021 (top) and the HP LVVC (bottom).

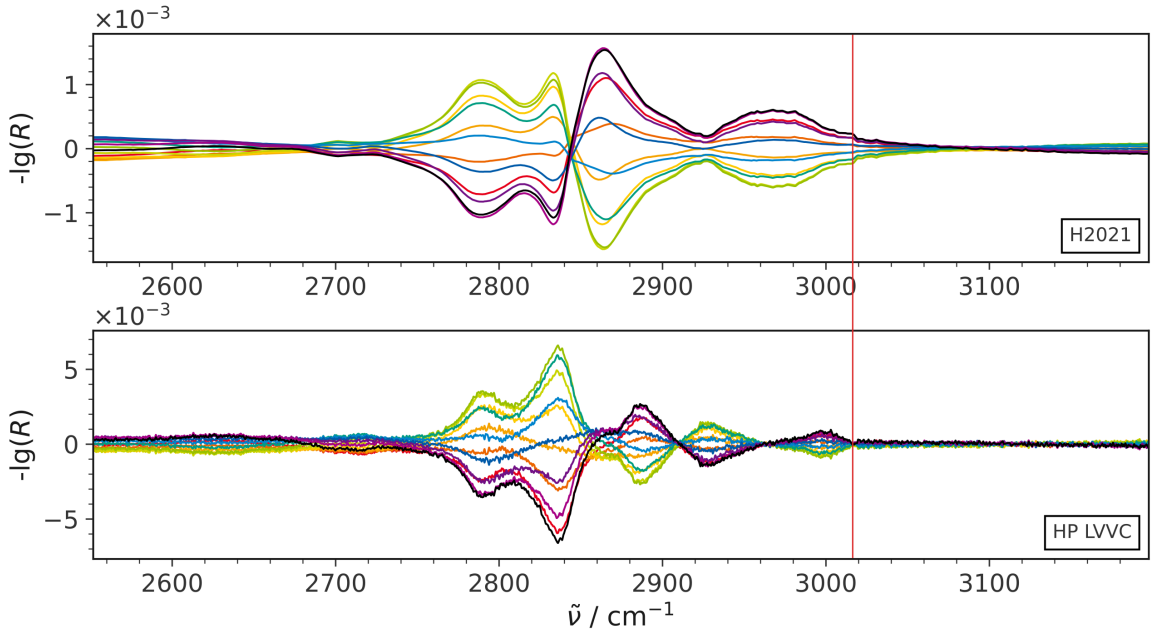

Figure 5.16: Comparison of CH regions of the PSD spectra during CO_2 activation over $AuCeO_2$ at 10 bar for CO_2 modulation using the H2021 (top) and the HP LVVC (bottom). The position of the Q-branch of CH_4 is indicated by a red line.

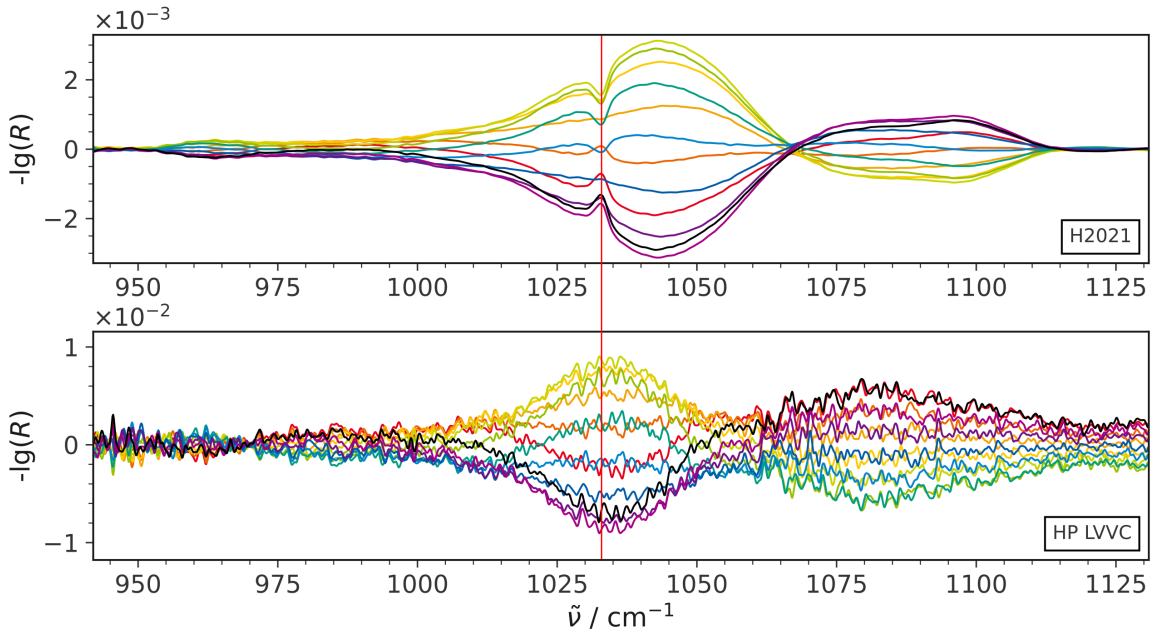

Figure 5.17: Comparison of the regions of the PSD spectra where a distinct MeOH signal is expected during CO_2 activation over $AuCeO_2$ at 10 bar for CO_2 modulation using the H2021 (top) and the HP LVVC (bottom). The position of the Q-branch of MeOH is indicated by a red line.

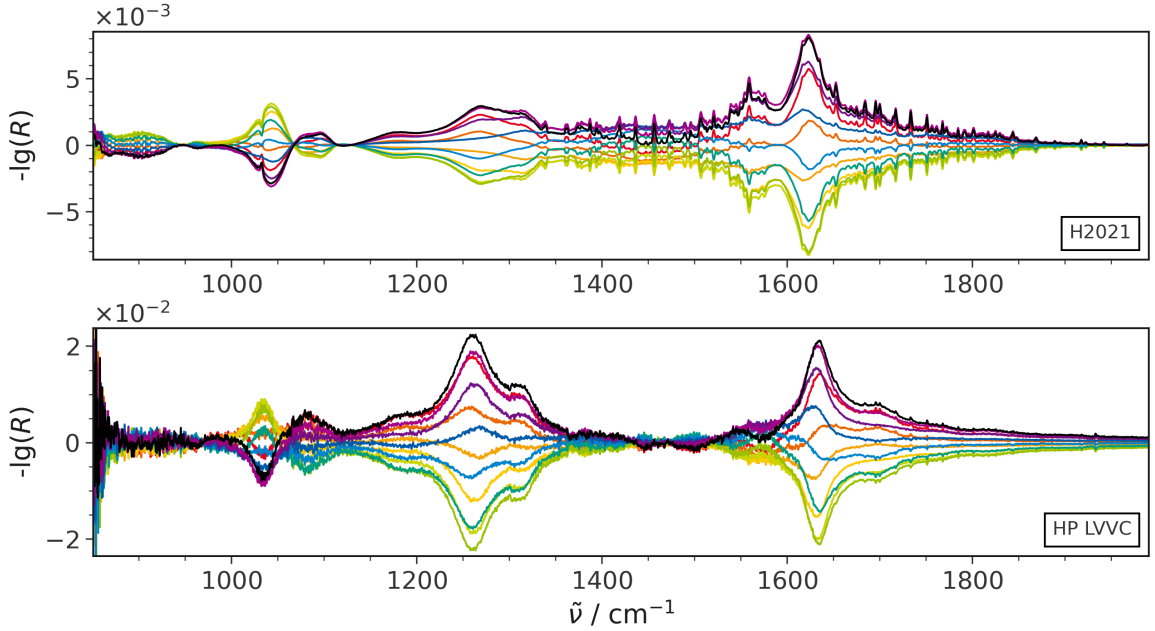

Figure 5.18: Comparison of the carbonate regions of the PSD spectra during CO_2 activation over $AuCeO_2$ at 10 bar for CO_2 modulation using the H2021 (top) and the HP LVVC (bottom).

Table 5.6: Most prominent signals, their time values derived from PSD and assignments from the full spectrum of the CO_2 activation over Au/CeO_2 in fig. 5.14 (CO_2 modulation) using the HP LVVC. Negative signs indicate signals that decrease when turning CO_2 on, the period length is 729 s.

$\tilde{\nu}$ / cm^{-1}	t / s	Assignment
1082	26	Carbonates
2077	26	CO_2 (g)
3630	26	CO_2 (g)
1310	41	Carbonates
2836	(-) 41	Methoxy
1698	45	Carbonates
1260	59	Carbonates
1633	77	Carbonates
2099	77	CO (g)
3000	81	CH
2790	(-) 85	Methoxy
2886	95	Methoxy
1036	(-) 122	Methoxy
2928	(-) 122	Methoxy

(toward MeOH and CH_4) makes it difficult to draw clear conclusions.
Furthermore, the adsorbate structure in the carbonate region does not really match the findings from the RWGSR experiments (see section 5.1), where important contributions of bidentate carbonates to CO formation via the associative pathway were observable and where it was possible to exclude all contributions of formate species, not because of their absence but because of their late appearance in the mechanism. The patterns of both these species cannot be observed in the spectra measured using the HP LVVC, even though in the experiments with the commercial H2021 and its long residence times, they have been detectable (see figs. 5.16 and 5.18).

Interpretation The signals at 2836 and 2886 cm^{-1} have already been seen in works of Badri and coworkers [64] as a pair of signals, that seem to transform into one another when reoxidizing the methoxy covered ceria surface. A similar behavior has been observed for the signal at 2790 cm^{-1}, blue-shifting roughly 10 cm^{-1} when the system is being reoxidized. Here, this shift is not observable, indicating, that either the reoxidation is not strong enough with 75 % H_2 in the atmosphere or that methoxy is consumed. And knowing that all of the methoxy-signals decrease when switching CO_2 on, it indeed seems, that the adsorbed methoxy is consumed one way or another. The most probable way for this should be an increasing desorption of MeOH into the gas phase, as the experiments in the previous section with the commercial cell have proven MeOH to emerge from the system (see section 5.2.1). The large amount of CO_2 (25 %) may facilitate replacing adsorbed methoxy by forming carbonates, as indicated by diverse signals in the carbonate region (see table 5.6).
Another way of consuming methoxy may be its transformation into other adsorbates but when looking at the signals and their time values in table 5.6, a species would have to be found, that shows a positive time value at least comparable to the methoxy species' signals. But as four out of five supposed methoxy signals respond as the latest group of signals in the PSD spectra, this hypothesis faints, as there appears to be no such species available. Thus the other possibility of methoxy leaving the surface as MeOH via the gas phase seems more likely, even though there is no doubt-free evidence for this process yet. However, such an evidence may be provided e. g. by conducting *operando* measurements including gas phase monitoring of products as it has

been the case for the experiments utilizing the H2021 in section 5.2.1. With this setup, almost identical to the one used here except for the reaction cell and of course the second spectrometer, it has been possible to prove the emergence of MeOH through *operando* gas phase analysis. This fact may at least serve as a hint, that the system can and is likely to produce MeOH even in this slightly different setup.
Interestingly, it was impossible to confirm any presence of formates in the spectra, as characteristic signals at about 2850 and 2940 cm^{-1} and in the carbonate region between 1300 and 1400 cm^{-1} (see the RWGSR experiments in tables 5.1 and 5.2) are missing in the PSD spectra when using the HP LVVC (see fig. 5.16), even though at least the intense CH signals have been present in the experiments using the commercial H2021-cell in section 5.2.1. Therefore, and as the clear methoxy-signals indicate an activity of the system towards MeOH-formation, the arguments of Rezvani *et al.* cannot be proven, who proposed a formate-mediated mechanism based on the results of H/D-SSITKA [50] for their experimental setup. But as already mentioned, when looking at the CH region of the commercial H2021-cell in fig. 5.16, signals at 2864 and at around 2969 cm^{-1} have been identified, that better fit these assignments and are therefore likely to be linked to formate species.
But in the case of the experiments using the commercial H2021-cell, a far higher CO production has been observed as well (see fig. 5.15), which means, that the stronger presence of formates may only indicate an elevated RWGSR-activity. This may as well have been the case in the study of Rezvani *et al.*, where a large part of the CO_2 conversion goes into CO formation too [50]. However, information that still needs to be gathered to support this claim is the activity data of the system and its selectivities towards CO, MeOH and perhaps CH_4 with this cell. Nevertheless, the experiments performed in this work have provided important preliminary insights that have already allowed to propose a plausible mechanism (see fig. 5.20) which can now be strengthened by future *operando* experiments.

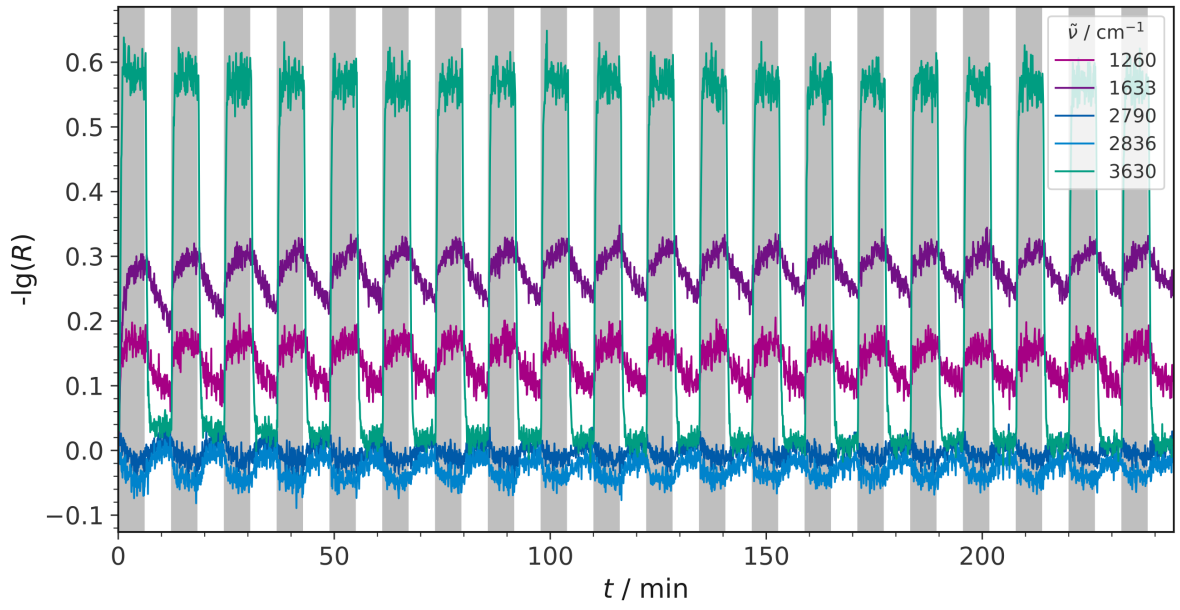

Figure 5.19: Time evolution of selected methoxy (2790 and 2836 cm^{-1}), carbonate (1260 and 1633 cm^{-1}) and CO_2 (3630 cm^{-1}) signals during the whole CO_2 modulation experiment. CO_2 was switched on in the gray areas and switched off in the white areas.

Proposing a reaction mechanism One important observation that the proposed mechanism will build upon is, that the methoxy species observed show a decreasing behavior during phases with reaction gas atmosphere while increasing during the H_2/Ar phase.
As already discussed in the wake of the experimental series described in section 5.2.1, this is the only set of signals exhibiting such a behavior, while all other adsorbates show an opposite trend, which is depicted in fig. 5.19 for some selected signals. This suggests, that methoxy species are formed during the reductive H_2 phase and presumably desorb in the reaction gas phase when CO_2 enters the system.
Therefore, it appears as if the methoxy species are displaced during the reaction phase by adsorbing CO_2 and the emerging carbonate species. However, the latter may convert wholly or partially to methoxy in the purely reducing H_2/Ar phase and restore the surface loading with this adsorbate species. In case of the previous experiments with the commercial H2021-cell it was even possible to identify a characteristic signal of gaseous MeOH at 1033 cm^{-1} pointing in the opposite direction than the signals of adsorbed methoxy did (see section 5.2.1), which supports the previously established hypothesis.
Concerning formates, they seem not to be involved in the supposed mechanism as this species's specific features lack in the spectra. On the other hand there are signals in table 5.6 that may indicate the involvement of different not further identified carbonate species.
The absence of signals from gold-related species in the spectra is another interesting observation that requires more in-depth studies. As in the case of the RWGSR in section 5.1, actively participating gold hydrides have been identified to play a crucial role in the formation of CO, but here no comparable species have been observed. Even in the previous section where the same setup in comparable experiments but with the commercial cell has produced significant amounts of CO, no gold-related species were observable. This raises the question of whether the role of gold in this mechanism is only electronic in nature, or whether it was simply not possible to detect these species under the high pressure conditions applied. But this question has to be addressed in future investigations. In particular, a comparison of bare ceria and gold-loaded catalysts with different loadings would be a promising series of experiments for the future.
Furthermore, activities of the catalysts used here still have to be quantified, especially using the HP LVVC, where not even qualitative evidence of MeOH formation exists, apart from some indications by the adsorbed methoxy species discussed above. However, if the assumptions made here are correct, some new conclusions can be drawn about the activation of CO_2 over Au/CeO_2 at elevated pressures (in this case 10 bar), which are illustrated in fig. 5.20 and explained in the following: **1.** It seems like long residence times tend to favor CO formation via the RWGSR visible when comparing results from the high void volume H2021-cell and the low void volume HP LVVC. **2.** Contrary to propositions from literature, stating an important active role of formates during MeOH formation, there are first indications, that they are not involved due to their absence despite clear evidence of adsorbed methoxy-species present. **3.** Methoxy seems to be a species that tends to accumulate on the surface and which needs to be displaced to be released in the form of MeOH. This is indicated by the decreasing behavior of the methoxy signals in table 5.6 and figs. 5.16 and 5.17 when the second reactant (CO_2) is switched on in the reaction phase and furthermore by an increasing behavior after turning the CO_2 supply off, entering a reductive H_2-phase, in which the carbonates that have been formed during the reaction phase decrease in intensity, thus seemingly being hydrogenated to methoxy.

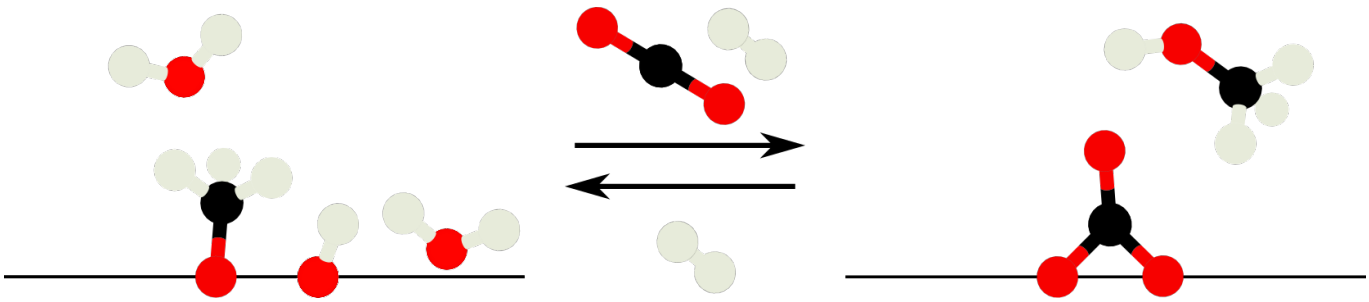

Figure 5.20: Proposed behavior (non-stoichiometric) of the Au/CeO_2 catalyst during the modulation procedure applied in the high pressure CO_2-activation experiments.

6 Application of MES to Cu/CeO_2

6.1 Understanding the working principle of the WGSR mechanism over Cu/CeO_2

Large parts of the following chapter have been adapted with permission from already published work [65]. Copyright 2022 American Chemical Society.

Cu/CeO_2 catalysts are very promising materials for low temperature (LT) WGS, showing good conversions [66–69]. Previous studies have revealed, that the catalytic activity increases with the Cu loading [70, 71], therefore most studies have focused on catalysts with high Cu loading [66, 68, 72]. However, low loaded catalysts such as the materials investigated here, show higher conversions normalized to the Cu content [71]. In the literature on supported metal oxide catalysts such as this system, two main mechanisms are currently discussed: the redox and the associative mechanism. Which mechanism is ultimately more important and dominant has to be clarified for each system individually [73, 74].
Up to now, especially for Cu/CeO_2 catalysts, the interaction of metallic copper with oxygen vacancies has been proposed to increase the reactivity [75]. This is backed up by studies in which the defect-rich ceria is proposed to be primarily active in the dissociation of water, whereas metallic copper is proposed to provide adsorbed CO for the reaction [76]. However, in later studies, carbonates have been proposed to act as intermediates using *operando* SSITKA-DRIFTS (steady-state isotropic transient kinetic analysis-diffuse reflectance infrared Fourier transform spectroscopy) and *in situ* DRIFTS [66, 77].
When studying this system, several techniques were used such as *operando* UV/Vis, Raman and quasi *in situ* XPS together with ME-DRIFTS to obtain a holistic picture of the reaction mechanism [65].
Initial results from *operando* Raman and UV/Vis spectroscopy are consistent with a redox mechanism, although no direct correlation of activity with overall reducibility is shown when comparing ceria supports with different surface facets. Further investigations of the subsurface and bulk oxygen dynamics via *operando* Raman spectroscopy included a detailed analysis of the redox-sensitive F_{2g} mode, which, when coupled with the application of $H_2^{18}O$, has been able to underline the importance of oxygen transport properties and its surface availability thus being another hint towards a redox mechanism. But in order to fully determine whether a redox or associative mechanism was involved, ME-DRIFTS was applied as it is primarily focused on the surface adsorbates and their temporal succession during the reaction. Proving or disproving their involvement would be the final step in assessing the reaction mechanism at hand.

Experimental details A measurement series consisted of 20 periods of 292 s each. For each spectrum, five consecutive interferograms were averaged so that a spectrum is acquired approximately every 3.7 s. This value is also used to approximate the experimental uncertainties of the time values derived from phase sensitive detection (PSD).
The catalyst investigated here is polycrystalline copper-loaded (0.46 wt%) ceria (Cu/CeO_2 sheets) for which a maximum CO conversion of roughly 7 % was observed during non-modulated steady-state experiments. The copper-free samples taken as reference show a smaller activity of about 1 % [65]. Activities during modulation have not been measured quantitatively but the spectra undoubtedly show the conversion of CO to CO_2.

As background, the catalyst itself was used after a 15 min pretreatment in either H_2O atmosphere (100 $mL_n min^{-1}$ of 8 vol% H_2O in Ar) or CO atmosphere (100 $mL_n min^{-1}$ of 2 vol% CO in Ar) at the reaction temperature of 190 °C and a subsequent gas phase modulation procedure identical to one modulation period of the desired experiment, which ensures a reproducible state of the sample. The atmosphere during the background measurement was the same as during the respective pre-treatment. Spectra were measured from 850 to 4000 cm^{-1} with a resolution of 0.2 cm^{-1}, an aperture of 6 mm and a mirror speed of 120 kHz on a Bruker INVENIO-R.
During ME-DRIFTS the sample is constantly exposed to a gas phase similar to one of the three pretreatments described above. In the case of constant H_2O (kept at 8 vol%), a flow of CO is pulsed over the sample at the same time, varying from 0 to 2 vol%, and in the case of constant CO (kept at 2 vol%), a flow of H_2O is pulsed, varying from 0 to 8 vol%. In all cases, the total flow rate is 100 $mL_n min^{-1}$, balanced with Ar.

6.1.1 CO modulation reveals no active adsorbate species

In order to investigate the adsorbate dynamics and the possibility of an associative mechanism over Cu/CeO_2 sheets, the first ME-DRIFTS experiment carried out was applying CO modulation to the system (i.e. switching between 0 and 2 vol% with a constant flow of 8 vol% H_2O/Ar), which is shown in fig. 6.1. Similar experiments were also carried out using other Cu/CeO_2 samples with different surface terminations such as polyhedra, cubes and rods as well as the respective bare supports [65]. But as those show a comparable general behavior despite slight differences observed in the spectral patterns, the in-depth discussion here will be focused on polycrystalline ceria sheets. From what is visible in fig. 6.1, carbonates (850-1800 cm^{-1}), carbonyls (2000-2200 cm^{-1}) and hydroxyls (3400-3800 cm^{-1}) can be identified as candidates for potential active species taking part in the reaction.

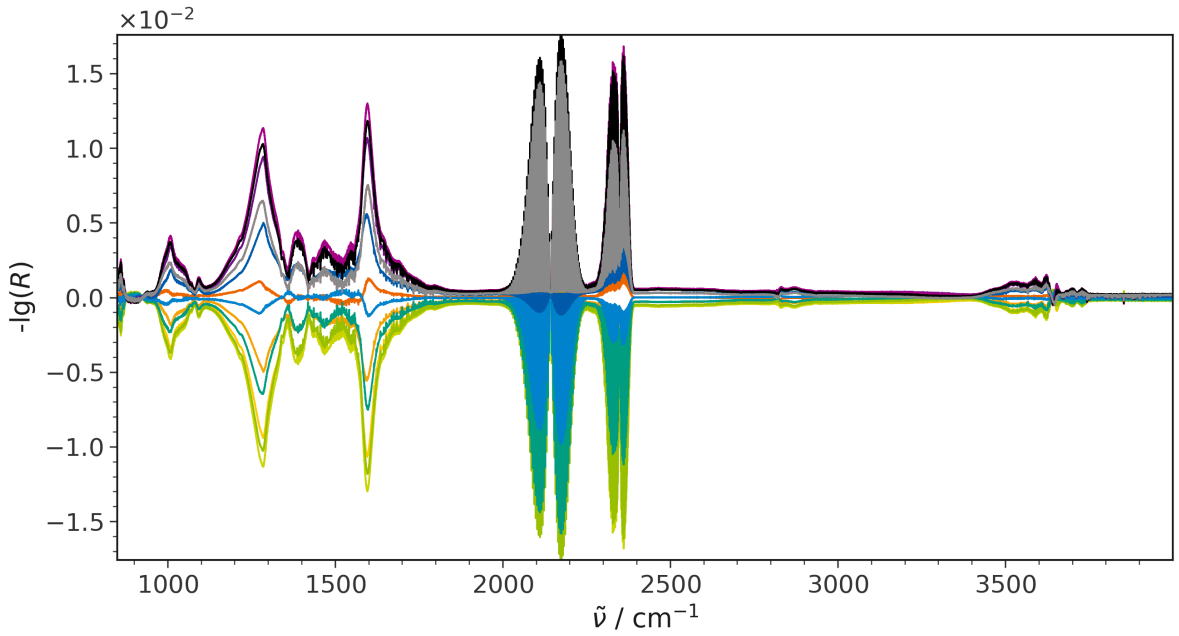

Figure 6.1: Full PSD spectra of the WGSR over Cu/CeO_2 sheets during CO modulation. Image taken from [65].

The carbonate region in fig. 6.1 is defined by intense signals at 1009, 1285, 1388, 1434, 1470, 1547 and 1597 cm^{-1}. The strongest features at 1285 and 1597 cm^{-1} can be attributed to the bidentate carbonates [11, 46], while the other signals are due to other carbonate-like species, such as bridged formates [45, 46].
Regarding the potential involvement of adsorbed CO-species, interestingly no signals are detected in the characteristic carbonyl region, except for the contributions of gaseous CO (see fig. 6.3). As preceding studies have shown that a sensitive detection of CO adsorbates is unaffected by the presence of CO in the gas phase [30], it is possible to exclude a substantial participation of CO adsorbates in the WGSR over Cu/CeO_2. This is consistent with non-transient *in situ* DRIFTS studies on low-loaded Cu/CeO_2, where no adsorbed CO was found at temperatures above 150 °C [71]. Furthermore improving temporal resolution in an additional series of experiments, with spectra being recorded every 0.5 s, did not result in any CO associated adsorbate signals.

However, when the mode of modulation is reversed by switching H_2O, a weak signal appears at about 2109 cm^{-1}, which is typical of CO-Cu^+ adsorbates (see fig. 6.3 for enlarged view and table 6.2) [78]. Given that this signal is only weak and occurs in only one modulation mode, it can be assumed, that adsorbed CO plays a negligibly small (if any) role within the WGSR mechanism. In order to confirm this behavior, steady-state DRIFTS experiments were also carried out on Cu/CeO_2 sheets (see fig. 6.2), which strongly indicate the presence of CO adsorbates under these experimental conditions. These show a band visible at 2109 cm^{-1} under CO/Ar, which significantly decreases under reactive conditions. The contribution of the well-known electronic transition at 2025 cm^{-1} [34], which is visible in steady-state experiments as well, remains constant and therefore cannot appear in the ME-DRIFTS spectra. Hence, the steady-state experiments fully support the ME-DRIFTS results.

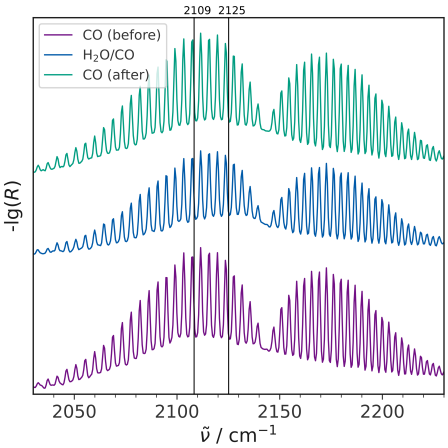

Figure 6.2: Steady-state DRIFT spectra of Cu/CeO_2 sheets. The sample itself at 190 °C under argon was used as the background spectrum and was then exposed to 2 vol% CO/Ar, 2 vol% CO/8 vol% H_2O/Ar and 2 vol% CO/Ar. All spectra were recorded at 190 °C after approximately 30 min in the respective gas atmosphere, the total flow rate was set to 100 $ml_n min^{-1}$. Modified image taken from [65].

Within the hydroxyl region, signals occur at 3530, 3622, 3642 and 3653 cm^{-1}, as well as features from the combination bands of gaseous CO_2 located at around 3610 and 3710 cm^{-1} [79]. A hydroxyl feature that can be seen at 3620 cm^{-1} is assigned to a triple bonded OH group (type III) [80], while those at 3642 and 3653 cm^{-1} are assigned to double bonded OH (type II-B and II*-B) [44], capable of transforming into each other (see below), depending on the oxidation state. Assignment of the signal at 3530 cm^{-1} is not as straightforward. So far, hydroxyl signals within 3520-3660 cm^{-1} have been attributed to bi- and tri-coordinate species [81], in agreement with the other assignments in the hydroxyl region.
Time values taken from the PSD spectra, revealing the succession of signals within a single modulation period and therefore providing valuable information about the mechanism are given in table 6.1.
The first signals to appear are those of gaseous CO, the reactant (23 s), and the reaction product CO_2 (40 s). The carbonate signals have significantly larger time values (45-50 s), similar to the hydroxyls at 3530 and 3622 cm^{-1}. The hydroxyl signal at 3653 cm^{-1} (II*-B) is increasing and that at 3642 cm^{-1} (II-B) is decreasing in the more reductive phase during the CO pulse, as would be expected from their previously reported redox behavior (see table 6.1) [44]. However, since these signals are reported to convert into one another, it is initially puzzling that they do not occur at the exact same time (with opposite sign). The deviation observed may be due to their overlapping with other signals, thereby confusing their time values, as was discussed in

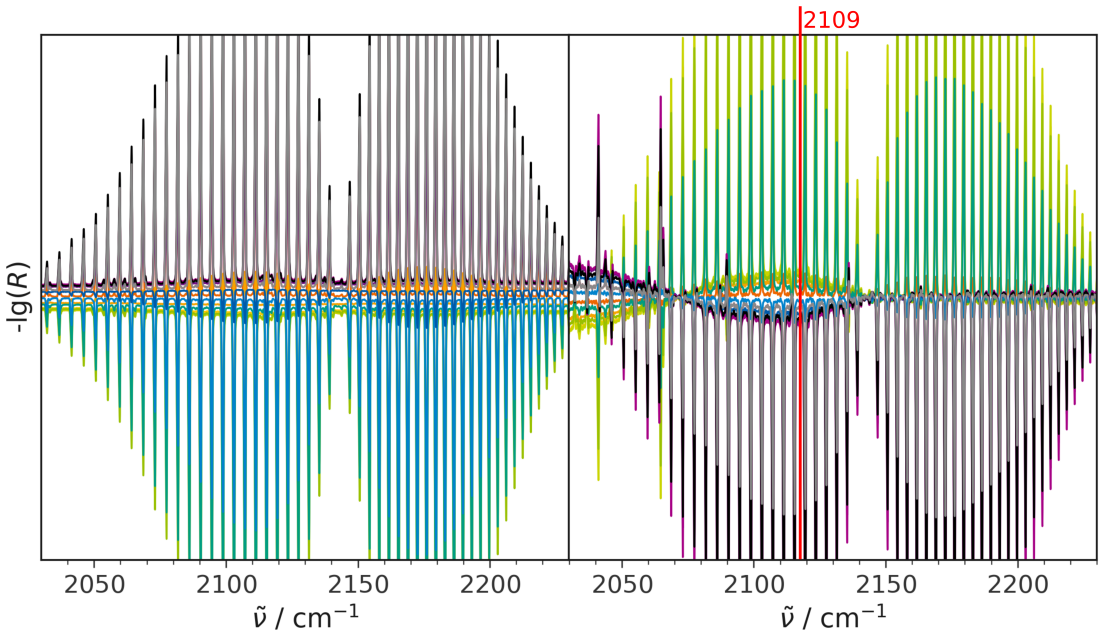

Figure 6.3: Carbonyl region of the PSD spectra of the WGSR over Cu/CeO_2 sheets during CO (**left**) and H_2O modulation (**right**). Image taken from [65].

Table 6.1: Most prominent signals, their time values derived from PSD and assignments from the full spectrum of the WGSR over Cu/CeO_2 in fig. 6.1 during CO modulation. Negative signs indicate signals that decrease when turning CO on, the period length is 292 s.

$\tilde{\nu}$ / cm^{-1}	t / s	Assignment
2064	23	CO (g)
2361	**40**	**CO_2 (g)**
3622	45	OH (III)
3530	45	OH (type III)
1597	45	Bidentate carbonate
1285	45	Bidentate carbonate
1009	46	Bidentate carbonate
3642	(-) 46	OH (II-B)
1470	48	Carbonates
1434	49	Carbonates
1547	50	Carbonates
1388	50	Carbonates
3653	73	OH (II*-B)

more detail earlier [30].
Considering the experimental uncertainty of 3.7 s for the time values, all species found in the carbonate and hydroxyl region are unlikely to be involved in formation of the product CO_2. Only the signals of bidentate carbonate and the OH signals at 45 and 46 s slightly overlap with the error range of CO_2. To investigate, whether these species may be involved, the following a different modulation approach of pulsing H_2O will be applied.

6.1.2 Corroborating evidence for a redox mechanism with H_2O modulation

Although the CO modulation experiments indicated that all the observed adsorbate signals are unlikely to be actively involved in the reaction mechanism, additional ME-DRIFTS experiments were performed using an inverted modulation procedure to get an even clearer picture of the role of the observed adsorbates. In these experiments, the 2 vol% CO/Ar flow remained constant while water was pulsed periodically from 0 to 8 vol% of the total flow. The corresponding spectra are presented in fig. 6.4. The spectra generated with the two modulation approaches (CO or H_2O modulation) are compared in fig. 6.5. Qualitative tracking of CO_2 production during these experiments using a second IR spectrometer at the exhaust showed that both modulation approaches lead to similar CO_2 conversions, indicating that the same (dynamic) conditions are reached that enable the WGS reaction.

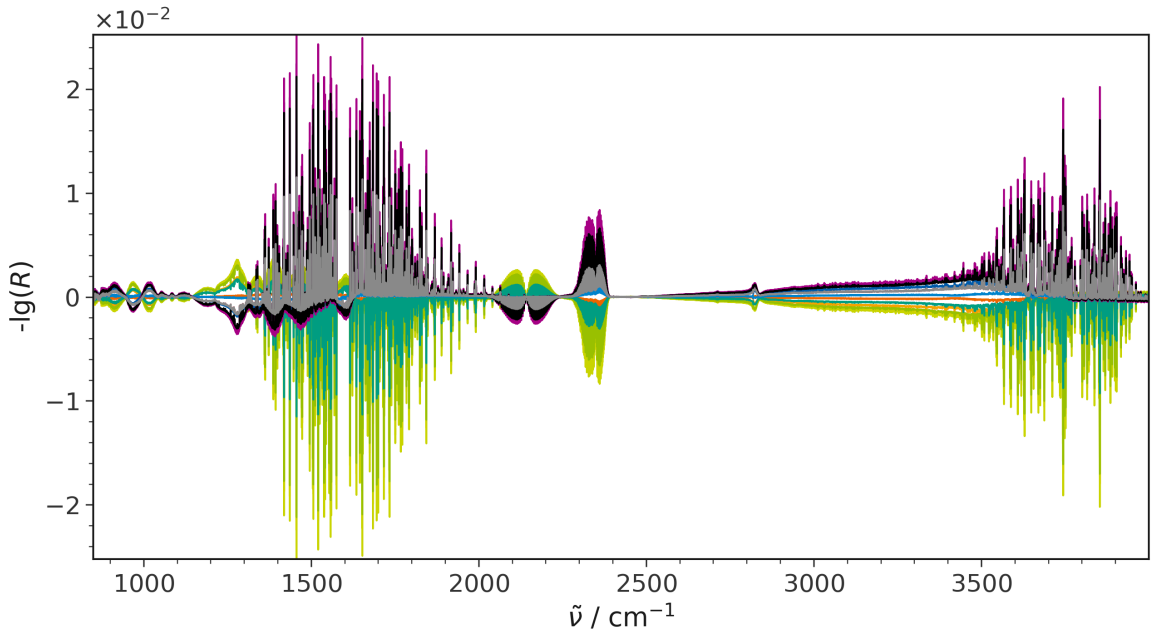

Figure 6.4: Full PSD spectra of the WGSR over Cu/CeO_2 sheets during H_2O modulation. Image taken from [65].

Analysis of the time values shows that all signals detected occur or vanish more or less simultaneously with the pulsed H_2O signal, excluding signals from CO_2 and weakly adsorbed H_2O, which lag behind by 3-5 s (see table 6.2). No clear signals are present in the hydroxyl region (see fig. 6.5), implying the absence of hydroxyls being actively involved in H_2 formation. However, it has to be pointed out, that signals of weak hydroxyls can be covered by contributions of gaseous and weakly adsorbed water in this part of the spectrum. Furthermore,

Table 6.2: Most prominent signals, their time values derived from PSD and assignments from the full spectrum of the WGSR over Cu/CeO_2 in fig. 6.4 during H_2O modulation. Negative signs indicate signals that decrease when turning H_2O on, the period length is 292 s.

$\tilde{\nu}$ / cm^{-1}	t / s	Assignment
2824	47	Formate CH
968	(-) 49	Carbonates
2183	(-) 50	CO (g)
1280	(-) 50	Carbonates
1942	51	H_2O (g)
1605	(-) 51	Carbonate
1392	(-) 51	Carbonates
1469	(-) 52	Carbonates
1017	52	Carbonates
3471	54	H_2O (ads)
2109	(-) 54	$CO\text{-}Cu^+$
912	54	Carbonates
2368	**56**	**CO_2 (g)**

the presence of a very unstable and fast-reacting hydroxyl species, as suggested in the literature, remains a possibility [71].
Comparison of the results obtained from both modulation experiments shows that spectroscopic evidence for an associative mechanism is lacking. Even though there are a few adsorbate signals present in the spectra of both the CO and H_2O modulation (see fig. 6.5), temporal analysis reveals that for the CO modulation all the adsorbate signals appear after formation of the product (see table 6.1) with only a few signals like bidentate carbonate and some triple-bonded OH appearing quite close but still after the product. But the error range surrounding each of the signal's time values of 3.7 s has at least a small overlap with the error range of the product signal's time value. However, for the H_2O modulation the signals appear slightly before formation of the product (see table 6.2), while those signals from bidentate carbonate and triple-bonded OH are completely absent, which were the only signals in the CO modulation that had a small semblance of legitimacy as active species.
To confirm the findings that the pattern of bidentate carbonates seen in fig. 6.1 cannot be observed when pulsing H_2O (see fig. 6.5), it was tried to back up that finding by D_2O modulation experiments which were intended to probe the carbonate region with less contamination from gaseous water signals. These experiments did indeed reveal the carbonate region, but nevertheless only validated the previous results of H_2O modulation experiments, i.e. the absence of any signal from an active species such as bidentate carbonate, attributable to CO_2 formation. Therefore the spectra are not shown here but are given in [65].
The lack of coherence in the observed signals can be explained by the occurrence of sorption processes when pulsing the particular reactant CO or H_2O into the system, and not by an active involvement in the reaction. Another possibility would be, that when recalling what was discussed concerning different initial states for modulation experiments in section 3.2 (see fig. 3.2), it may as well be possible, that two different states of the system that are not or hardly related were probed and that the results of both experiments cannot be directly compared. For example, the reaction may take a different pathway depending on the pretreatment of the catalyst system. Addressing the open question, whether or not the data sets from both modulation approaches are complementary, one may in future experiments apply the approach of modulating at different period lengths, an approach that has been discussed in section 3.2 and which will be applied in the following

chapter on the CO oxidation over a comparable Cu/CeO_2-polyhedra material.

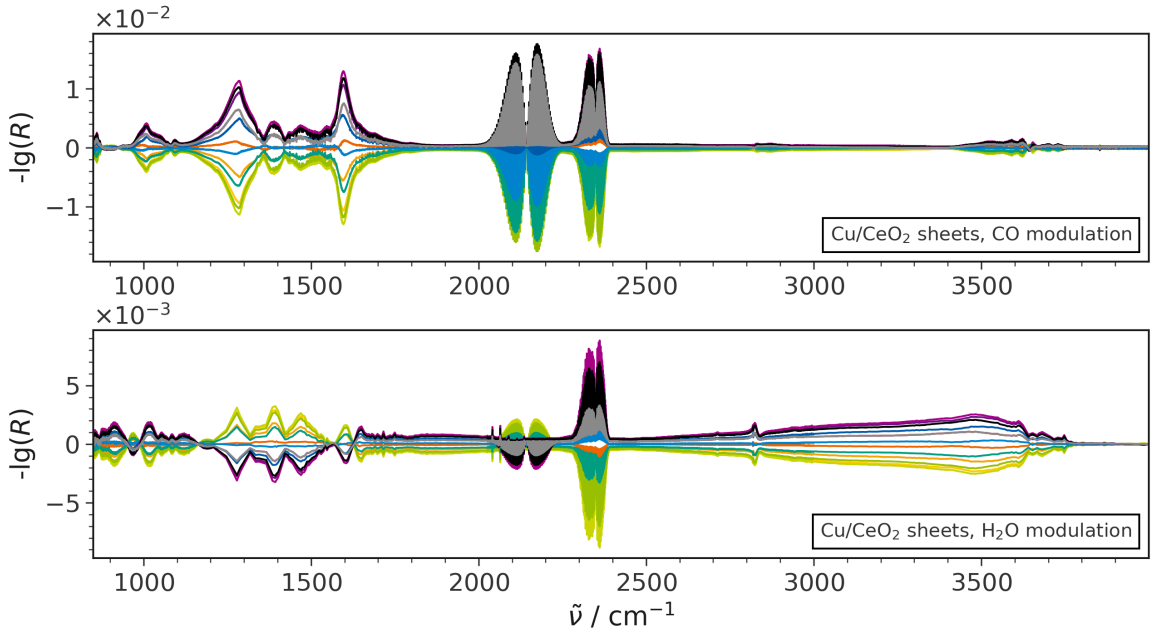

Figure 6.5: Comparison of the full PSD spectra of the WGSR over Cu/CeO_2 sheets during CO and H_2O modulation. Spectra of H_2O modulation are shown after subtraction of contributions from gaseous water. Image taken from [65].

6.2 Investigating the complex interplay of copper states during CO oxidation over Cu/CeO_2 polyhedra

Unlike the WGSR over Cu/CeO_2, where it was not possible to probe the copper state via CO adsorbates because the only copper-ceria interaction is proposed to be electronic [65], the aim is now to shed light on the copper redox behavior of these samples by subjecting them to a prototype reaction, that is CO oxidation, like it was possible for gold-ceria samples in section 4.1, where contributions of the active gold states were identified and tracked. To better understand the presumably more complex copper system, it was planned to investigate it from different perspectives. Therefore, two alternative modulation approaches were applied, as in sections 5.1 and 6.1, with in this case either CO or O_2 being pulsed while the other gas flowed constantly over the surface. This corresponds to different pretreatments of the catalyst and can lead to different "states" (e. g. concerning the degree of reduction of the system) being reached during modulation. To investigate if this state of the system is already reached and whether it is the same for both types of experiments, decreasing modulation period lengths were applied, as discussed in section 3.2. This was not possible in the case of the WGSR and RWGSR studies in the previous chapters because only the commercial H2021 high void volume cell was available. Here, the HP LVVC from section 5.2.2 was used, which allowed for rapid gas phase exchanges. These rapid exchanges, combined with varying times to reach the new state after pulsing the second reactant, allowed to use ME-DRIFTS to study more than one "snapshot" of a reaction mechanism to which the discussions were limited before. The goal here is to investigate whether the relative intensities of the individual species'

signals change as the period length (i.e. the time that the system is exposed to the reaction) is shortened, and thus to draw conclusions about possible short-lived species such as intermediates of the reaction.

Experimental details Experimental and modulation parameters were basically kept the same as for the period length-study in section 4.3. Briefly, 20 periods with a length of 60, 121 and 243 s were cycled for each data set. During these CO modulation experiments, the CO concentration was switched between 0 and 2 mol%, while the O_2 concentration was kept constant at 10 mol% with Ar as an inert carrier gas. For O_2 modulation the only difference was that 10 mol% O_2 were periodically switched on and off, while 2 mol% CO were kept constant. The overall flow rate was 100 $mL_n min^{-1}$. After baking out the samples at 250 °C to remove any residuals, they were treated for 15 min in a 10 % O_2 in Ar atmosphere at reaction temperature, which was set to 37 °C. Background spectra were measured after one modulation period at reaction temperature as pretreatment. Spectra were measured from 850 to 3850 cm^{-1} with a resolution of 0.5 cm^{-1}, an aperture of 3 mm and a mirror speed of 40 kHz on a Bruker INVENIO-R.
Unfortunately, these data sets were only measured in an *in situ*-mode, thus activities are not available. But during long-time studies under these conditions, a small CO conversion of 0.1 % was measured for the copper-ceria polyhedra, a comparable sample to the copper-ceria sheets used in the WGSR experiments. Each interferogram measured was converted into a spectrum so that one spectrum is acquired approximately every 1.5 s.

6.2.1 Applying different period lengths during CO modulation to find intermediate species

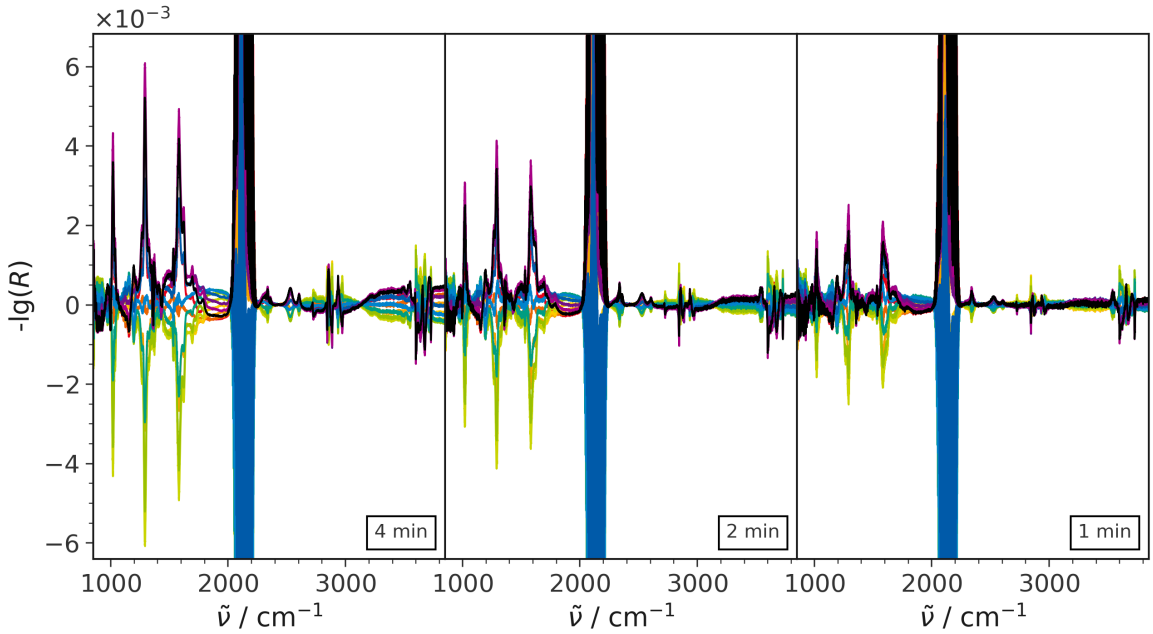

Figure 6.6: Comparison of the full PSD spectra of CO oxidation over Cu/CeO_2 polyhedra recorded using the HP LVVC at different period lengths (4, 2, 1 min) during CO modulation. The CO signal is not fully shown to make the other signals visible.

Signal positions The most important information from the full spectra in fig. 6.6 is, that there is conversion observable for all three period lengths, as at least small CO_2-signals between 2300 and 2400 cm^{-1} are visible.

Apart from that, signals in the carbonate, CH and hydroxyl region are visible. Their intensities increase with increasing period length, while their pattern remains about the same. However, since the focus of this discussion is on the active copper states, which can best be probed via the CO adsorbates in the carbonyl region, further consideration of the other regions will be omitted.

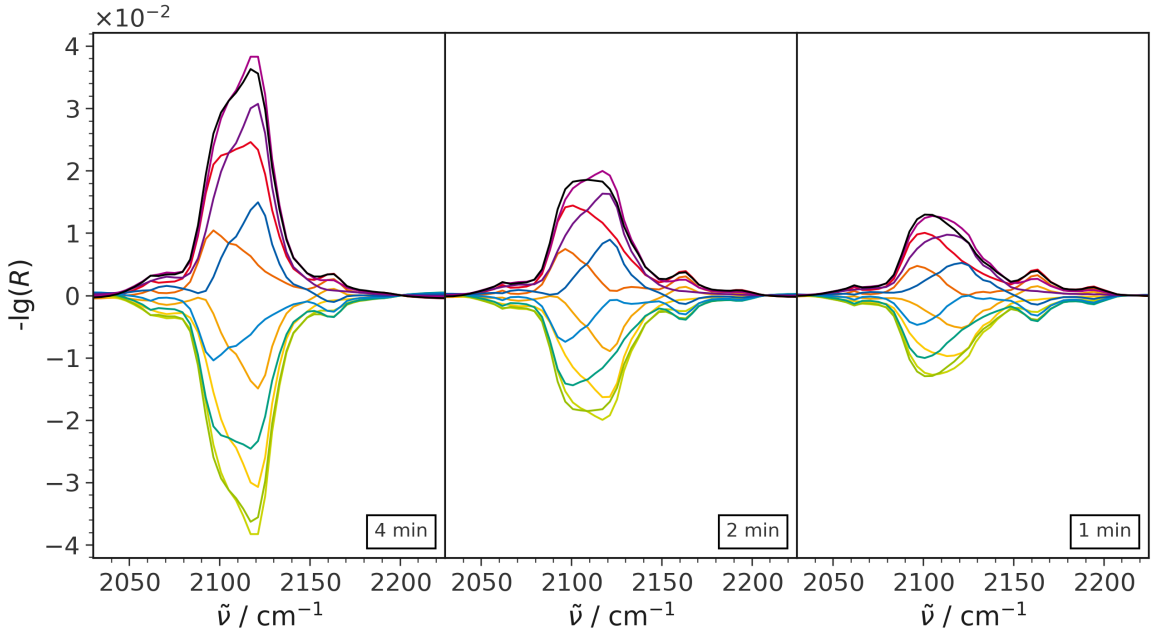

Figure 6.7: Comparison of the carbonyl area PSD spectra of CO oxidation over Cu/CeO_2 polyhedra recorded utilizing the HP LVVC at different period lengths (4, 2, 1 min) during CO modulation after gas phase removal.

Within the carbonyl region of the Cu/CeO_2 polyhedra shown in detail in fig. 6.7, most signals appear in all three data sets and become more intense with increasing period lengths.
Signals at 2100 and 2120 cm^{-1}, which are assigned to CO adsorbed to Cu^0 (2100 cm^{-1}) and Cu^+ (2120 cm^{-1}) [82–84], are visible at all three period lengths but with shifting relative intensities. While the overall intensity of these signals increases with period length, the signal at 2100 cm^{-1} seems to gain less intensity compared to the neighboring one at 2120 cm^{-1}, which becomes the dominant one of both at higher period lengths. A signal at 2164 cm^{-1} keeps constant in intensity and shape for all period lengths and is assigned to CO adsorbed to bare ceria [82]. A weak signal at 2071 cm^{-1} is visible, that increases in intensity when increasing the period length and has previously been assigned to CO adsorbed to small metallic copper clusters [83, 84]. Another signal appears at 2195 cm^{-1} and is strongest for the shortest period length of 1 min, becomes weaker with increasing period lengths and is totally gone at a period length of 4 min. Due to its high wavenumber and according to literature, this signal is assigned to CO adsorbed to Cu^{2+} [82, 85].
From the relative time values given in table 6.3, those of CO_2 can unfortunately not been taken into account, as the signal intensity is not high enough to really stand out from the background. Therefore, the time values are highly likely to be altered by background participation and not suited for discussion, as already elaborated concerning other signals in section 4.1.
Looking at the time values in table 6.3 it can be seen, that signals of CO adsorbed to Cu^{2+} or bare ceria are the first to appear in all data sets with one exception at 4 min, where the Cu^{2+}-related signal is not visible at all. The next signals in line are those of CO on metallic copper at 2097 cm^{-1} followed by CO on small metallic

Table 6.3: Most prominent carbonyl signals of the CO oxidation over Cu/CeO_2 during CO modulation at different period lengths, their time values derived from PSD normalized to the respective period length and their respective assignments.

4 min			2 min			1 min		
$\tilde{\nu}$ / cm^{-1}	$\frac{t}{t_{per}}$	Assignment	$\tilde{\nu}$ / cm^{-1}	$\frac{t}{t_{per}}$	Assignment	$\tilde{\nu}$ / cm^{-1}	$\frac{t}{t_{per}}$	Assignment
2209	**0.01**	**CO (g)**	**2209**	**0.00**	**CO (g)**	**2209**	**0.00**	**CO (g)**
-	-	CO-Cu^{2+}	2195	0.02	CO-Cu^{2+}	2160	0.04	CO-CeO_2
2160	0.03	CO-CeO_2	2160	0.03	CO-CeO_2	2195	0.04	CO-Cu^{2+}
2097	0.10	CO-Cu^0	2097	0.09	CO-Cu^0	2097	0.10	CO-Cu^0
2071	0.13	CO-$Cu_n{}^0$	**2361**	**0.10**	**CO_2 (g)**	2071	0.14	CO-$Cu_n{}^0$
2122	0.16	CO-Cu^+	2071	0.14	CO-$Cu_n{}^0$	2122	0.15	CO-Cu^+
2361	**0.26**	**CO_2 (g)**	2122	0.16	CO-Cu^+	**2361**	**0.17**	**CO_2 (g)**

copper particles at 2071 cm^{-1}. The last signal that appears in the carbonyl range of all three period lengths is the one of CO adsorbed to Cu^+.
All of this gives the impression, that besides the differences between the spectra collected at different period lengths in fig. 6.7, the temporal behavior of all these signals is quite similar, so it becomes important to check on the error. In absolute numbers the tolerance of the time values is about 1.5 s, the time needed to acquire one spectrum. But in order to compare the time values from different period lengths, they were normalized to the respective period length. This translates into an error of this parameter of 0.025 for a period length of 1 min, of 0.012 for 2 min and of 0.006 for 4 min. So increasing the period length obviously reduces the error. Therefore, all time values recorded at a period length of 4 min are well separated without overlapping error regions, making the sequence depicted in table 6.3 unambiguous. But for shorter period lengths the data becomes more blurry. For a period length of 2 min and a resulting error of 0.012, some signals come in pairs that cannot unequivocally be separated. These consist of CO-Cu^{2+} and CO-CeO_2 as well as CO-$Cu_n{}^0$ and CO-Cu^+. When applying a period length of only 1 min, the increasing error of 0.025 makes the signals of CO-CeO_2 and CO-Cu^{2+} overlap as well as all other signals of CO-Cu^0, CO-$Cu_n{}^0$ and CO-Cu^+. But common to all experiments at different period lengths is a large gap between the fast-responding CO adsorbed to bare ceria and Cu^{2+} and all the other species at metallic copper and Cu^+.

Data interpretation In stark contrast to the results from CO oxidation over Au/CeO_2, where the reaction happens quite fast and strong, in this case there is barely a reaction happening, as the tiny CO_2-signals in fig. 6.6 and the long-time conversions of about 0.1 % indicate. Therefore, the signals of most carbonyl species in fig. 6.7 were observed to rise with increasing period length. This was not the case for Au/CeO_2 in fig. 4.8, where the signals of the active species only slightly increased with period length. If just following the argumentation given for the accumulating CO-CeO_2-species in the case of Au/CeO_2 and apply it to Cu^0 and Cu^+, the conclusion could be drawn, that species are observed that accumulate on the surface. Additionally, the fact, that there is a change in intensity of Cu^0 compared to Cu^+ may indicate, that species adsorbed to Cu^+ can more easily accumulate than those at metallic copper sites.
Another possible conclusion can be drawn from the signal associated with the small uncharged copper clusters at 2071 cm^{-1}. Its increase with period length may indicate that some of the CO-Cu^0 species may form these smaller clusters in the course of the modulation experiment, transferring part of the intensity of the CO-Cu^0 signal at 2097 cm^{-1} to the signal at 2071 cm^{-1}, thereby changing the intensity ratio of CO-Cu^0 at 2097 cm^{-1} relative to CO-Cu^+ at 2122 cm^{-1}. However, since the conversions are so low and there is a risk that mostly

sorption dynamics are observed in this case, therefore, the interpretation of these data must be made with caution.
CO-Cu^{2+} is not visible in table 6.3 at a period length of 4 min, indicating that it might be a short lived surface species, related to the most oxidized state of Cu that is only existent after the relatively oxidizing pure O_2-phase preceding the reaction gas phase with both O_2 and the pulsed CO. Its contribution may therefore be marginalized in the case of higher period lengths and thus longer exposition time of the surface to the pure O_2-atmosphere, compared to species that appear as more stable by not answering that fast to changes in the gas atmosphere such as CO on less oxidized copper species, as has been discussed in [43].
Interestingly, the CO-CeO_2-signal's intensity stays completely the same for all three period lengths applied. This may indicate, that this species is already saturated on the surface and only minor changes still occur. Another idea might be, that this site is not really preferred for CO adsorption on this catalyst and only tiny alterations of this species are observed, as most of the dynamics happens at the Cu sites. Concerning the hypothesis of already pre-saturated CeO_2-sites, it can be seen from raw single-channel spectra shown in the top panel of fig. 6.8 recorded after the experiment with a modulation period length of 1 min, that this is not the case and that there is no indication for already existent CO-CeO_2-species (2163 cm^{-1}), although there is significant accumulation of all the other CO adsorbates. Therefore, it seems like the adsorption is not that favored compared to the copper-sites and seems to be saturated surprisingly fast as shown by the almost identical signal intensities at 2163 cm^{-1} in fig. 6.7.

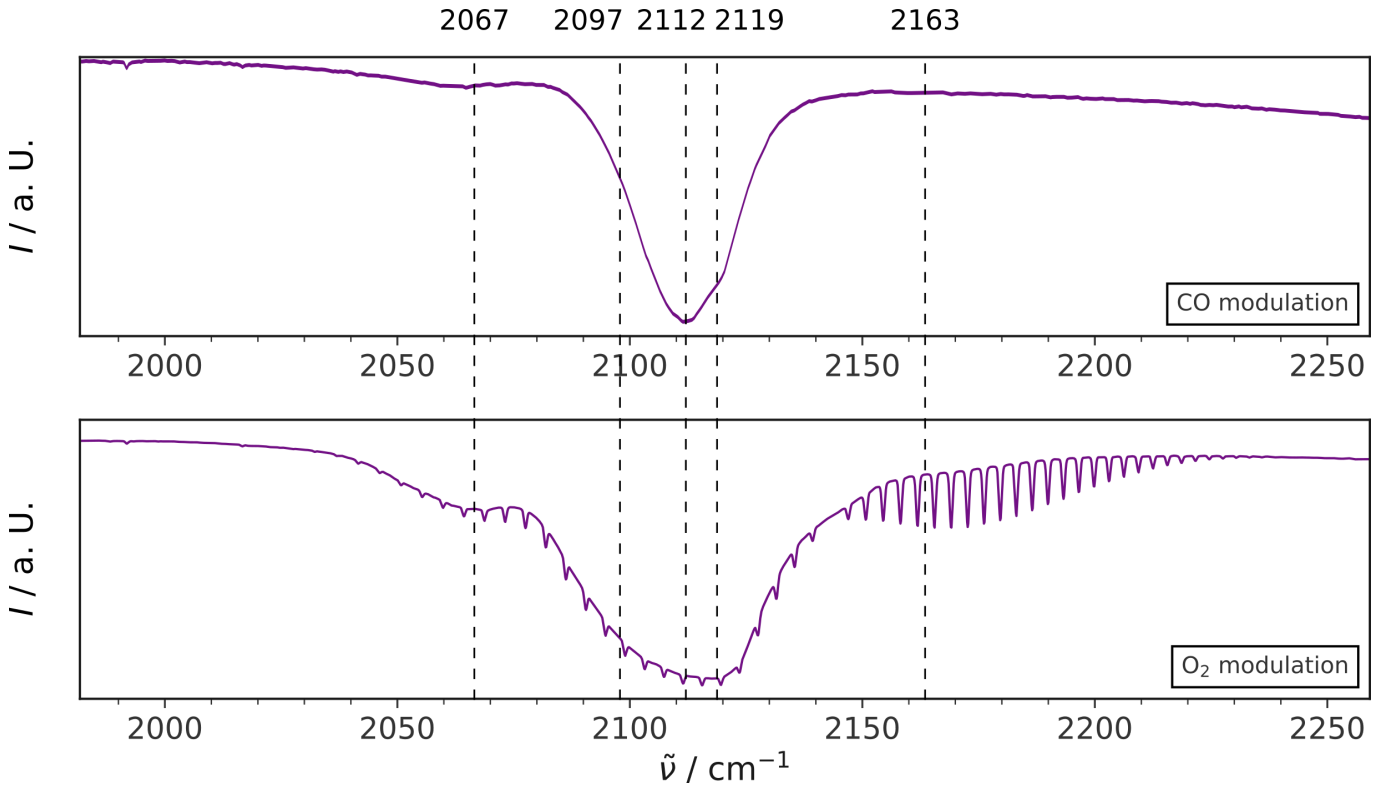

Figure 6.8: Unprocessed single channel spectra of the CO species remaining on the surface after the respective modulation experiment with a period length of 1 min. Above is displayed that after the CO modulation experiment with 10 % O_2 still in the gas phase and below that after the O_2 modulation experiment with 2 % CO remaining in the atmosphere.

6.2.2 Changing to O_2 modulation to investigate the dependence on the modulation approach.

In fig. 6.9 a tiny conversion is visible, as again small CO_2-signals between 2300 and 2400 cm^{-1} are present. As for the CO modulation experiments, carbonate, CH and hydroxyl signals are visible as well. Their intensities increase with period length, while their pattern remains about the same. Again, the focus of this discussion is on the state of copper, thus the carbonyl region, therefore the discussion of the other regions will be left out.

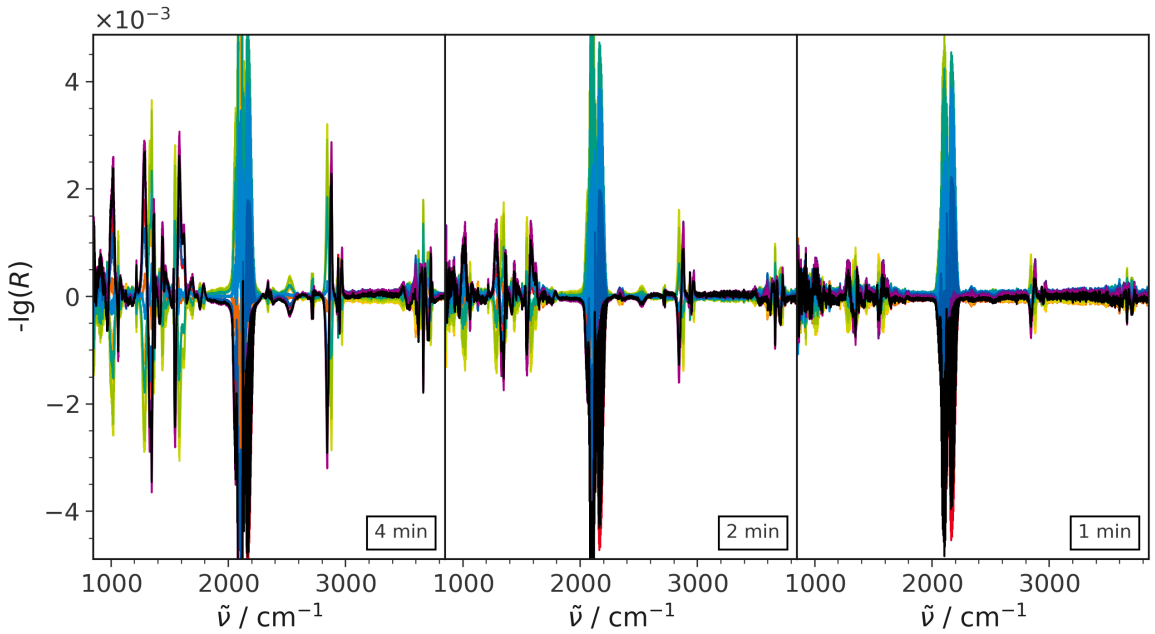

Figure 6.9: Comparison of the full PSD spectra of CO oxidation over Cu/CeO_2 polyhedra recorded using the HP LVVC at different period lengths (4, 2, 1 min) during O_2 modulation. The CO signal is not fully shown to make the other signals visible.

During O_2 modulation, while the signal pattern in the carbonyl range remains constant, its overall amplitude is increasing with period length. Signals are visible at 2064, 2097, 2115, 2138 and 2164 cm^{-1}. Most of the signals have a counterpart in the CO modulation experiments, and only slight shifts of up to 5 cm^{-1} are visible for the CO-Cu^+-signal. A signal assigned to CO on Cu^{2+} which has been observed for CO modulation at 2195 cm^{-1} is not visible for any of the O_2 modulation experiments. CO adsorbed on bare ceria at 2164 cm^{-1} is barely visible in the foothill of an other signal at 2138 cm^{-1}, that has not been observed in the CO modulation spectra (see fig. 6.7). This signal can be assigned to CO adsorbed to reduced ceria with a high Ce^{3+} content [78, 86], which is consistent with the in this case more reductive treatment of the sample.
Regarding the time values it can be seen, that the signals in all experiments approximately follow the same sequence, comparable to the observations in case of CO modulation. The first species observed for all period lengths after the reactant CO is that of CO adsorbed on bare ceria. For period lengths of 1 and 2 min it is then followed by the species at 2138 cm^{-1} and shortly after CO-Cu^0. In the case of a period length of 4 min, the sequence of the latter two signals is reversed, but still almost identical with 0.16 and 0.17 respectively. After that, the sequence is the same for all period lengths with CO-Cu^+ being the last carbonyl species before CO_2 emerges. But as the time values of most signals observed are quite identical, this seems to be within tolerance of each data point. As already mentioned for CO adsorption, the absolute experimental tolerance is 1.5 s but all time values were normalized to the respective period length, which yields dimensionless errors of 0.025

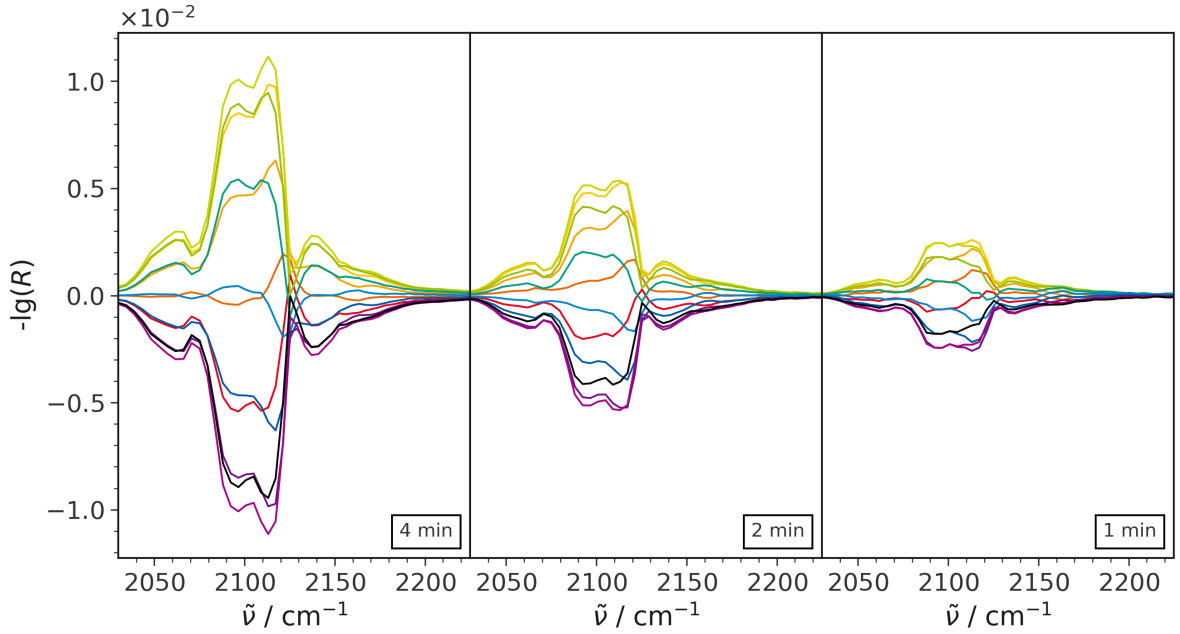

Figure 6.10: Comparison of the carbonyl area PSD spectra of CO oxidation over Cu/CeO_2 polyhedra recorded utilizing the HP LVVC at different period lengths (4, 2, 1 min) during O_2 modulation after gas phase removal.

for a period length of 1 min, 0.012 for 2 min and 0.006 for 4 min. That means, that CO adsorbed to Cu^+, Cu^0, small Cu^0-clusters and the species at 2138 cm^{-1} all lie within the error range of each other and are not clearly separated temporally for any of the period lengths. A similar behavior of these species has already been observed for CO modulation, where there was a clear division between fast- and late-responding signals, the latter of which included the aforementioned species' signals of Cu^+, Cu^0 and small Cu^0-clusters there as well. In this case only very small CO_2-signals are observed as well, thus their time values are not very well suited for discussion, as they may be highly influenced by their surrounding.

Data interpretation The fact, that all signal-amplitudes in the carbonyl region almost linearly increase with period length without regard of their nature leads to the conclusion, that this behavior may be linked to sorption dynamics only. In this case, CO adsorbates accumulated during the CO-phase prior to the reaction phase just get consumed during the latter and their places refilled again during the CO-phase. Together with the fact, that there is barely product visible in the form of CO_2, the conclusion may be drawn, that this is more or less only a discussion of CO adsorption and desorption.
When comparing the signals observed for this type of pulsing (see fig. 6.10) to the spectra generated after CO modulation (see fig. 6.7), it can be noted, that the same signals apart from the one assigned to CO-Cu^{2+} during CO modulation are visible, but with different intensities. Furthermore, the signal at 2138 cm^{-1} that is quite intense for O_2 modulation has not been visible in the case of CO modulation.
One reason for the temporal behavior of CO-CeO_2, which is the first signal to separately emerge, followed by the large bulk of Cu-related species, may be that first the adsorption to the more abundant site of bare ceria takes place. At a low loading of only 0.46 wt% copper, an adsorption of CO at copper sites is of course possible as well but seems less likely compared to the adsorption on the wide ceria surface with its countless available

Table 6.4: Most prominent carbonyl signals of the CO oxidation over Cu/CeO_2 during O_2 modulation at different period lengths, their time values derived from PSD normalized to the respective period length and their respective assignments.

4 min			2 min			1 min		
$\tilde{\nu}$ / cm^{-1}	$\frac{t}{t_{per}}$	Assignment	$\tilde{\nu}$ / cm^{-1}	$\frac{t}{t_{per}}$	Assignment	$\tilde{\nu}$ / cm^{-1}	$\frac{t}{t_{per}}$	Assignment
2209	**(-) 0.03**	**CO (g)**	**2209**	**(-) 0.01**	**CO (g)**	**2209**	**(-) 0.00**	**CO (g)**
2163	(-) 0.14	CO-CeO_2	2163	(-) 0.14	CO-CeO_2	2163	(-) 0.10	CO-CeO_2
2097	(-) 0.16	CO-Cu^0	2138	(-) 0.19	CO-Ce^{3+}	2138	(-) 0.20	CO-Ce^{3+}
2138	(-) 0.17	CO-Ce^{3+}	2097	(-) 0.19	CO-Cu^0	2097	(-) 0.21	CO-Cu^0
2063	(-) 0.17	CO-$Cu_n{}^0$	2063	(-) 0.20	CO-$Cu_n{}^0$	2063	(-) 0.21	CO-$Cu_n{}^0$
2113	(-) 0.17	CO-Cu^+	2113	(-) 0.20	CO-Cu^+	2113	(-) 0.24	CO-Cu^+
2361	**0.22**	**CO_2 (g)**	**2361**	**0.44**	**CO_2 (g)**	**2361**	**0.44**	**CO_2 (g)**

adsorption sites. Interestingly though is the fact, that CO adsorbed to bare ceria only exhibits such a small response to the external stimulation. As already discussed for CO modulation, a first guess may be, that there is a plethora of residual CO preadsorbed on ceria but only a small amount may be answering. But as visible in the single-channel spectra in the lower panel of fig. 6.8, there is only a small fraction of already adsorbed CO on CeO_2, way less than for the other CO adsorbates. This may be due to lower adsorption energies of CO on bare ceria compared to CO on various copper sites, with CO-CeO_2 lying at about -0.2 eV [31], while CO adsorbed to diverse copper species is reported to exhibit a four times higher adsorption energy of about -0.8 eV [82]. In all experiments CO-CeO_2 is one of the fastest-responding species but exhibits only small answers to the external modulation and is way less abundant on the surface than the other CO adsorbates on copper species. Therefore, it can be assumed, that in case of Cu/CeO_2, lower quantities of CO-CeO_2 are visible than e. g. in the case of Au/CeO_2, where there is evidence for a reaction-linked CO spillover from the active gold site that helps populating the ceria surface with carbonyls (see section 4.1). These results are consistent with the fact that the experiments in section 4.1 and earlier studies by Schilling *et al.* [31] have shown, that bare ceria is not active under the chosen conditions at atmospheric pressure and 37 °C. Thus it can be stated, that for CO-CeO_2 primarily sorption processes are observed.

With respect to the observed CO-copper species, it is not possible to unambiguously identify an active species catalyzing the reaction. On the one hand, the small effects in the spectra caused by only very low CO conversions of about 0.1 % may be no problem to detect with the sensitive method of ME-DRIFTS, as has been shown in [49]. There ME-DRIFTS was performed at very low reactant concentrations, while it was still possible to obtain valuable mechanistic information. On the other hand, for the reaction over Cu/CeO_2 discussed here, the potential contributions of the setup to the activities were not dissected. So all of these data must be viewed critically, as it is not completely sure that all of the conversion is really caused by the catalyst.

But it can be assumed, that primarily sorption dynamics of CO on Cu/CeO_2 are observed for CO-CeO_2 signals, which appear fast but are unstable due to a low adsorption energy and more stable copper carbonyls which are detected later in the experiment. This behavior may be due to the abundance of copper on the surface being quite low on the investigated samples with only 0.46 wt%.

Furthermore, different species' signals have been observed, that seem to be oxidation-state-related such as CO-Cu^{2+}, which appears only in the more oxidized conditions during CO modulation with constant O_2 supply. CO adsorbed to more reduced ceria at 2138 cm^{-1} is only observed under reducing conditions of O_2-modulation with CO being constantly present.

Unfortunately, it was not possible to fully map the possible states in which the reaction could be observed using ME-DRIFTS, as only a weak reaction was visible. Nevertheless, valuable information was obtained, that it is possible to discriminate between different CO species, which are linked to specific oxidation states of the material. This clearly indicates the presence of slightly different sites on the surface during different modulation approaches, although most of the signals related to metallic copper or copper (I) show a quite similar behavior for both modulation approaches.
This study can nevertheless serve as a reference point for the system at low conversions, where the reaction begins. Together with future studies of this system at higher temperatures, it will be possible to obtain a complete picture of the dynamics observed in MES-PSD and to clarify which are due to the reaction and which are only caused by sorption processes.

7 Summary

In this work it was shown, that using MES-PSD in combination with DRIFTS, new insights into reaction mechanisms such as CO oxidation, (reverse) water-gas shift (RWGSR/WGSR) and CO_2 activation to form MeOH are readily accessible. In this respect, MES-PSD allows to reduce the amount of signals in the spectra to those actively responding to the external periodic stimulation (modulation), which in most cases is a good indicator of an active involvement in the mechanism under investigation. Furthermore, the ability of this method to provide additional information on the sequence of the observed signals is useful to immediately obtain at least a first idea of the reaction sequence, as was accomplished e. g. for the WGSR over Cu/CeO_2. In this case, by discussing the results of basically two modulation experiments (pulsing CO or pulsing H_2O), it was possible to judge whether the mechanism runs via adsorbates (associative) or was solely due to the redox activity of the material. The redox mechanism proved to be the one at work and, in combination with other *operando* spectroscopic techniques, a full picture of the relevant surface processes was obtained, including the type of adsorbates involved as well as the influence of the metal on the reaction.
In other cases, such as the CO oxidation or the RWGSR over Au/CeO_2, it was even possible to prove and refine existing concepts of the reaction mechanism from the literature and provide direct spectroscopic evidence for the surface species that are actively involved in product formation.
In the case of CO oxidation, it was demonstrated, that carbonate and hydroxyl species were not involved in product formation, as all potentially active species were found in the carbonyl region. (Dynamically formed) single atomic gold sites were identified as active species and it was shown, that CO adsorbed on larger gold clusters or even on the ceria surface is not involved in product formation.
In the case of the RWGSR, it was demonstrated, that the literature suggestion, that an associative, adsorbate-mediated reaction mechanism leads to product formation is correct. It was shown, that the active species are bidentate carbonate and specific hydroxyl species. Formate, which has also been discussed in the literature, appears to form only after the reaction and is therefore excluded as a relevant species.
The analysis of the high pressure CO_2 activation with *operando*-MES has revealed, that under these conditions three reactions may occur in parallel. These are the formation of CO and methane as well as the desired MeOH. The coexistence of these possible pathways has hindered the unambiguous interpretation of the time values extracted by PSD. Nevertheless it was possible to gain insight into a possible pathway to MeOH via adsorbed methoxy species. The interpretation of these data was further complicated by the fact that the reaction cell was not suitable for rapid gas phase exchange.
The design and application of a more suitable low void volume *in situ* cell has greatly improved the clarity of the spectra and the interpretation of the data generated, e. g. by further strengthening the pattern of active species such as adsorbed methoxy. Therefore, it was possible to propose a mechanism of MeOH formation via the adsorption of CO_2 as carbonates and their subsequent hydrogenation to form methoxy, followed by a release as MeOH as more CO_2 adsorbs and forms carbonates to replace the accumulated methoxy.
Similar custom made reaction cells have not only been successfully used in high-pressure experiments, but have also furthered the understanding of CO oxidation over Au/CeO_2 and Cu/CeO_2. Since these low volume reaction cells allow rapid total gas phase exchange within seconds, the period lengths in the experiments could be reduced. This is not only beneficial for increasing the time efficiency of the measurements, but also has a clear advantage when targeting fast-reacting intermediates of the reaction. With a reduced period length,

more stable species that tend to appear later in the mechanism and perhaps accumulate during the reaction are less abundant at the time when the gas phase exchange occurs, but if a species is only an intermediate of the reaction and tends not to accumulate, perhaps passing through a maximum abundance, that species will be much more intense in this data set.
For the CO oxidation over Au/CeO_2 this cell and its rapid gas phase exchange allowed to drastically reduce the abundance of more stable but non-reactive species such as CO adsorbed on larger Au clusters, which almost disappeared from the spectra, as well as CO on bare ceria sites. The signal of CO-CeO_2 has been observed decreasing with period length, indicating that this is primarily an accumulating species that becomes more intense the longer it is exposed to the reaction atmosphere, correlating with the parameter of period length.
In the case of the CO oxidation over Cu/CeO_2, the focus was primarily on potential active copper carbonyls during reaction, other than for the WGSR, for which only electronic effects of copper on the reaction were reported, which could not be explored by observing adsorbed CO. The CO oxidation was chosen as a model reaction, allowing to gather information on the active copper states, even though only a small conversion was observed in the MES-PSD data. Experiments with decreasing period lengths and their comparison with existing data provided further information about the oxidation state of copper on this catalyst, especially its evolution over time. However, as the conversions measured under the chosen conditions were only small, the identified intermediate species, such as CO adsorbed on Cu^{2+}, cannot be unambiguously related to the reaction alone but may to some extent as well be due to sorption processes which will need to be further elucidated in future studies. Nevertheless, the present results of CO oxidation over Cu/CeO_2 can serve as a reference point for the behavior of the system at very low conversions.

To summarize the results of this work in relation to its objective, we must first recapitulate the latter, which was to first install and apply the novel spectroscopic method of ME-DRIFTS in combination with PSD, to prove its efficiency for currently studied reaction systems and to finally explore and expand its potential applications. We have seen how this approach has first of all allowed to reduce the immense complexity of DRIFT spectra in heterogeneous catalysis. In most of the examples presented here, the number of active signals, e. g. in the carbonate region, shrank to a low single-digit number originating from one or two potential candidate species. The welcome side effect, that MES-PSD provides additional temporal information, further enhances the signal assignment advantages of this method over “conventional” steady-state or even time-resolved DRIFTS by further facilitating the assignment of related signals, since they should appear at the same time.
This temporal information is also useful when it comes to elucidating reaction mechanisms. It allows to sort the emerging signals, and thus the related species, according to their time of emergence relative to the appearance of the reactants and products, and therefore to obtain immediate evidence for a possible reaction mechanism in only one single experiment. However, since the information obtained from a single experiment is limited in its significance, additional experiments, such as changing the modulation approach by varying the periodically pulsed reactant between experiments, decreasing/increasing the period length of the modulation experiment, or pulsing isotopically labeled gases were presented, that provide a comprehensive picture of the surface processes observable by DRIFT spectroscopy, and increase the understanding of the transient processes during the reaction mechanism manifold.

8 Outlook

Considering future applications of MES-PSD in our group, I am confident that the approaches explored here will contribute to an even better understanding of reaction mechanisms on a regular basis.
At the beginning of my Ph.D., I started with just a few pieces of equipment, a vague idea of how to combine them, and a vision of a new and powerful ready-to-use method in our group's inventory. This was eventually achieved, and in this work it was demonstrated that this method is applicable to different types of reactions and their peculiarities within a short adaptation time of a few hours to a few days, which is definitely worth the effort.

Impact on understanding catalyzed reactions Before addressing the remaining open questions arising from this work, one must first emphasize the impact that MES-PSD can have on the field of heterogeneous catalysis. As a method that allows a deep mechanistic understanding of the reaction over a catalyst at work, the knowledge thus gained can bring us a step closer to system optimization and thus to a rational catalyst design. It has been shown, that MES-PSD in combination with DRIFT spectroscopy can greatly contribute to this end, providing a variety of interesting mechanistic details of a wide range of reactions and allowing to address open questions in new ways, some of which will be discussed in more detail in the following paragraphs.

Low void volume cells make MES data much more meaningful To better understand reaction mechanisms, the importance of an adapted reaction cell was demonstrated. In all MES experiments, a rapid exchange of the gas phase is essential to induce the largest possible effects on the surface by the abrupt change in concentration, thus maximizing the intensity of the active species in the spectra. For example, in all RWGSR experiments a commercial reaction cell with a high volume and therefore slow exchange rate was used, whereas in high-pressure MeOH formation experiments presented here, the performance of such a high-volume cell was compared to that of a low-volume custom made cell. There it was found, that the clarity of the signals increased significantly together with the time resolution and sharpness of the effects. So while rudimentary experiments with a non-optimal cell are possible and can still yield good results, the use of a well-designed cell will be the basis of future modulation experiments. And because the current version of the reactor cell is very simple, it can be easily adapted to very different reaction conditions, including higher temperatures and pressures as the ones discussed here, with only minor modifications to the cooling circuit or consumables (O-rings).

Reverse Water-Gas Shift Reaction (RWGSR) over Au/CeO_2 still holds secrets about active gold hydrides For the RWGSR, although the reaction mechanism over the catalyst utilized here has been understood quite well, there are still limitations of the experiment when it comes to resolving the various potentially active gold hydride species calculated and partially observed in [11]. So far, it was only possible to clearly see one of these species assigned to weakly adsorbed undissociated H_2 in this work, although at least one other species assigned to dissociated H-atoms was expected to be found based on previous experiments presented

in [11]. As discussed there, the signal of dissociated H-atoms on gold has been observed in the case of gold-ceria polyhedra, whereas in this work investigating gold-ceria sheets, these species were not visible. Therefore the use of other types of samples in future experiments may provide interesting insights into the succession of different gold-hydride species. The use of one of the self-designed low void volume reaction cells (LVVC, HP LVVC) should also lead to better resolved time values and thus a clearer picture of the mechanistic succession. A reduction in period lengths would also be possible, opening the way to possibly elucidate more short-lived species. Especially the behavior of the gold hydrides under these reaction conditions would be of great interest.

High pressure CO_2 activation must become more selective toward one reaction product Concerning the high pressure CO_2-activation and MeOH formation experiments, an open question concerns the quantification of the catalyst activity in *operando* experiments in combination with a comparison of catalysts loaded with different amounts of gold. This will also allow the influence of gold on the reaction to be addressed and its role in the reaction mechanism to be elucidated. So far, it is still up for debate, whether gold has a purely electronic contribution to the reaction, whether species such as gold hydrides are involved at all, or whether the parameters of the spectra accumulation are perhaps not perfectly suited for their detection. But with future *operando* ME-DRIFTS experiments I am quite confident, that light can be shed on these open questions and that the rather complex interplay of the three possible parallel reactions of CO, MeOH and methane formation will be disentangled.
However, as far as mechanistic insights are concerned, before postulating an unambiguous MeOH formation mechanism, the parameters of the reaction and, if necessary, the catalyst itself have to be adapted to become more selective towards MeOH formation. Otherwise, it will remain challenging to decide, whether the observed signals belong to a species that actively contributes to one specific reaction.

For the Water-Gas Shift Reaction (WGSR), additional experiments could clarify remaining questions Further investigation of the WGSR over Cu/CeO_2 revealed that ME-DRIFTS reinforced the findings of other techniques about the dominant presence of a redox mechanism, i.e. there are no surface adsorbates that are undoubtedly actively involved in the reaction mechanism. A further investigation that might be of interest here would be to use different period lengths for the two modulation approaches, to prove that the data from CO and H_2O modulation are complementary and to check for potential fast-reacting intermediates.
This would include the use of one of the custom reaction cells, which allows for faster gas phase exchange and thus a better grasp on the aforementioned fast-reacting species, although the latter are not very likely based on what is currently known about the system.
Perhaps more promising in terms of active surface adsorbates, including those of CO, is the study of the same reaction over higher loaded copper-ceria systems, as the active contribution of copper carbonyls in their case has been reported in the literature [77, 87]. Although these higher loaded systems have been extensively studied in the literature, transient methods such as MES may still provide valuable information about the sequence of reaction steps that occur during the reaction.

Extending the application of MES to UV/Vis Returning to the low-loaded systems and the assumed purely electronic contribution of copper, a potential application of ME-UV/Vis spectroscopy could be very interesting. It might be possible to elucidate which electronic effects are involved in the enhancement of the activity of copper-loaded materials compared to bare ceria. First conceptual studies of such a ME-UV/Vis approach have been published in [23], but to my knowledge there have been no further applications of this technique. In the

course of my Ph.D. research, first steps were taken towards the application of this technique by installing all the hardware that allows communication between a UV/Vis spectrometer (Jasco 770), the aforementioned 4/2 valve and a control unit built by the electronics workshop of the chemistry department. Initial results looked promising, but due to unforeseen technical issues with the spectrometer, which could not be reliably triggered externally to take measurements, this project had to be abandoned for the time being. But with the arrival of a new promising spectrometer, I am quite confident that a resumption of the project should lead to the desired result, a working ME-UV/Vis apparatus, which in the next step can be applied to those systems where ME-DRIFTS cannot provide any further information like the WGSR over low-loaded Cu/CeO_2.

It remains a challenge to apply IR spectroscopy to indium oxide A major challenge is the application of IR spectroscopy to In_2O_3, another promising catalyst material. A variety of approaches was applied to study the behavior of this material in its pure as well as gold- and copper-loaded form toward CO oxidation and (R)WGSR via MES and steady-state DRIFTS, but under reductive conditions this material absorbs all of the incident IR light, making it impossible to measure spectra. This behavior has been further investigated by our group and has led to the use of a variety of different spectroscopic techniques such as UV/Vis, Raman and impedance spectroscopy to circumvent the use of IR techniques [13, 88]. Therefore, the future application of at least ME-UV/Vis spectroscopy may help to further narrow the knowledge gap that exists because IR techniques are so far not applicable.

Exploring ME-Raman as a promising technique UV/Vis is not the only other type of spectroscopy whose utility for mechanistic studies in heterogeneous catalysis can be dramatically enhanced by combining it with MES-PSD. The same work by Nuguid *et al.* that introduced ME-UV/Vis [23] also proposed an approach for the application of ME-Raman spectroscopy, which was further elaborated in [22], and there is an even older publication by Urakawa *et al.* that touched on the subject as early as 2011 [24], but there have been no more recent studies than these since 2019.
The great potential of this technique for future studies lies in the fact that it provides complementary information to ME-DRIFTS. But it may also be used when ME-DRIFTS is not applicable, as in the case of highly absorbing materials such as In_2O_3. Another area of investigation could be the study of materials at high temperatures where conventional IR spectroscopic techniques become blind.
An example, where easier access to information complementary to DRIFTS studies would have been practical is the elucidation of the Mars-van Krevelen type mechanism in the case of CO oxidation over Au/CeO_2 materials. The investigation of the role of species that are difficult to study with IR, such as peroxides, superoxides, or the associated surface oxygen vacancies during the reaction [31, 32], could have been greatly simplified by ME-Raman and/or UV/Vis, and enriched with the temporal information that should be readily available from these methods.

CO oxidation over Cu/CeO_2 has major open questions left Regarding the results of CO oxidation over Cu/CeO_2, it has to be noted, that the experimental conditions chosen were not suitable to approach higher conversions. Therefore, at the present low catalyst activities, caution is still required in data interpretation, since the dynamics observed in the PSD spectra could also be caused, at least in part, by reaction-independent sorption processes.
The experimental conditions were chosen to make the results as comparable as possible to the experiments over Au/CeO_2 in section 4.3, but in the future it seems necessary to move to higher temperatures to really

trigger the reaction and elucidate its mechanism.
Nevertheless, valuable information about the catalyst system at the time of the onset of the reaction and minimal conversion was obtained, that will be useful for studying certain spectral features in more detail, such as the signal observed for CO-Cu^{2+}, the transient nature of which was revealed by comparing experiments with different period lengths.

Different period-length approach helps to see reaction intermediates This approach of studying the system at different period lengths, which has been used for Cu/CeO_2 and Au/CeO_2, is indeed promising and has led in the studies of both catalysts either to the clear identification of transient species such as CO-Cu^{2+} or to the unambiguous exclusion of species, that might have appeared active in a single modulation experiment, as was the case for CO-CeO_2 and CO adsorbed on larger gold clusters for the Au/CeO_2 system.
The use of this approach, which is only truly effective in combination with the application of a low residence time reaction cell such as the ones presented in this work (LVVC, HP LVVC), will be of great interest for future in-depth studies of reaction mechanisms and may help to better interpret MES data. This is very important because the response of the system is clearly linked to its initial state and e. g. combining the results obtained from different modulation approaches (either pulsing reactant A or B) may or may not make sense depending on whether the system oscillates between the same states in both experiments or whether they are completely different. Thus, the approach of comparing different modulation period lengths along with the modulation of different gases may lead to a better understanding of the system's transition between these states and thus allow the experimenter to judge whether the data can be joined or not.

MES detects low concentrations of active species in gas sensing experiments Beyond the scope of this work, various colleagues in our research group have already begun to successfully apply this technique to other reactions in heterogeneous catalysis and even to the field of gas sensing.
In gas sensing, a master student of mine has applied ME-DRIFTS to elucidate the mechanism of EtOH gas sensing over gold-loaded and bare SnO_2, and his results were published in [49]. In this area of research, the amount of reactant is always kept very low to resemble the working conditions of the gas sensor, but this comes at the cost of very low abundances of intermediates and other interesting species, making them difficult to follow spectroscopically. To this end, ME-DRIFTS is perfectly suited to highlight the signals of the active species, and allow their selective observation. Further applications to different materials and/or analyte molecules are therefore already planned in our group and will deepen the understanding of chemical gas sensors at work.

Propane-ODH demonstrated the potential of different modulation approaches and isotope MES for complex reactions Another interesting direction in which our group has advanced is the application of MES-PSD and its combination with isotope exchange experiments to narrow down the number of signals appearing in the PSD spectra even further, enabling to deepen mechanistic insights.
In a joint work with my colleague Leon Schumacher [29], ME-PSD was applied to the complex oxidative dehydrogenation (ODH) of propane over ceria-supported vanadium. A large number of complementary modulation experiments was used to exploit the resulting synergies in the interpretation of the spectra to more precisely identify the species actively involved in the reaction.
For this purpose, in several experiments both reactants were added either pulsed or constant, while the other reactant was added exactly the other way round, either constant or pulsed. This has already allowed to gain

deeper insights and to exclude or confirm one or the other species that may initially have seemed to be active, especially in the area of surface vanadia structures.
These insights were then further deepened by the use of isotope exchange MES, which was introduced by Pavelko *et al.* in 2014 [28] but has not really taken off since then. In this approach, a reactant, in this case propane, is exchanged for an isotopically labeled equivalent, in this case d8-propane. This experiment almost completely prevents the appearance of signals in the PSD spectrum that can only be attributed to sorption processes of species that are not actually involved, and shows, in addition to the sorption behavior of the labeled and unlabeled product, only those signals for which the corresponding species is affected by the isotope exchange.
This approach of combining different modulation approaches with the rather unexplored technique of isotopic MES has led to a much deeper understanding of the species involved, the mechanism at work and thus the propane ODH over ceria-supported vanadia in general. Due to the great success of this approach, further studies of other vanadia-loaded systems are currently under way, demonstrating the usefulness of MES, but also about combined modulation approaches with pulsing different reactants and even isotopically labeled MES.

Overcoming the limitations imposed by overlapping signals A major problem that has been discussed in almost all of the chapters here and that limits the power of MES-PSD data is the overlap of neighboring signals that affect the time values extracted from the phase angles by blurring their error region to an unknown extent. If this barrier could be overcome, e. g., as it was possible for broad background absorptions that overlap with possibly active signals [49], the significance of the obtained PSD spectra would be drastically increased.
A similar approach as applied in case of broad backgrounds is conceivable, where the unwanted signal was subtracted in the time-resolved spectra stage before the PSD was applied. But fitting functions to the area of overlap and guessing what to remove can introduce its own errors and come with additional complexity.
Another way might be to apply some mathematical method that performs similar to what the Fourier transform does in separating the different frequencies contained in a periodic signal, only with different phase angles, i.e., time shifts of the periodic function describing the system's response to the external modulation. However, the mathematical toolbox has not yet been further explored, so investigating the possibilities in this area may be a worthwhile endeavor.

Bibliography

[1] W. Reschetilowski, *Einführung in die Heterogene Katalyse*, Springer Berlin Heidelberg, Berlin, Heidelberg, **2015**.

[2] M. D. Porosoff, J. G. Chen, *Journal of Catalysis* **2013**, *301*, 30–37.

[3] Y. Denkwitz, A. Karpenko, V. Plzak, R. Leppelt, B. Schumacher, R. Behm, *Journal of Catalysis* **2007**, *246*, 74–90.

[4] D. Trimm, *Applied Catalysis A: General* **2005**, *296*, 1–11.

[5] C. Ratnasamy, J. P. Wagner, *Catalysis Reviews* **2009**, *51*, 325–440.

[6] A. F. Diwell, R. R. Rajaram, H. A. Shaw, T. J. Truex, *Studies in Surface Science and Catalysis* **1991**, *71*, 139–152.

[7] M. Baerns, A. Behr, A. Brehm, J. Gmehling, K.-O. Hinrichsen, H. Hofmann, U. Onken, R. Palkovits, A. Renken, *Technische Chemie*, 2. Auflage, Wiley, Weinheim, **2014**.

[8] D. Baurecht, U. P. Fringeli, *Review of Scientific Instruments* **2001**, *72*, 3782–3792.

[9] P. Müller, I. Hermans, *Industrial & Engineering Chemistry Research* **2017**, *56*, 1123–1136.

[10] A. Filtschew, K. Hofmann, C. Hess, *The Journal of Physical Chemistry C* **2016**, *120*, 6694–6703.

[11] M. Ziemba, J. Weyel, C. Hess, *Applied Catalysis B: Environmental* **2022**, *301*, 120825.

[12] M. Ziemba, C. Hess, *Catalysis Science & Technology* **2020**, *10*, 3720–3730.

[13] M. Ziemba, C. Schilling, M. V. Ganduglia-Pirovano, C. Hess, *Accounts of Chemical Research* **2021**, *54*, 2884–2893.

[14] G. L. Chiarello, Y. Lu, M. Agote-Arán, R. Pellegrini, D. Ferri, *Catalysts* **2021**, *11*, 116.

[15] B. S. Patil, P. D. Srinivasan, E. Atchison, H. Zhu, J. J. Bravo-Suárez, *Reaction Chemistry & Engineering* **2019**, *4*, 667–678.

[16] E. del Río, S. E. Collins, A. Aguirre, X. Chen, J. J. Delgado, J. J. Calvino, S. Bernal, *Journal of Catalysis* **2014**, *316*, 210–218.

[17] A. Urakawa, R. Wirz, T. Bürgi, A. Baiker, *The Journal of Physical Chemistry B* **2003**, *107*, 13061–13068.

[18] A. Waheed, C. Cao, Y. Zhang, K. Zheng, G. Li, *New Journal of Chemistry* **2022**, *46*, 5361–5367.

[19] A. Urakawa, T. Bürgi, H.-P. Schläpfer, A. Baiker, *The Journal of Chemical Physics* **2006**, *124*, 054717.

[20] M. A. Serrer, A. Gaur, J. Jelic, S. Weber, C. Fritsch, A. H. Clark, E. Saraçi, F. Studt, J. D. Grunwaldt, *Catalysis Science and Technology* **2020**, *10*, 7542–7554.

[21] D. Ferri, M. A. Newton, M. Di Michiel, G. L. Chiarello, S. Yoon, Y. Lu, J. Andrieux, *Angewandte Chemie International Edition* **2014**, *53*, 8890–8894.

[22] R. J. G. Nuguid, D. Ferri, A. Marberger, M. Nachtegaal, O. Kröcher, *ACS Catalysis* **2019**, *9*, 6814–6820.

[23] R. J. G. Nuguid, D. Ferri, O. Kröcher, *Emission Control Science and Technology* **2019**, *5*, 307–316.

[24] A. Urakawa, W. Van Beek, M. Monrabal-Capilla, J. R. Galán-Mascarós, L. Palin, M. Milanesio, *The Journal of Physical Chemistry C* **2011**, *115*, 1323–1329.

[25] V. Marchionni, M. Nachtegaal, D. Ferri, *ACS Catalysis* **2020**, *10*, 4791–4804.

[26] C. Xu, X. Xu, J. Su, Y. Ding, *Journal of Catalysis* **2007**, *252*, 243–248.

[27] M. Eigen, *Discussions of the Faraday Society* **1954**, *17*, 194–205.

[28] R. G. Pavelko, J. K. Choi, A. Urakawa, M. Yuasa, T. Kida, K. Shimanoe, *Journal of Physical Chemistry C* **2014**, *118*, 2554–2563.

[29] L. Schumacher, J. Weyel, C. Hess, *Journal of the American Chemical Society* **2022**, *144*, 14874–14887.

[30] J. Weyel, M. Ziemba, C. Hess, *Topics in Catalysis* **2022**, *65*, 779–787.

[31] C. Schilling, M. Ziemba, C. Hess, M. V. Ganduglia-Pirovano, *Journal of Catalysis* **2020**, *383*, 264–272.

[32] C. Schilling, C. Hess, *The Journal of Physical Chemistry C* **2018**, *122*, 2909–2917.

[33] F. Bozon-Verduraz, A. Bensalem, *Journal of the Chemical Society Faraday Transactions* **1994**, *90*, 653.

[34] H. Daly, J. Ni, D. Thompsett, F. Meunier, *Journal of Catalysis* **2008**, *254*, 238–243.

[35] C. Yang, L. L. Yin, F. Bebensee, M. Buchholz, H. Sezen, S. Heissler, J. Chen, A. Nefedov, H. Idriss, X. Q. Gong, C. Wöll, *Physical Chemistry Chemical Physics* **2014**, *16*, 24165–24168.

[36] C. Wöll, *ACS Catalysis* **2020**, *10*, 168–176.

[37] P. G. Lustemberg, P. N. Plessow, Y. Wang, C. Yang, A. Nefedov, F. Studt, C. Wöll, M. V. Ganduglia-Pirovano, *Physical Review Letters* **2020**, *125*, 256101.

[38] C. Yang, X. Yu, S. Heißler, A. Nefedov, S. Colussi, J. Llorca, A. Trovarelli, Y. Wang, C. Wöll, *Angewandte Chemie International Edition* **2017**, *56*, 375–379.

[39] M. Ziemba, M. V. Ganduglia-Pirovano, C. Hess, *Faraday Discussions* **2021**, *229*, 232–250.

[40] P. Ghosh, M. Farnesi Camellone, S. Fabris, *The Journal of Physical Chemistry Letters* **2013**, *4*, 2256–2263.

[41] Y.-G. Wang, D. Mei, V.-A. Glezakou, J. Li, R. Rousseau, *Nature Communications* **2015**, *6*, 6511.

[42] D. Karhánek, https://assets.thermofisher.com/TFS-Assets/CAD/Specification-Sheets/PS51812-Praying-Mantis.pdf, **2023**.

[43] V. Marchionni, D. Ferri, O. Kröcher, A. Wokaun, *Analytical Chemistry* **2017**, *89*, 5801–5809.

[44] A. Badri, C. Binet, J. C. Lavalley, *Journal of the Chemical Society - Faraday Transactions* **1996**, *92*, 4669–4673.

[45] G. N. Vayssilov, M. Mihaylov, P. S. Petkov, K. I. Hadjiivanov, K. M. Neyman, *The Journal of Physical Chemistry C* **2011**, *115*, 23435–23454.

[46] F. Romero-Sarria, L. M. Martínez T, M. A. Centeno, J. A. Odriozola, *The Journal of Physical Chemistry C* **2007**, *111*, 14469–14475.

[47] D. Vovchok, C. Zhang, S. Hwang, L. Jiao, F. Zhang, Z. Liu, S. D. Senanayake, J. A. Rodriguez, *ACS Catalysis* **2020**, *10*, 10216–10228.

[48] W. O. Gordon, Y. Xu, D. R. Mullins, S. H. Overbury, *Physical Chemistry Chemical Physics* **2009**, *11*, 11171–11183.

[49] M. Pfeiffer, C. Hess, *The Journal of Physical Chemistry C* **2022**, *126*, 3980–3992.

[50] A. Rezvani, A. M. Abdel-Mageed, T. Ishida, T. Murayama, M. Parlinska-Wojtan, R. J. Behm, *ACS Catalysis* **2020**, *10*, 3580–3594.

[51] G. Ertl, H. Knözinger, J. Weitkamp, *Handbook of Heterogeneous Catalysis*, Wiley, Weinheim, **2008**.

[52] S. G. Jadhav, P. D. Vaidya, B. M. Bhanage, J. B. Joshi, *Chemical Engineering Research and Design* **2014**, *92*, 2557–2567.

[53] M. Saito, K. Murata, *Catalysis Surveys from Asia* **2004**, *8*, 285–294.

[54] E. L. Kunkes, F. Studt, F. Abild-Pedersen, R. Schlögl, M. Behrens, *Journal of Catalysis* **2015**, *328*, 43–48.

[55] Y. Hartadi, D. Widmann, R. J. Behm, *Journal of Catalysis* **2016**, *333*, 238–250.

[56] X.-M. Liu, G. Q. Lu, Z.-F. Yan, J. Beltramini, *Industrial & Engineering Chemistry Research* **2003**, *42*, 6518–6530.

[57] A. M. Abdel-Mageed, A. Klyushin, A. Rezvani, A. Knop-Gericke, R. Schlögl, R. J. Behm, *Angewandte Chemie* **2019**, *131*, 10431–10436.

[58] C. T. Campbell, C. H. F. Peden, *Science* **2005**, *309*, 713–714.

[59] J. Graciani, K. Mudiyanselage, F. Xu, A. E. Baber, J. Evans, S. D. Senanayake, D. J. Stacchiola, P. Liu, J. Hrbek, J. Fernández Sanz, J. A. Rodriguez, *Science* **2014**, *345*, 546–550.

[60] Coblentz Society, https://webbook.nist.gov/cgi/cbook.cgi?ID=C67561&Type=IR-SPEC&Index=1#IR-SPEC, **2023**.

[61] Coblentz Society, https://webbook.nist.gov/cgi/cbook.cgi?ID=C74828&Type=IR-SPEC&Index=1#IR-SPEC, **2023**.

[62] L. P. Gonçalves, J. Mielby, O. S. G. Soares, J. P. Sousa, D. Y. Petrovykh, O. I. Lebedev, M. F. R. Pereira, S. Kegnæs, Y. V. Kolen'ko, *Applied Catalysis B: Environmental* **2022**, *312*, 121376.

[63] S. M. Fehr, I. Krossing, *ChemCatChem* **2020**, *12*, 2622–2629.

[64] A. Badri, C. Binet, J. C. Lavalley, *Journal of the Chemical Society - Faraday Transactions* **1997**, *93*, 1159–1168.

[65] M. Ziemba, J. Weyel, C. Hess, *ACS Catalysis* **2022**, *12*, 9503–9514.

[66] Z. Ren, F. Peng, J. Li, X. Liang, B. Chen, *Catalysts* **2017**, *7*, 48.

[67] J. Ning, Y. Zhou, W. Shen, *Science China Chemistry* **2021**, *64*, 1103–1110.

[68] M. Lykaki, S. Stefa, S. Carabineiro, M. Soria, L. Madeira, M. Konsolakis, *Catalysts* **2021**, *11*, 753.

[69] Y. Zhou, A. Chen, J. Ning, W. Shen, *Chinese Journal of Catalysis* **2020**, *41*, 928–937.

[70] J. Ning, Y. Zhou, A. Chen, Y. Li, S. Miao, W. Shen, *Catalysis Today* **2020**, *357*, 460–467.

[71] D. Vovchok, C. J. Guild, J. Llorca, W. Xu, T. Jafari, P. Toloueinia, D. Kriz, I. Waluyo, R. M. Palomino, J. A. Rodriguez, S. L. Suib, S. D. Senanayake, *Physical Chemistry Chemical Physics* **2017**, *19*, 17708–17717.

[72] S. Y. Ahn, H. S. Na, K. W. Jeon, Y. L. Lee, K. J. Kim, J. O. Shim, H. S. Roh, *Catalysis Today* **2020**, *352*, 166–174.

[73] Y. Chen, J. Lin, X. Wang, *Chemical Communications* **2022**, *58*, 208–222.

[74] W.-H. Chen, C.-Y. Chen, *Applied Energy* **2020**, *258*, 114078.

[75] X. Wang, J. A. Rodriguez, J. C. Hanson, D. Gamarra, A. Martínez-Arias, M. Fernández-García, *Journal of Physical Chemistry B* **2006**, *110*, 428–434.

[76] L. Barrio, M. Estrella, G. Zhou, W. Wen, J. C. Hanson, A. B. Hungría, A. Hornés, M. Fernández-García, A. Martínez-Arias, J. A. Rodriguez, *Journal of Physical Chemistry C* **2010**, *114*, 3580–3587.

[77] A. L. Cámara, S. Chansai, C. Hardacre, A. Martínez-Arias, *International Journal of Hydrogen Energy* **2014**, *39*, 4095–4101.

[78] S.-C. Yang, S. H. Pang, T. P. Sulmonetti, W.-N. Su, J.-F. Lee, B.-J. Hwang, C. W. Jones, *ACS Catalysis* **2018**, *8*, 12056–12066.

[79] K. Isokoski, C. A. Poteet, H. Linnartz, *Astronomy and Astrophysics* **2013**, *555*, A85.

[80] A. Laachir, V. Perrichon, A. Badri, J. Lamotte, E. Catherine, J. C. Lavalley, J. El Fallah, L. Hilaire, F. Le Normand, E. Quéméré, G. N. Sauvion, O. Touret, *Journal of the Chemical Society Faraday Transactions* **1991**, *87*, 1601–1609.

[81] P. Bera, A. L. Cámara, A. Hornés, A. Martínez-Arias, *The Journal of Physical Chemistry C* **2009**, *113*, 10689–10695.

[82] A. Chen, X. Yu, Y. Zhou, S. Miao, Y. Li, S. Kuld, J. Sehested, J. Liu, T. Aoki, S. Hong, M. F. Camellone, S. Fabris, J. Ning, C. Jin, C. Yang, A. Nefedov, C. Wöll, Y. Wang, W. Shen, *Nature Catalysis* **2019**, *2*, 334–341.

[83] X. Guo, J. Li, R. Zhou, *Fuel* **2016**, *163*, 56–64.

[84] M. Manzoli, R. D. Monte, F. Boccuzzi, S. Coluccia, J. Kašpar, *Applied Catalysis B: Environmental* **2005**, *61*, 192–205.

[85] W. Ji, N. Wang, X. Chen, Q. Li, K. Lin, J. Deng, J. Chen, X. Xing, *Inorganic Chemistry* **2022**, *61*, 10006–10014.

[86] L. Kang, B. Wang, A. T. Güntner, S. Xu, X. Wan, Y. Liu, S. Marlow, Y. Ren, D. Gianolio, C. C. Tang, V. Murzin, H. Asakura, Q. He, S. Guan, J. J. Velasco-Vélez, S. E. Pratsinis, Y. Guo, F. R. Wang, *Angewandte Chemie International Edition* **2021**, *60*, 14420–14428.

[87] D. Gamarra, A. Martínez-Arias, *Journal of Catalysis* **2009**, *263*, 189–195.

[88] M. Ziemba, M. Radtke, L. Schumacher, C. Hess, *Angewandte Chemie International Edition* **2022**, *61*, e202209388.